INL/EXT-16-38233
Revision 0

Nonlinear Time Domain Seismic Soil-Structure Interaction (SSI) Deep Soil Site Methodology Development

Fiscal Year 2015 Report

September 2015

The INL is a U.S. Department of Energy National Laboratory
operated by Battelle Energy Alliance

INL/EXT-16-38233
Revision 0

Nonlinear Time Domain Seismic Soil-Structure Interaction (SSI) Deep Soil Site Methodology Development

Robert Spears and Justin Coleman

September 2015

Idaho National Laboratory
NS&T
Idaho Falls, Idaho 83415

http://www.inl.gov

Prepared for the
U.S. Department of Energy
Office of _____
Under DOE Idaho Operations Office
Contract DE-AC07-05ID14517

Nonlinear Time Domain Seismic Soil-Structure Interaction (SSI) Deep Soil Site Methodology Development

INL/EXT-16-38233
Revision 0

September 2015

Approved by:

Name Title [optional]	Date

EXECUTIVE SUMMARY

Currently the Department of Energy (DOE) and the nuclear industry perform seismic soil-structure interaction (SSI) analysis using equivalent linear numerical analysis tools. For lower levels of ground motion, these tools should produce reasonable in-structure response values for evaluation of existing and new facilities. For larger levels of ground motion these tools likely overestimate the in-structure response (and therefore structural demand) since they do not consider geometric nonlinearities (such as gaping and sliding between the soil and structure) and are limited in the ability to model nonlinear soil behavior. The current equivalent linear SSI (SASSI) analysis approach either joins the soil and structure together in both tension and compression or releases the soil from the structure for both tension and compression. It also makes linear approximations for material nonlinearities and generalizes energy absorption with viscous damping. This produces the potential for inaccurately establishing where the structural concerns exist and/or inaccurately establishing the amplitude of the in-structure responses.

Seismic hazard curves at nuclear facilities have continued to increase over the years as more information has been developed on seismic sources (i.e. faults), additional information gathered on seismic events, and additional research performed to determine local site effects. Seismic hazard curves are used to develop design basis earthquakes (DBE) that are used to evaluate nuclear facility response. As the seismic hazard curves increase, the input ground motions (DBE's) used to numerically evaluation nuclear facility response increase causing larger in-structure response. As ground motions increase so does the importance of including nonlinear effects in numerical SSI models.

To include material nonlinearity in the soil and geometric nonlinearity using contact (gaping and sliding) it is necessary to develop a nonlinear time domain methodology. This methodology will be known as, NonLinear Soil-Structure Interaction (NLSSI). In general NLSSI analysis should provide a more accurate representation of the seismic demands on nuclear facilities their systems and components.

INL, in collaboration with a Nuclear Power Plant Vender (NPP-V), will develop a generic Nuclear Power Plant (NPP) structural design to be used in development of the methodology and for comparison with SASSI. This generic NPP design has been evaluated for the INL soil site because of the ease of access and quality of the site specific data. It is now being evaluated for a second site at Vogtle which is located approximately 15 miles East-Northeast of Waynesboro, Georgia and adjacent to Savanna River. The Vogtle site consists of many soil layers spanning down to a depth of 1058 feet. The reason that two soil sites are chosen is to demonstrate the methodology across multiple soil sites.

The project will drive the models (soil and structure) using successively increasing acceleration time histories with amplitudes. The models will be run in time domain codes such as ABAQUS, LS-DYNA, and/or ESSI and compared with the same models run in SASSI. The project is focused on developing and documenting a method for performing time domain, non-linear seismic soil structure interaction (SSI) analysis. Development of this method will provide the Department of Energy (DOE) and industry with another tool to perform seismic SSI analysis.

ACKNOWLEDGEMENTS

CONTENTS

CONTENTS

EXECUTIVE SUMMARY iv

ACRONYMS xi

SOFTWARE xii

FIGURES

TABLES

ACRONYMS

DBE	Design Basis Earthquake
DOE	Department of Energy
INL	Idaho National Laboratory
NLSSI	NonLinear Soil Structure Interaction
NNSA	National Nuclear Security Administration
NRC	Nuclear Regulatory Commission
SSI	Soil-Structure Interaction

SOFTWARE

Abaqus Software, Version 6.12-2 (Abaqus/Standard and Abaqus/Explicit) [Dassault Systèmes 2012]

LS-DYNA Software, Version smp s R7.00 (LS-DYNA) [LSTC 2013]

Mathcad Software, Version 15.0 (Mathcad) [PTC 2011]

SASSI2000 Software (SASSI) [Lysmer et al. 1999]

SHAKE2000 Software (SHAKE) [Deng et al. 2000]

Nonlinear Time Domain Seismic Soil-Structure Interaction (SSI) Deep Soil Site Methodology Development

1. Introduction

The Department of Energy (DOE) and the nuclear industry perform seismic soil-structure interaction (SSI) analysis using equivalent linear numerical analysis tools. For lower levels of ground motion these tools should produce reasonable in-structure response values for evaluation of existing and new facilities. For larger levels of ground motion these tools likely overestimate the in-structure response (and therefore structural demand) since they do not consider geometric nonlinearities (such as gaping and sliding between the soil and structure). These tools could also underestimate the in-structure response (and therefore structural demand) where gapping, which could result in impact, is not addressed. Additionally, these tools are limited in their ability to model nonlinear soil behavior such as plasticity that causes permanent deformation. Instead, material nonlinearities are approximated with springs and viscous damping. For higher levels of ground motion these approximations may produce inaccurate in-structure responses.

Inaccurate in-structure response (seismic demand) for higher levels of ground motions may produce overly conservative analyses for existing and new nuclear facilities. It could also produce a situation where the high in-structure response location is not correctly identified. This may cause nuclear facility owners to spend more money than necessary to mitigate the perceived seismic risk. Development of a NonLinear Soil-Structure Interaction (NLSSI) methodology offers a more physics based solution that has the potential to remove additional conservatism from design and analysis of existing and new nuclear facilities. It also has potential to remove conservatism from seismic probabilistic risk assessments (SPRA) so that best estimate seismic risk numbers can be computed. Benefits of NLSSI include making evaluation possible for gapping and sliding, soil plasticity, inclined seismic waves, nonlinear structure behavior, and nonlinear seismic isolation.

Linear, frequency domain numerical analysis codes were developed in the early 1980s to provide a computationally efficient method for computing seismic nuclear facility response. These codes efficiently deal with the problem of modeling a finite domain (local soil and structure) in an infinite space (soil extends many miles to earthquake sources) by using the method of superposition. The input motions defined by the seismic hazards at nuclear facility sites were typically lower in the early 1980s than current seismic hazard curves. These lower seismic hazard curves tended to produce linear soil-structure response thus making equivalent linear codes applicable.

Nonlinear time domain analysis requires modeling of the local soil out to the point where the nuclear facility no longer significantly affects the soil response (free field soil behavior). Load time histories are used to bring the seismic waves into the model. Absorbing boundary conditions are used to pass the reflected seismic waves and local waves (that propagate away from the nuclear facility) out of the model. Over the years the computational power has greatly increased to a point where standard desktop computers can efficiently solve large problems. Seismic hazard curves and therefore input ground motions have also tended to increase at nuclear facility sites thus making the nonlinear effects potentially more important. This makes NLSSI a viable tool in soil structure analysis.

The NLSSI methodology is being developed using the commercially available time domain code LS-DYNA. However, this methodology is independent of a specific numerical tool and should be generally applicable to any time domain code that can meet the requirements of the method. Other time domain codes exist that have capability for performing NLSSI such as ABAQUS, Earthquake Soil/Rock Structure Interaction (ESSI), and Mastodon. ESSI is a nonlinear time domain code that is being developed at

University of California at Davis (UC Davis) for the Nuclear Regulatory Commission (NRC) and Mastodon is being developed at the Idaho National Laboratory.

This report documents development of a NLSSI methodology for a deep soil site. As free field validation, the nonlinear soil constitutive model is compared to actual data gathered by the Electric Power Research Institute (EPRI) in cooperation with the Taiwan Power Company (Taipower) at Lotung, Taiwan. As SSI validation, low amplitude seismic results are compared between NLSSI and the recently V&Ved version of SASSI at the Vogtle site (located approximately 15 miles East-Northeast of Waynesboro, Georgia and adjacent to Savanna River).

The structure used in the SSI model is a generic Nuclear Power Plant (NPP). The NLSSI models are primarily performed with the time domain code, LS-DYNA. However, the software Abaqus is also used as a time domain code and as an eigensolver for the structure. The linear SSI models are performed with the frequency domain code, SASSI.

2. Benchmarking and Validation

One part of benchmarking and validation for using NLSSI at a deep soil site is to compare NLSSI results to actual measured seismic data. The Electric Power Research Institute (EPRI) in cooperation with the Taiwan Power Company (Taipower) has conducted field experiments at Lotung, Taiwan. The field experiments include gathering material property data on the soil and measuring soil motion caused by seismic events. The soil motion is measured at many locations at and below the soil surface. The resulting soil motion and material property data are useful for validation of SSI analysis techniques.

The purpose of this study (documented in Appendix A) is to demonstrate that NLSSI can reasonably reproduce the actual measured soil motions at Lotung. The results of the study showed that NLSSI can reasonably reproduce the actual measured soil motions at Lotung.

3. Second Soil Site

The second soil site is a deep soil site at Vogtle. The Vogtle site is located approximately 15 miles East-Northeast of Waynesboro, Georgia and adjacent to Savanna River. The site consists of many soil layers spanning down to a depth of 1058 feet. Being a well-documented deep soil site, Vogtle makes a good location to compare deep soil column, linear and nonlinear evaluation techniques. Appendix B performs this comparison.

The study in Appendix B shows results for a deep soil column evaluated with linear techniques (SHAKE) and with nonlinear techniques (LS-DYNA/Abaqus). The soil surface, response spectra results showed good agreement between the linear and nonlinear techniques at low frequencies (< 6•Hz). Additionally, the soil surface, response spectra results showed good agreement between the linear and nonlinear techniques relative to natural frequency response of the soil column. The higher frequency response (> 6•Hz) amplitude diverged between the linear and nonlinear techniques. This difference is predictable given the differences in the linear and nonlinear hysteresis loops (and further discussion can be found in Sections 6.1 and 7).

4. Structure Model and Rayleigh Damping

The structural model is used as a reasonable structure for SSI analysis. It is evaluated as being linear elastic and Rayleigh damping is applied to approximate 4 % modal damping. The structural mesh is described in Section 4.1. The process used to select Rayleigh damping coefficients is discussed in Section 4.2 and a fixed base model and results are discussed in Section 4.3.

4.1 Structure Model

The structural mesh is shown in Figures 4.1-1 to 4.1-5. It is a continuous, linear elastic mesh with concrete material properties for the structure and steel material properties for the reactor vessel and the support for the reactor vessel. The elastic material properties for the concrete are a modulus of elasticity of 449,600 ksf, a Poisson's ratio of 0.20, and a density of 150 lbm/ft^3. The elastic material properties for the steel are a modulus of elasticity of 3,744,000 ksf, a Poisson's ratio of 0.30, and a density of 515 lbm/ft^3.

The structure is modeled with LS-DYNA mesh definitions and with Abaqus mesh definitions. The nonlinear SSI model is performed with LS-DYNA and the linear SSI model is performed with stiffness and mass matrices output from Abaqus/Standard. Because the two codes do not use the same element formulations, this causes some differences.

The reactor vessel solid mesh and point mass is tuned such that it has a first natural frequency with the reactor vessel inertial element near 6 Hz (and the modal analysis was performed in Abaqus/Standard). The reactor vessel mesh has a mass of 6,800 ton.

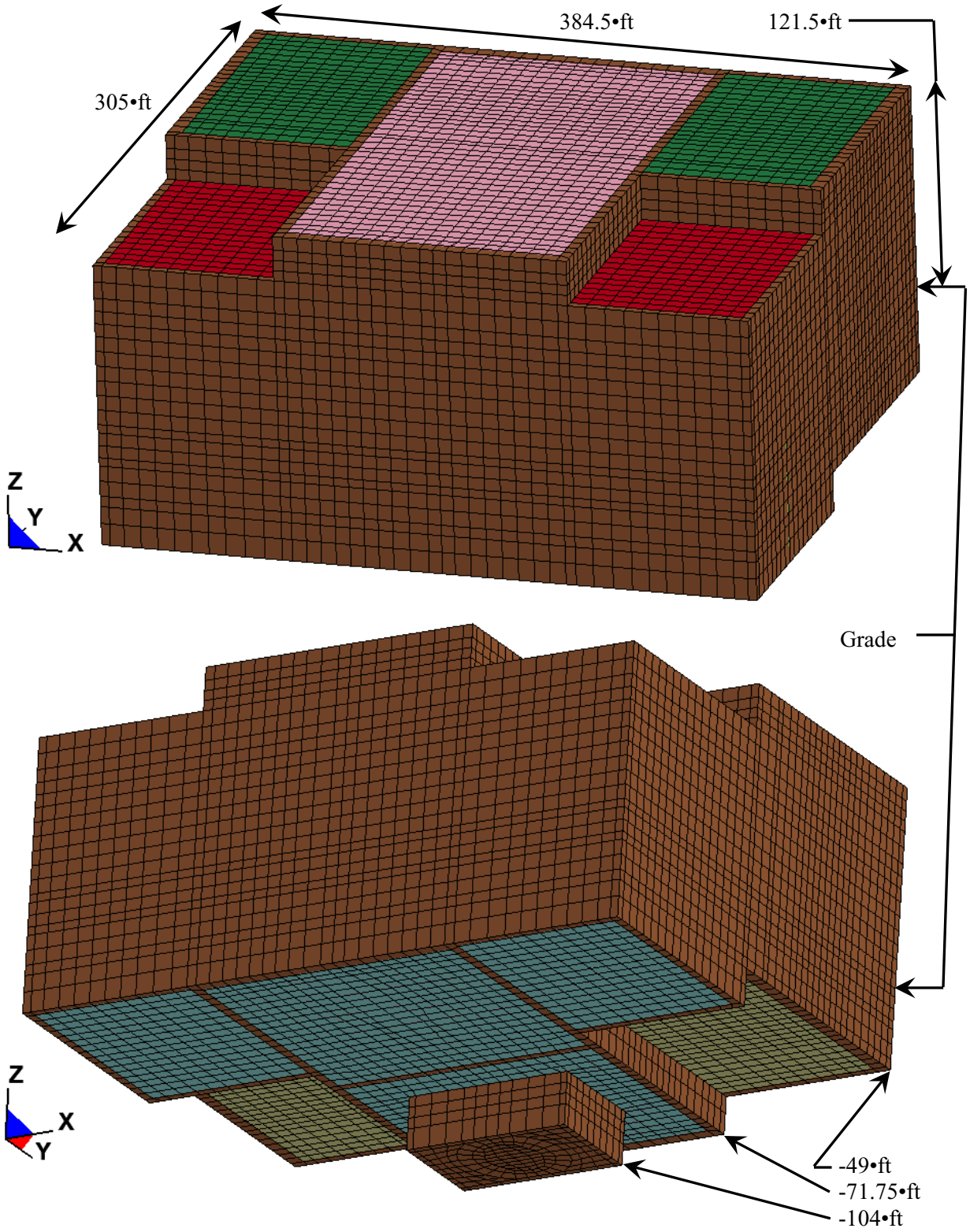

Figure 4.1-1. Finite element mesh of the structure.

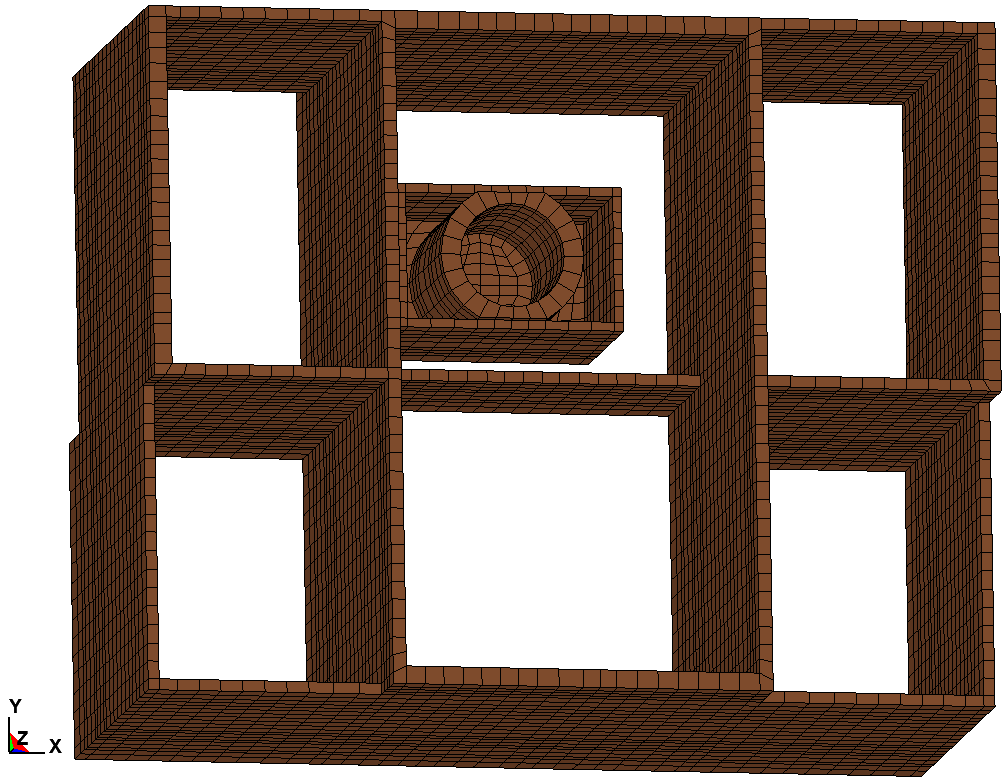

Figure 4.1-2. Linear Tshells (LS-DYNA) or incompatible modes linear bricks (Abaqus) walls and reactor area.

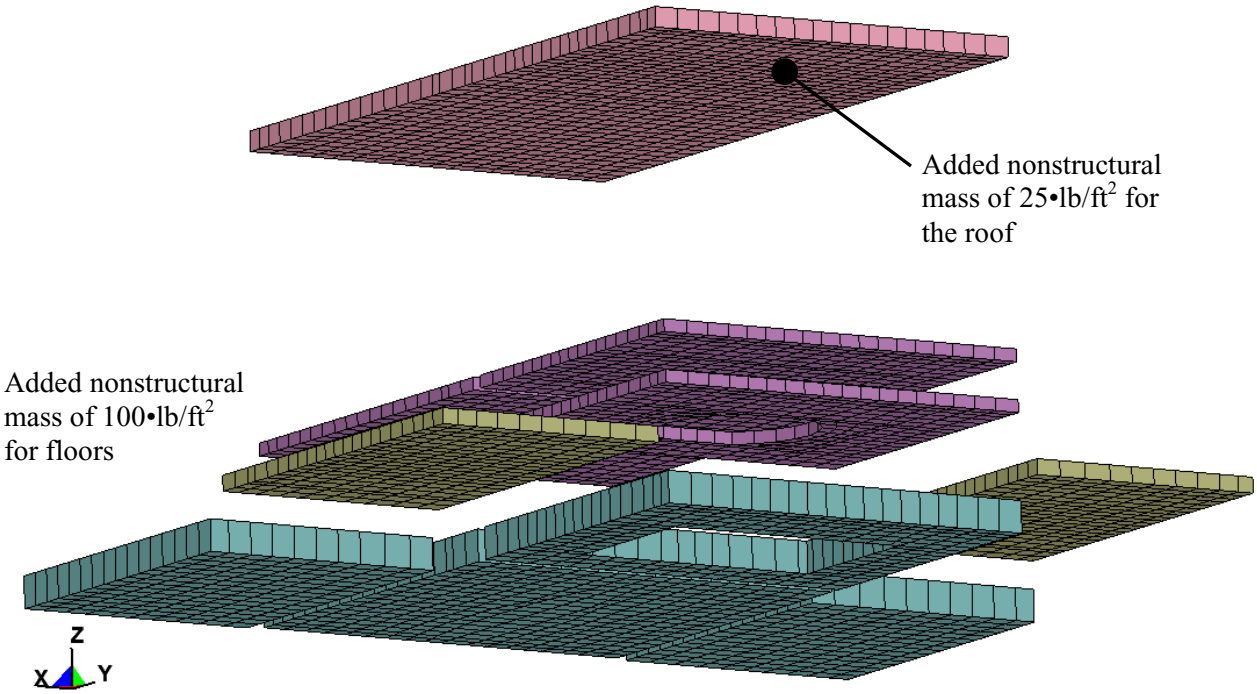

Figure 4.1-3. Linear Tshells (LS-DYNA) or incompatible modes linear bricks (Abaqus) floors and roof.

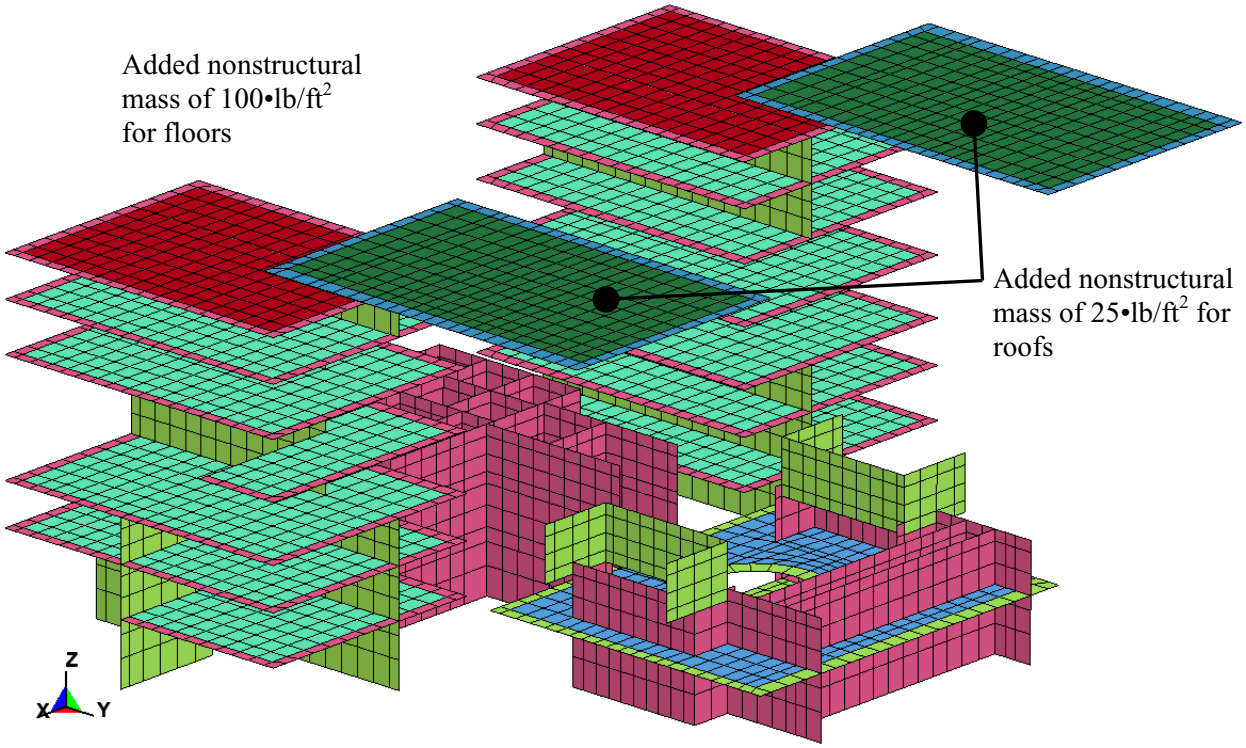

Figure 4.1-4. Linear shells (LS-DYNA/Abaqus) for the remaining floors and roofs. (

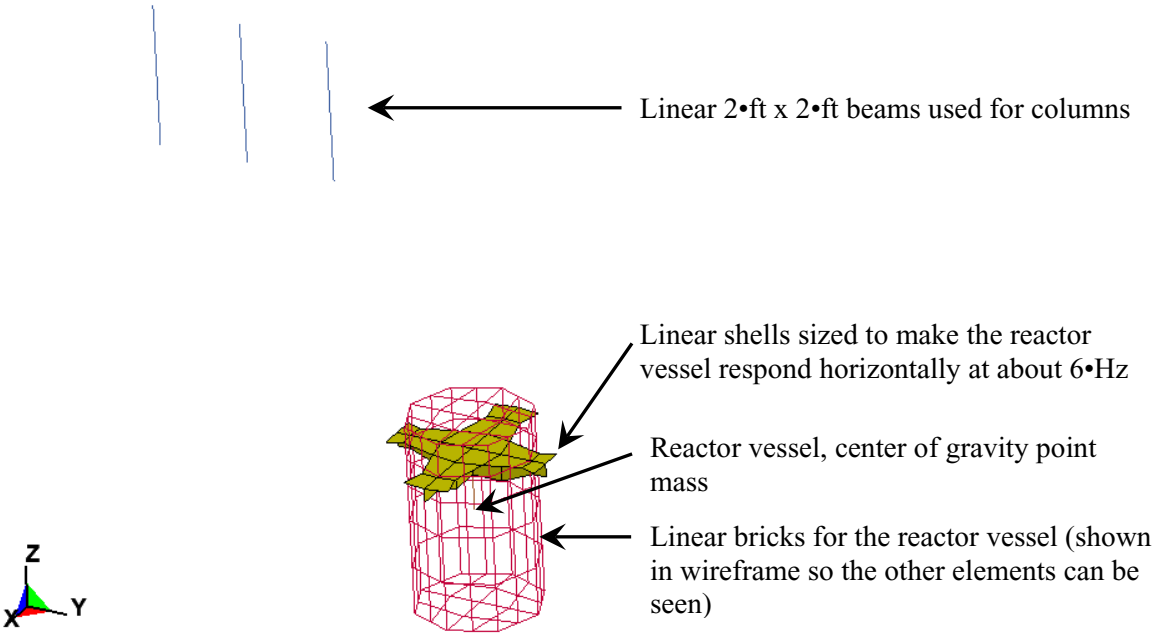

Figure 4.1-5. Remaining elements in the structure.

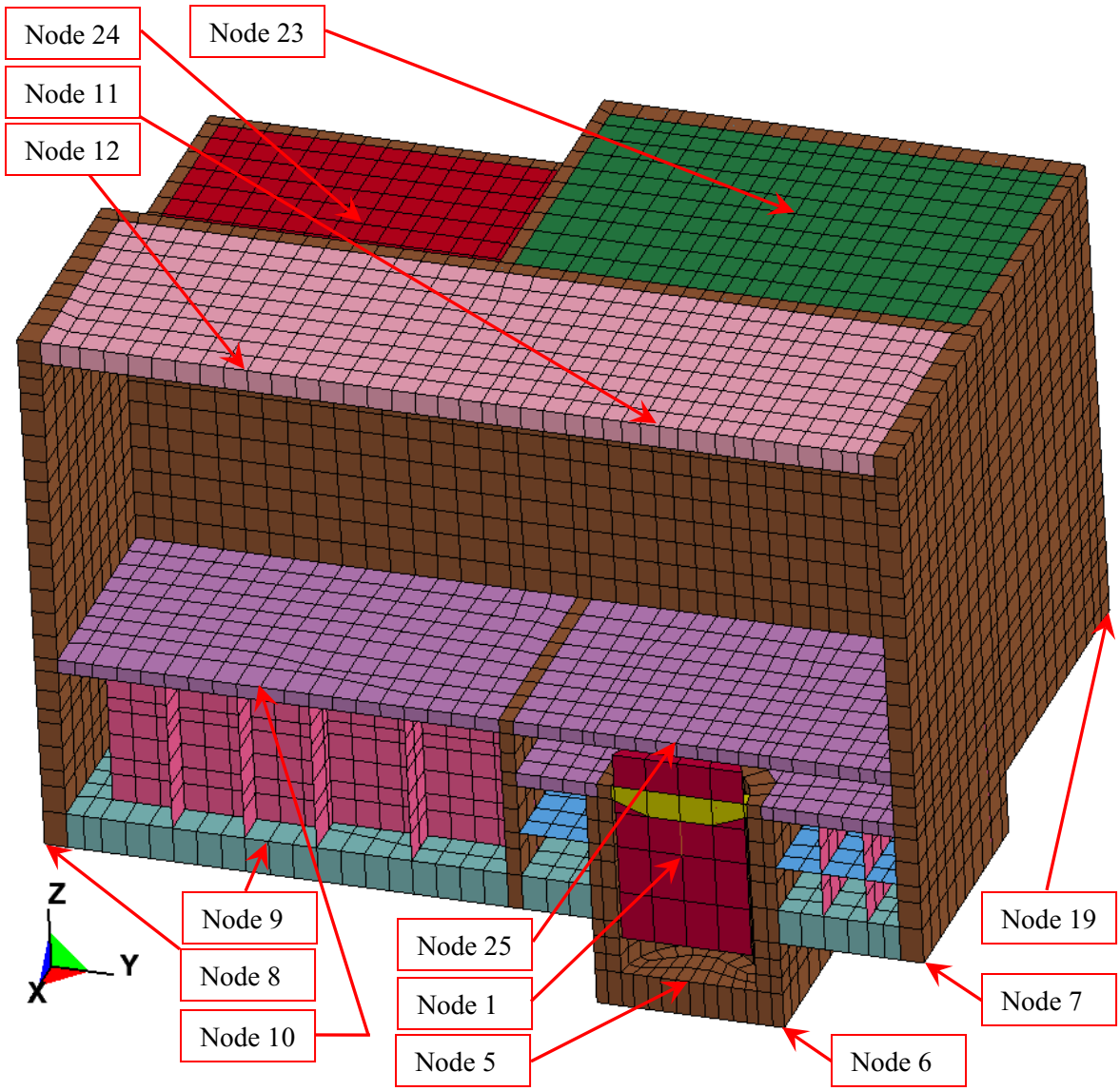

Figure 4.1-6. Most of the nodes used for output.

Figure 4.1-6 shows most of the nodes used for output. Node 20 is on the bottom corner of the structure at the most negative x and negative y coordinates. Node 21 is on the top of the bottom most floor under Node 24. Node 22 is on the top of the bottom most floor under Node 23. Considering that the outside dimensions of the cut-away portion of the structure are a mirror image of the portion in view, Nodes 13 – 18 are at mirror image locations to Nodes 19 – 24 respectively.

4.2 Rayleigh Damping

To approximate Rayleigh damping factors for the structure, effective mass is used. The effective mass is approximated with a fixed base modal analysis of the structure in Abaqus/Standard. To perform the fixed base analysis, every node that touched soil is restrained in x-, y-, and z-translation. Natural frequencies are then found for all frequencies between 0 Hz and 100 Hz. Plotting cumulative effective mass percentage at every natural frequency (as shown in Figure 4.2-1) provides evidence of where the predominate structural respond occurs. The steeper the cumulative effective mass percentage curve at a given frequency, the more that structure will respond at that frequency.

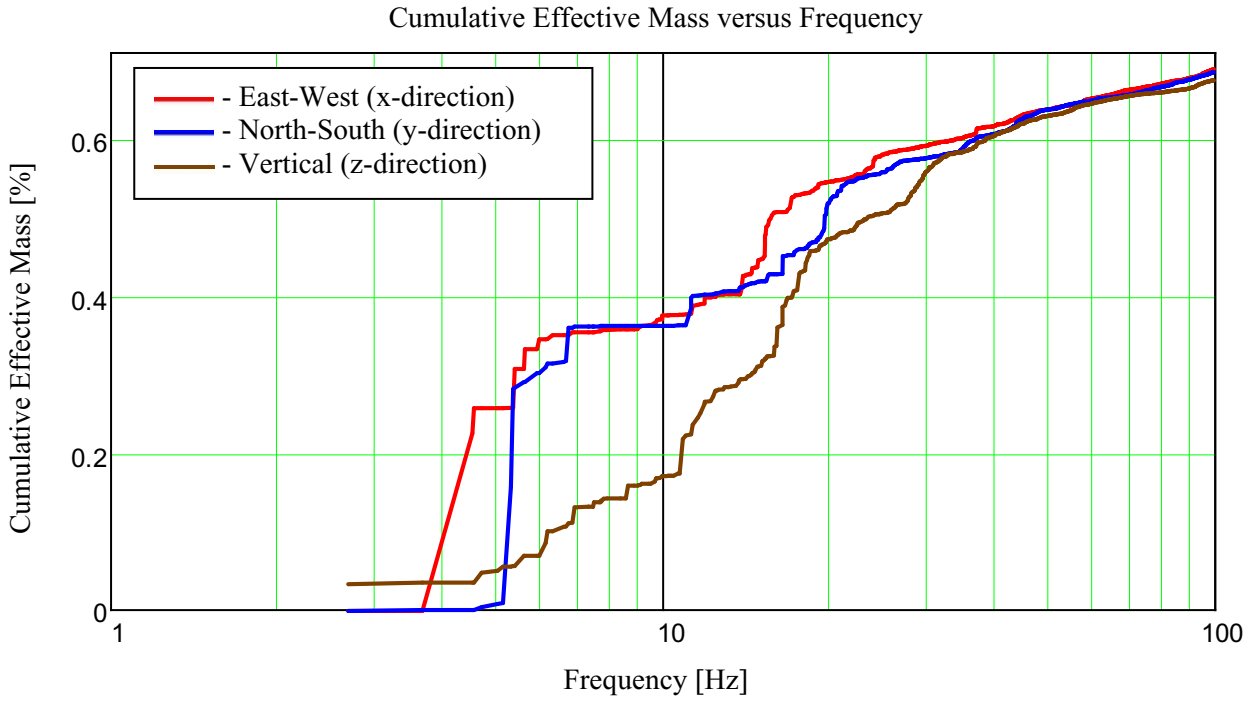

Figure 4.2-1. Cumulative effective mass versus frequency.

For all of the modeled mass to be considered, the cumulative effective mass curves should go to 100 %. Because the fixed base analysis fixed the motion on so many nodes, much of the structural mass is not able to participate.

To approximate Rayleigh damping factors for the structure, response spectra for an appropriate set of acceleration time histories are used. The acceleration time histories used for this (shown in Figure 4.2-2) are based on time histories at the soil surface from Cuesta et al. (2016).

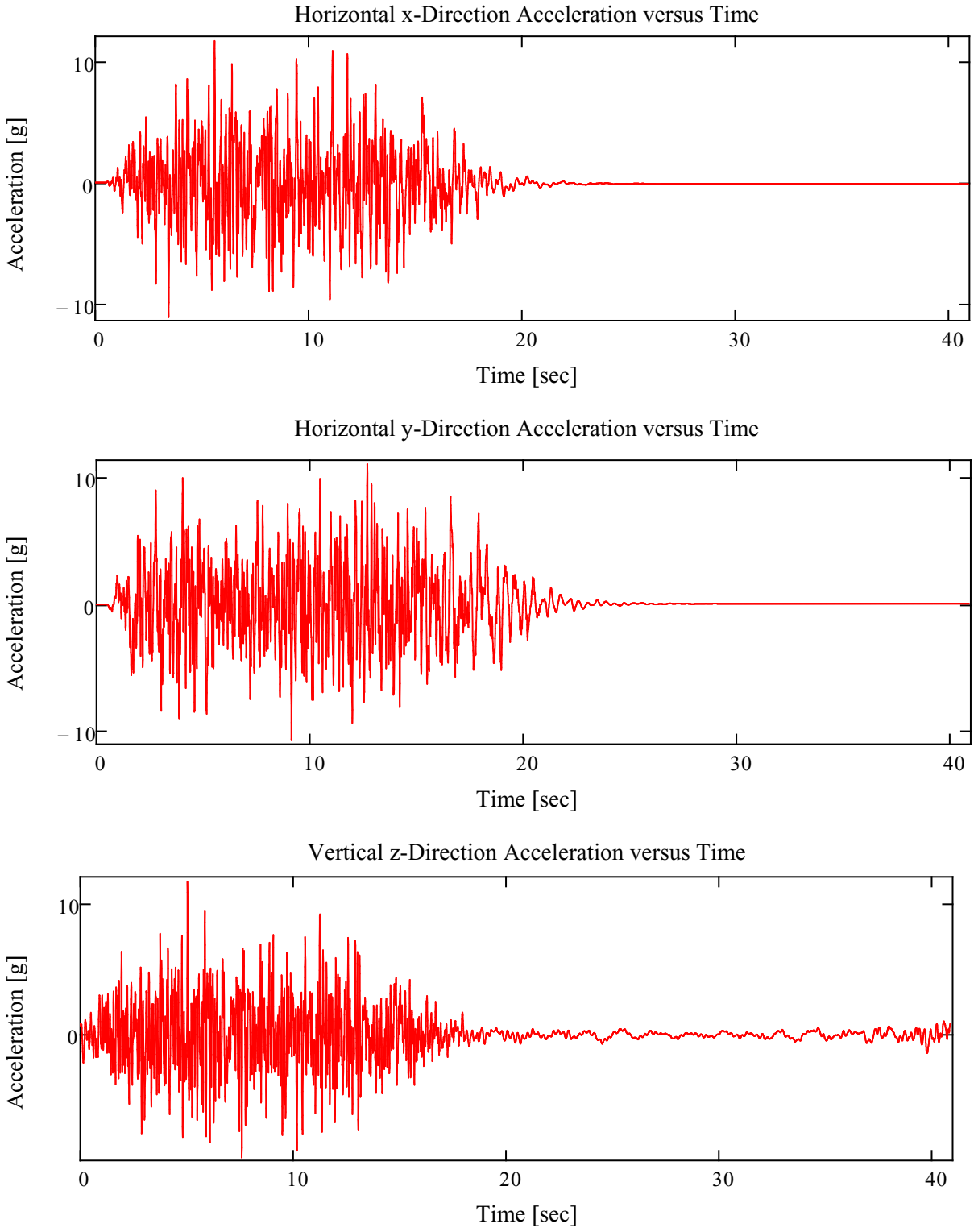

Figure 4.2-2. Horizontal and vertical acceleration time histories.

To establish Rayleigh damping coefficients, an iterative process is used. First response spectra for the desired 4 % modal damping are generated for the acceleration time histories in Figure 4.2-2. Second, Rayleigh damping coefficients are selected and Rayleigh damped response spectra are generated for the acceleration time histories in Figure 4.2-2. Third, the difference in response between the modal damped and Rayleigh damped plot are found and multiplied by the effective mass values at each frequency where an effect mass value exists. Fourth, all of these values are summed. For a good set of Rayleigh damping coefficients, the summed value should be at or near zero. If it is not, then new Rayleigh damping coefficients are selected and another iteration is performed. Using this process to select Rayleigh damping coefficients, the mass damping coefficient is "$\alpha = 1.51$" and the stiffness damping coefficient is "$\beta = 7.572 \cdot 10^{-4}$". Figure 4.2-3 shows the damping versus frequency plot for these Rayleigh damping coefficients. Figure 4.2-4 shows the Rayleigh damped (using the defined coefficients) and the 4 % modal damped response spectra.

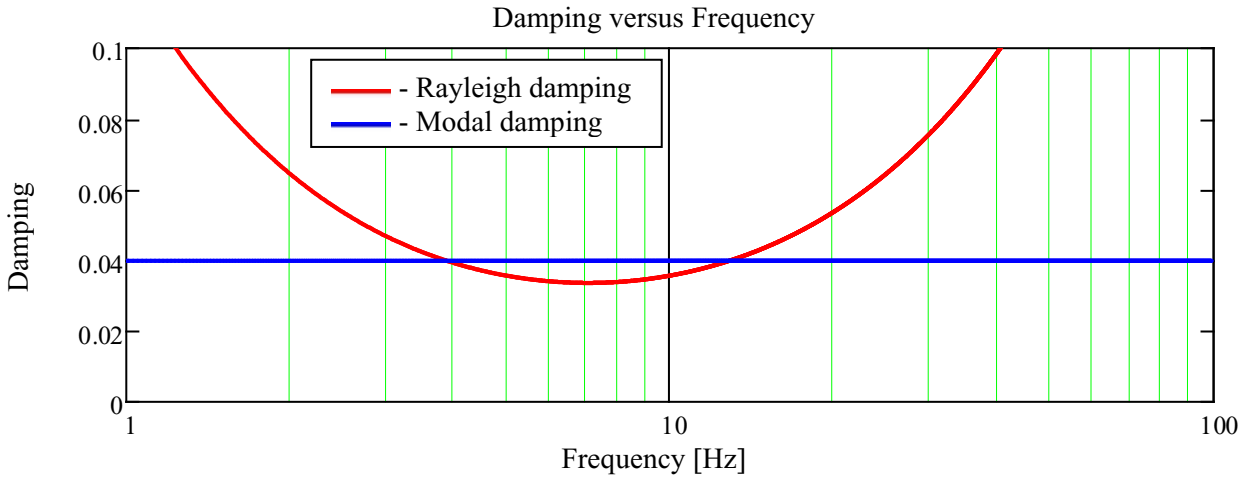

Figure 4.2-3. Damping versus frequency for Rayleigh damping and modal damping.

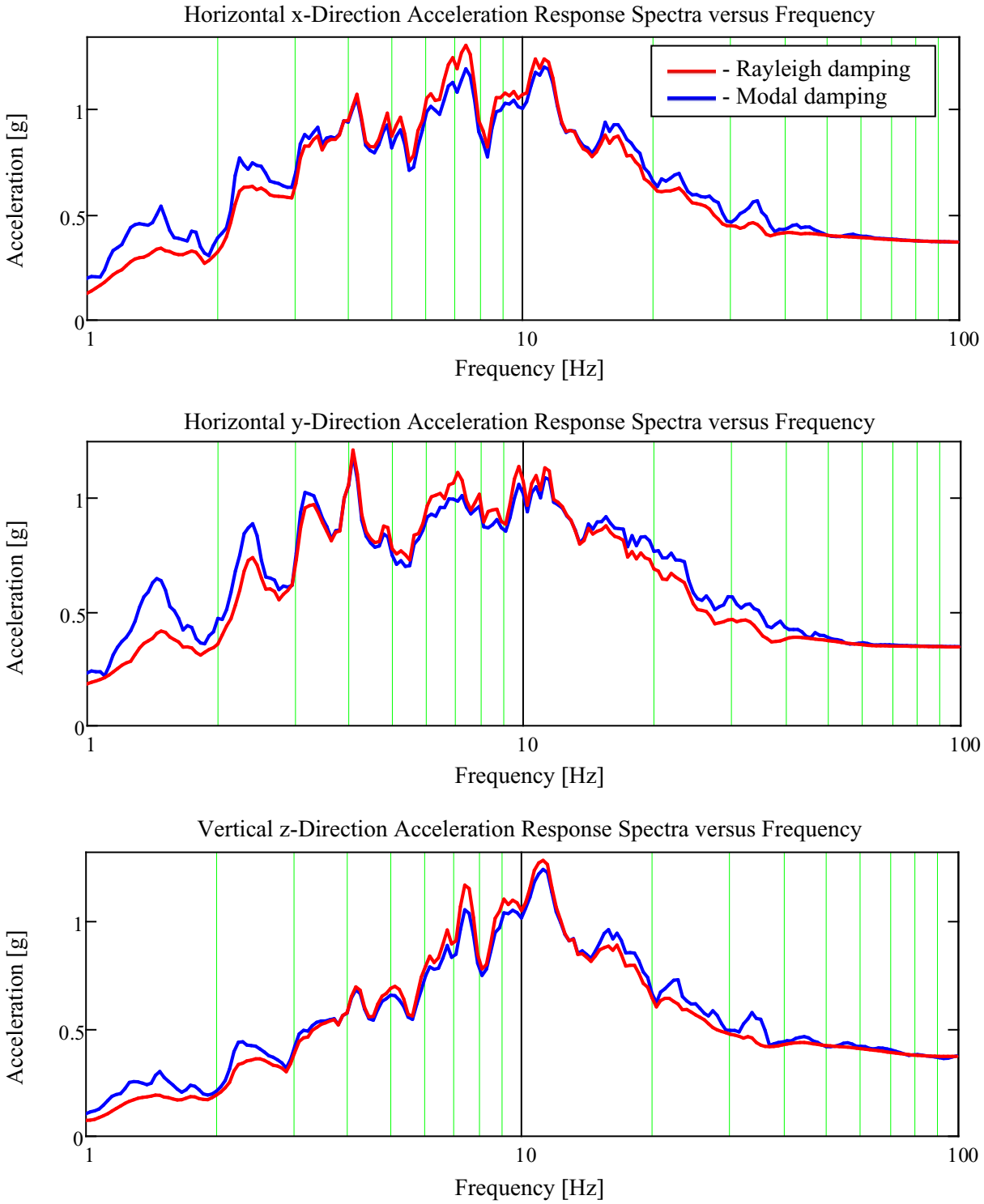

Figure 4.2-4. Rayleigh damped and the 4 % modal damped response spectra.

Figure 4.2.4 shows that the Rayleigh damped and the 4 % modal damped response spectra match reasonably well for the range where the structure responds. Consequently, the selected Rayleigh damping parameters are reasonable.

4.3 Fixed Base Model Structural Results

As a check of the linear elastic structure with Rayleigh damping, structure only fixed base seismic models are run in LS-DYNA and Abaqus/Standard. In the fixed base analysis, every node in the structure that touches soil has the acceleration time histories in Figure 4.2-2 applied to it. The LS-DYNA model run is performed with a dynamic relaxation step (using default parameters) to apply gravitational loading followed by the seismic evaluation step with Rayleigh damping. The Abaqus/Standard model run is performed with a nonlinear static step to apply gravitational loading followed by the seismic evaluation step with Rayleigh damping.

With the model runs complete, response spectra are generated and compared at nodes listed in Figure 4.1-6 (except the nodes that have the acceleration time histories applied to them). Figures 4.3-1 to 4.3-7 show these results.

There is one notable difference in the LS-DYNA and Abaqus/Standard models. Because of the way that the point mass is incorporated, the LS-DYNA model point mass (at Node 1) is more rigidly supported vertically than that of the Abaqus/Standard model. Other differences include the differences in element formulation between LS-DYNA. Scoping analyses were performed for comparison of the following element types:

- Solid linear bricks (LS-DYNA) versus solid linear bricks (Abaqus)
- Linear Tshells (LS-DYNA) versus linear continuum shells and linear incompatible modes bricks (Abaqus)
- Linear thin shells (LS-DYNA) versus linear thin shells (Abaqus)
- Linear beams (LS-DYNA) versus linear beams (Abaqus)

The comparison using the solid linear bricks showed very good agreement between LS-DYNA and Abaqus. However, the potential for significant differences in the model results existed in the other element types. Attempts were made to minimize these differences in the structural models. The figures demonstrate that differences do occur but there is reasonable agreement between the LS-DYNA and Abaqus model runs. Because LS-DYNA is used for the NLSSI models and Abaqus is used to translate the model into a form useable for SASSI, the differences in Figures 4.3-1 to 4.3-7 can be expected to translate into differences in the nonlinear and linear SSI models.

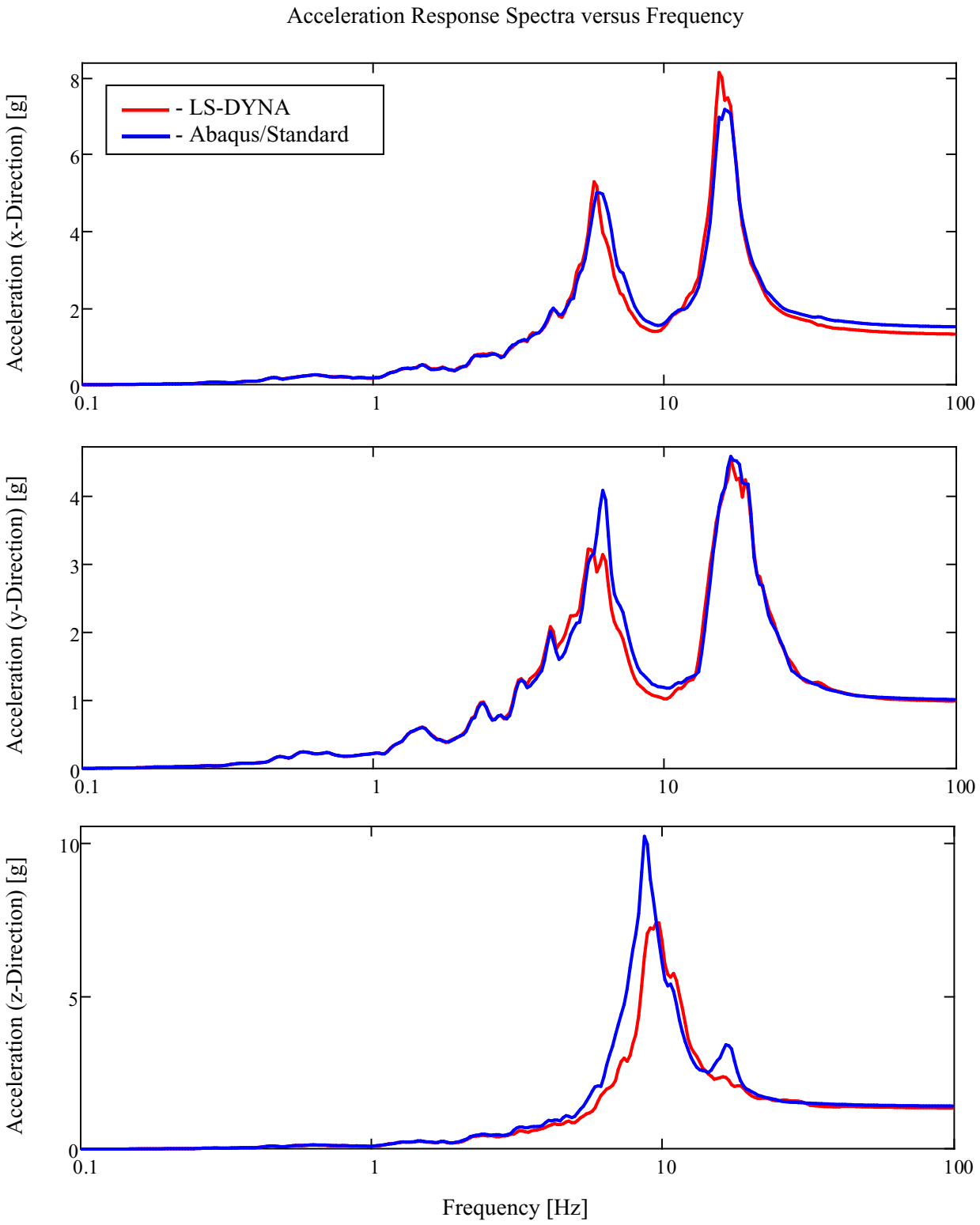

Figure 4.3-1. Node 1 acceleration response spectra from Abaqus/Standard and LS-DYNA.

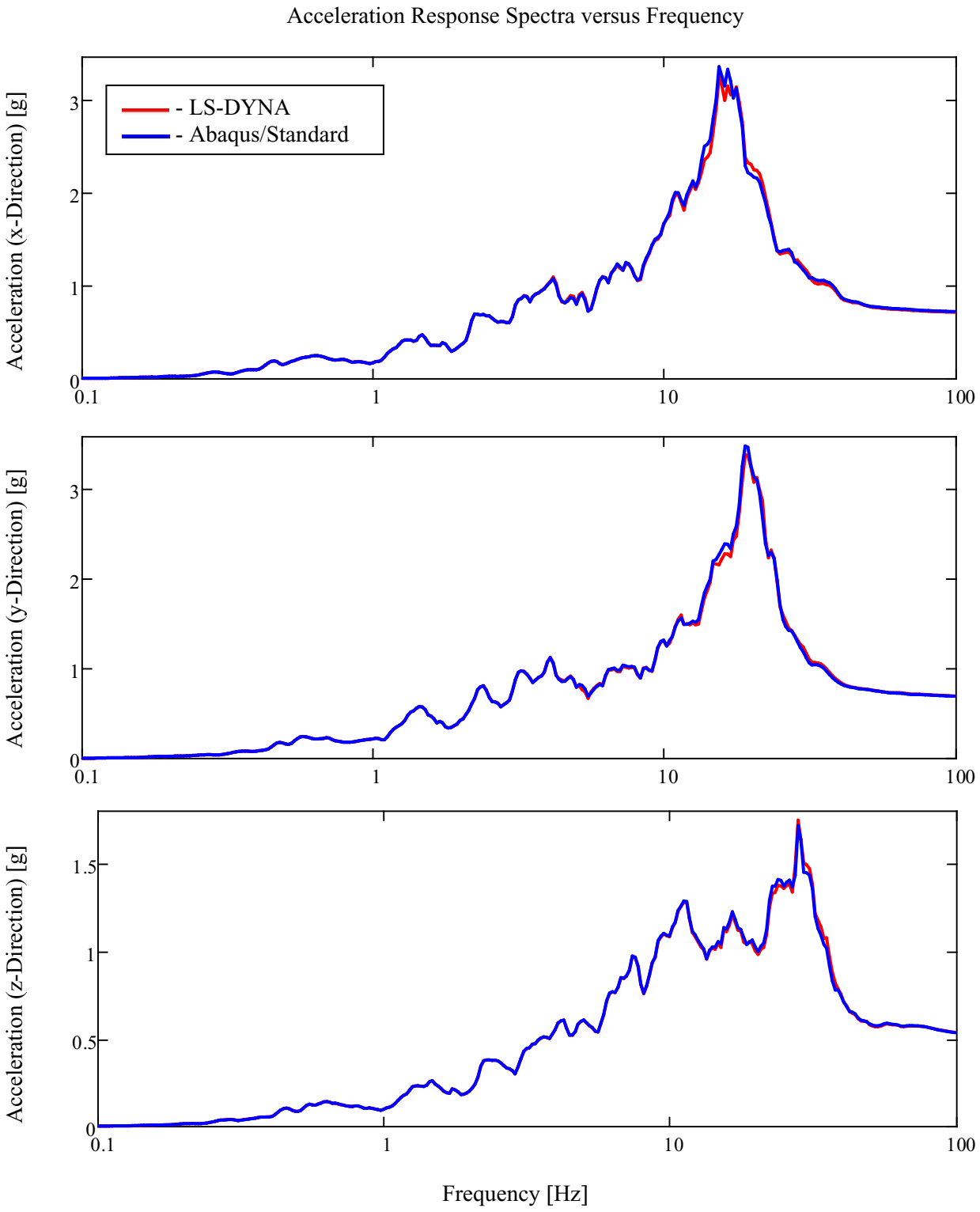

Figure 4.3-2. Node 10 acceleration response spectra from Abaqus/Standard and LS-DYNA.

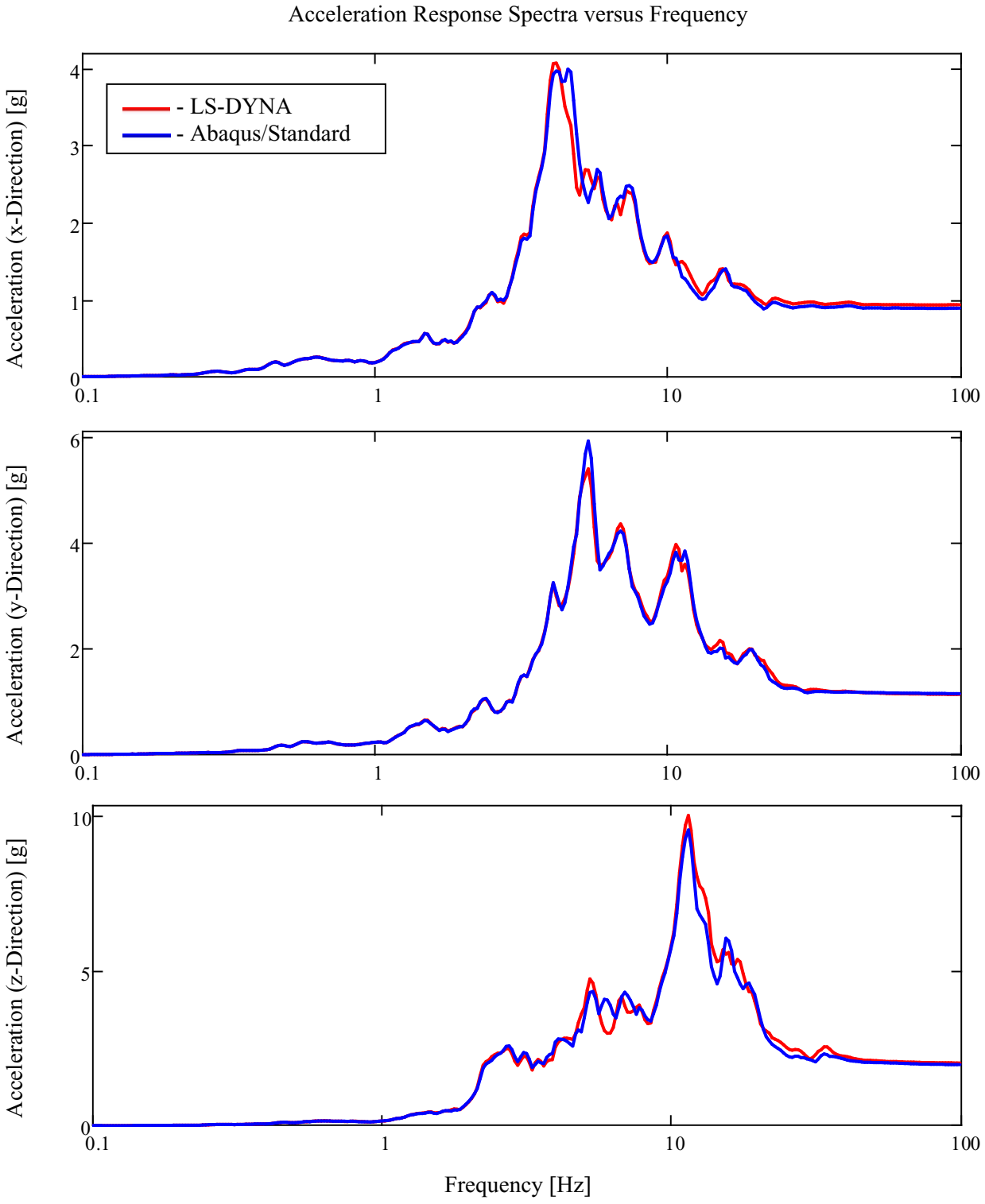

Figure 4.3-4. Node 11 acceleration response spectra from Abaqus/Standard and LS-DYNA.

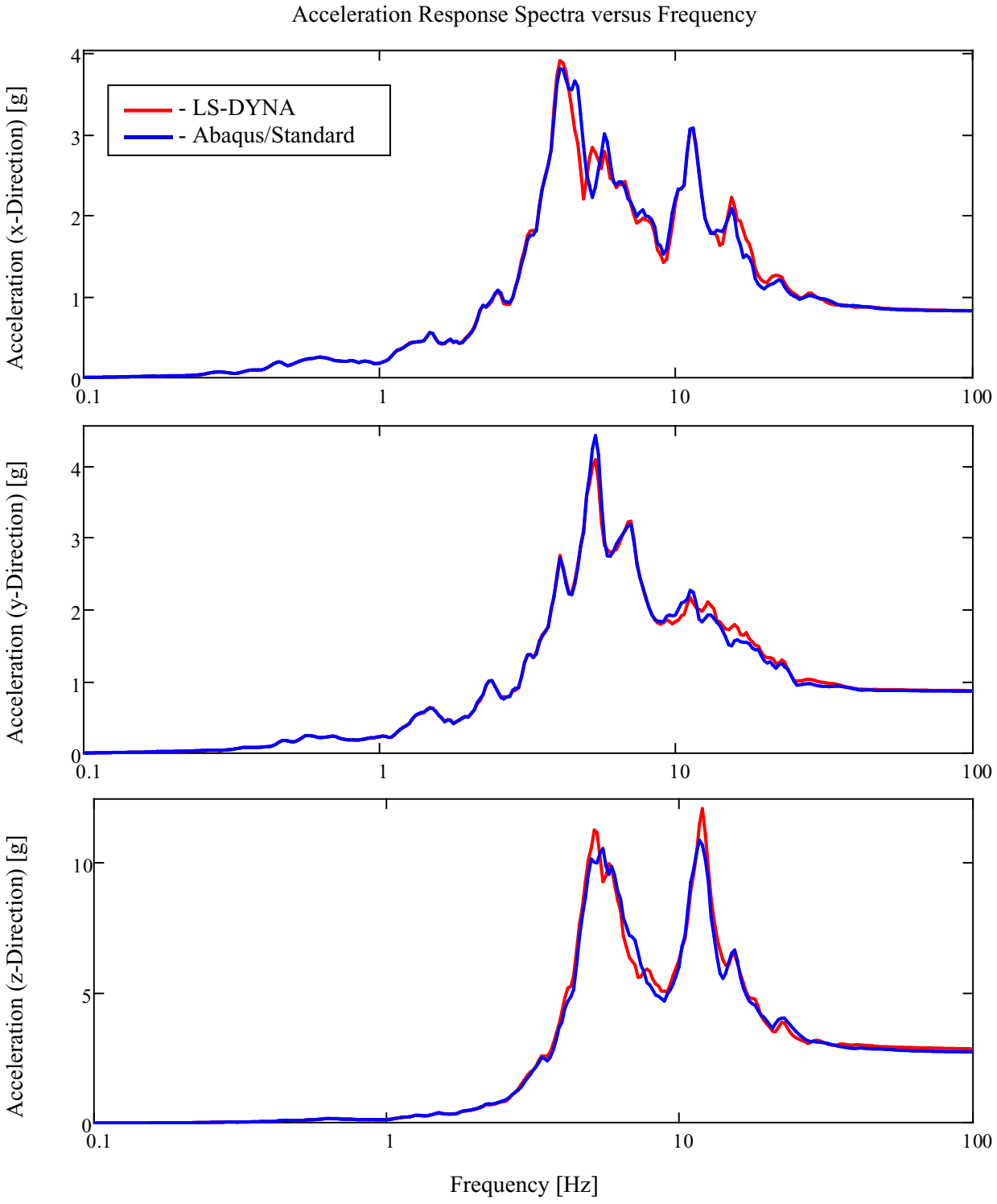

Figure 4.3-5. Node 23 acceleration response spectra from Abaqus/Standard and LS-DYNA.

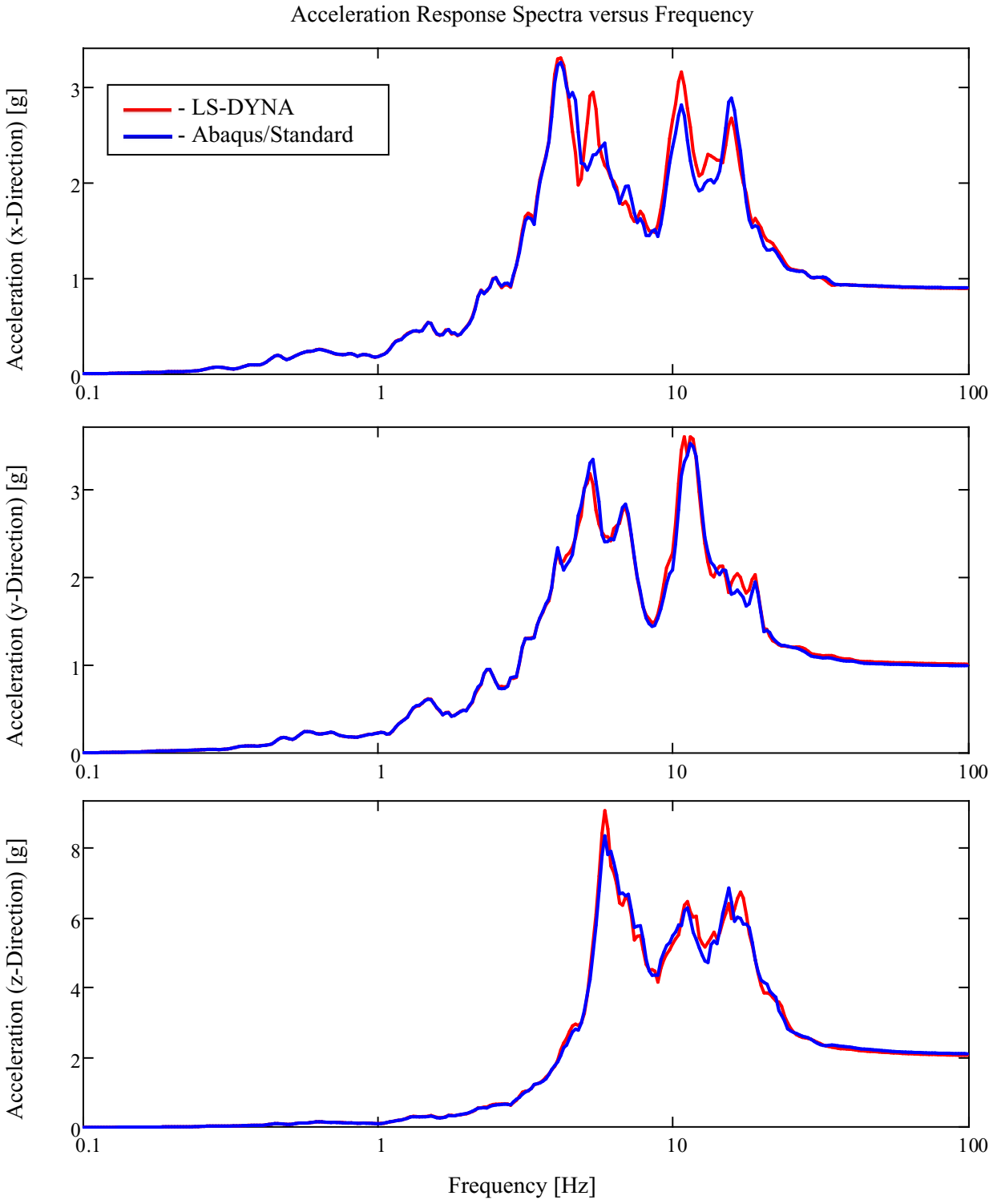

Figure 4.3-6. Node 24 acceleration response spectra from Abaqus/Standard and LS-DYNA.

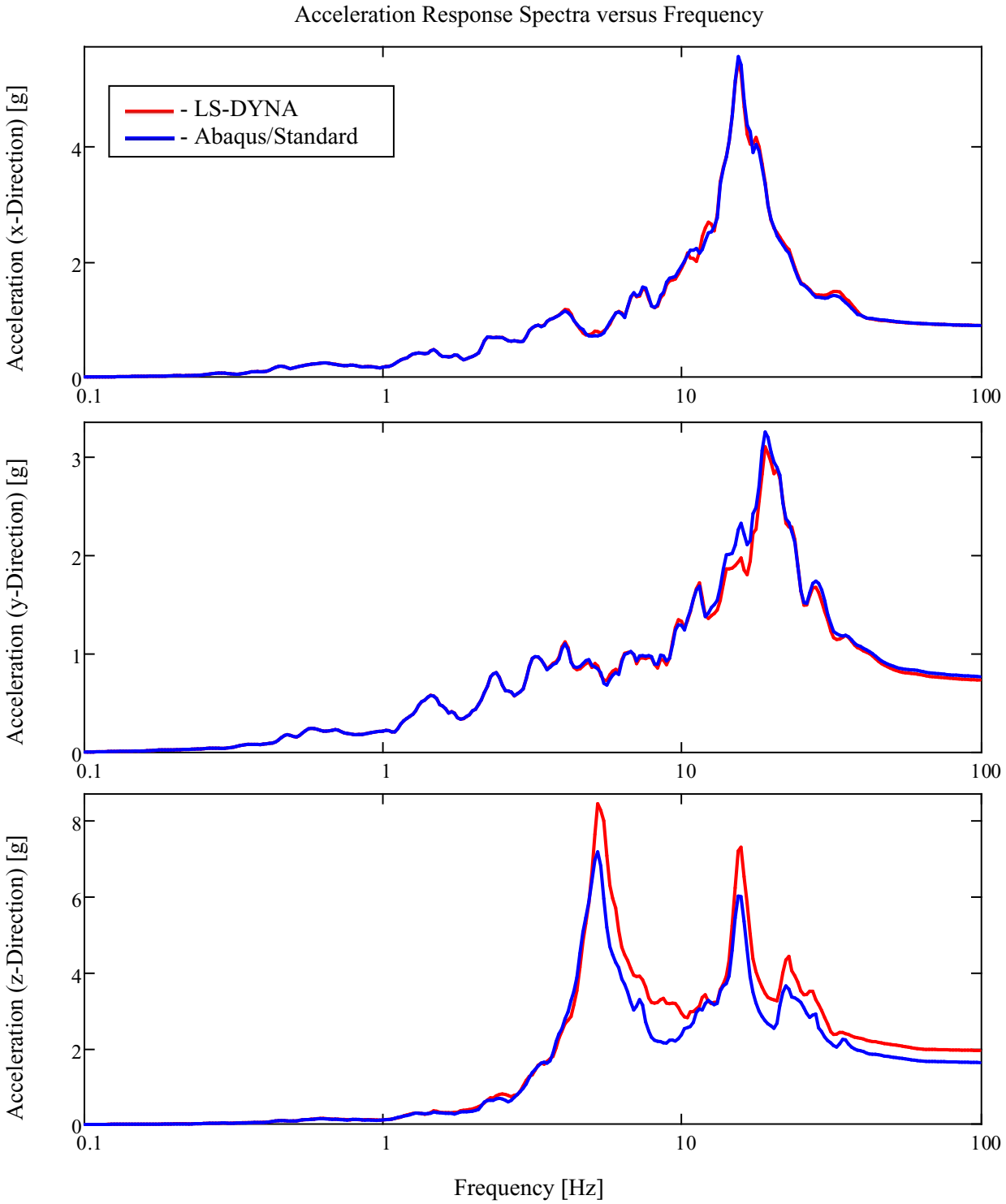

Figure 4.3-7. Node 25 acceleration response spectra from Abaqus/Standard and LS-DYNA.

5. Nonlinear Soil-Structure Interaction

The NLSSI model runs discussed in this section are performed with LS-DYNA using the structure described in Section 4.1 and the soil column down to 486•ft described in Appendix B. The meshes are described in Section 5.1, the contact modeling is described in Section 5.2, and model results are discussed in Sections 5.3.

5.1 NLSSI Model Mesh

Two NLSSI model meshes are generated for this study. Both model meshes use the same nonlinear soil and linear structure meshes (shown in Figures 5.1-1 to 5.1-3) but they differ in how the soil-structure interaction occurs. The first mesh is modeled with the structure constrained to the soil. This is referred to as the equivalent linear model due to the structure pushing and pulling on the soil (similar to SASSI). The second mesh is modeled with additional mesh (discussed in Section 5.2) between the structure and soil to mimic frictional contact with a coefficient of friction of 0.5. This is referred to as the nonlinear model as the structure can only push on the soil and not pull.

The soil mesh dimensions are shown in Figure 5.1-1. The depth is selected in an attempt to capture half space stiffness. The actual value for the depth was select by going to the bottom of the soil layer that occurred at the width of the building (384 ft) below the primary depth of the building (71.75 ft). This resulted in nonlinear soil being modeled to a depth of 486 ft. The horizontal dimensions of the model are more than twice the horizontal dimensions of the structure in an attempt to get the boundaries a significant distance from the structure.

Similar to the soil column described in Appendix B, the boundary conditions for the NLSSI models include non-reflective boundary conditions at the base, free boundary conditions at the top, and seismic load time histories applied to the top surface of the elastic bottom layer. The meshes for the different soil layers do not align so the layers are tied together with a constraint type definition (as opposed to a penalty type definition). (Note: Penalty contact is not desirable for this application because the interface spring could erroneously respond to the seismic input.) The tied contact is used because it is simple to define and should allow local waves to correctly pass or reflect.

As discussed in Appendix B, additional constraints are added to the side boundaries to mimic an infinite soil continuum. These constraints cause each set of nodes on the boundary at a given elevation (that form a "ring" around the model) to move horizontally and vertically together. This allows the shear and compressive plane waves to pass up through the model unimpeded while providing the support that would be received from neighboring elements in an infinite soil continuum. However, this causes horizontally propagating waves from the structure to be reflected back into the model rather than letting them pass out of the model. This is why the horizontal boundaries of the soil model need to be significantly distant from the structure. The horizontal boundaries of the soil model also need to be significantly distant from the structure to capture the correct static stiffness of the soil.

The soil meshing strategy is intended to produce accurate results while minimize computation time. Consequently, element sizes are closely managed. In an attempt to bring high frequency input into the base of the structure; soil elements below 71.75 ft are meshed with a height to pass up to 50 Hz vertical shear waves with at least 10 elements per wavelength. Mesh density of the soil elements beside the building (above 71.75 ft) is meshed with a height to pass up to 30 Hz vertical shear waves with at least 10 elements per wavelength. Considering the cumulative effective mass plots (shown in Figure 4.2-1), a large portion of the horizontal structural response occurs below 15 Hz. Consequently, the horizontal mesh density for all soil elements is meshed with a width to pass up to 15 Hz horizontal shear waves with at least 10 elements per wavelength. (Note: Compressive waves have a higher speed of sound which makes higher frequency wave passage possible in all directions with at least 10 elements per wavelength.)

The structure meshing strategy is also intended to produce accurate results while minimize computation time. The structural elements need to vary in size to accurately model the structure but an attempt is made to have them so that they require a similar time step to that of the soil (preferably requiring a slightly higher time step that the soil so that the soil primarily drives the time step).

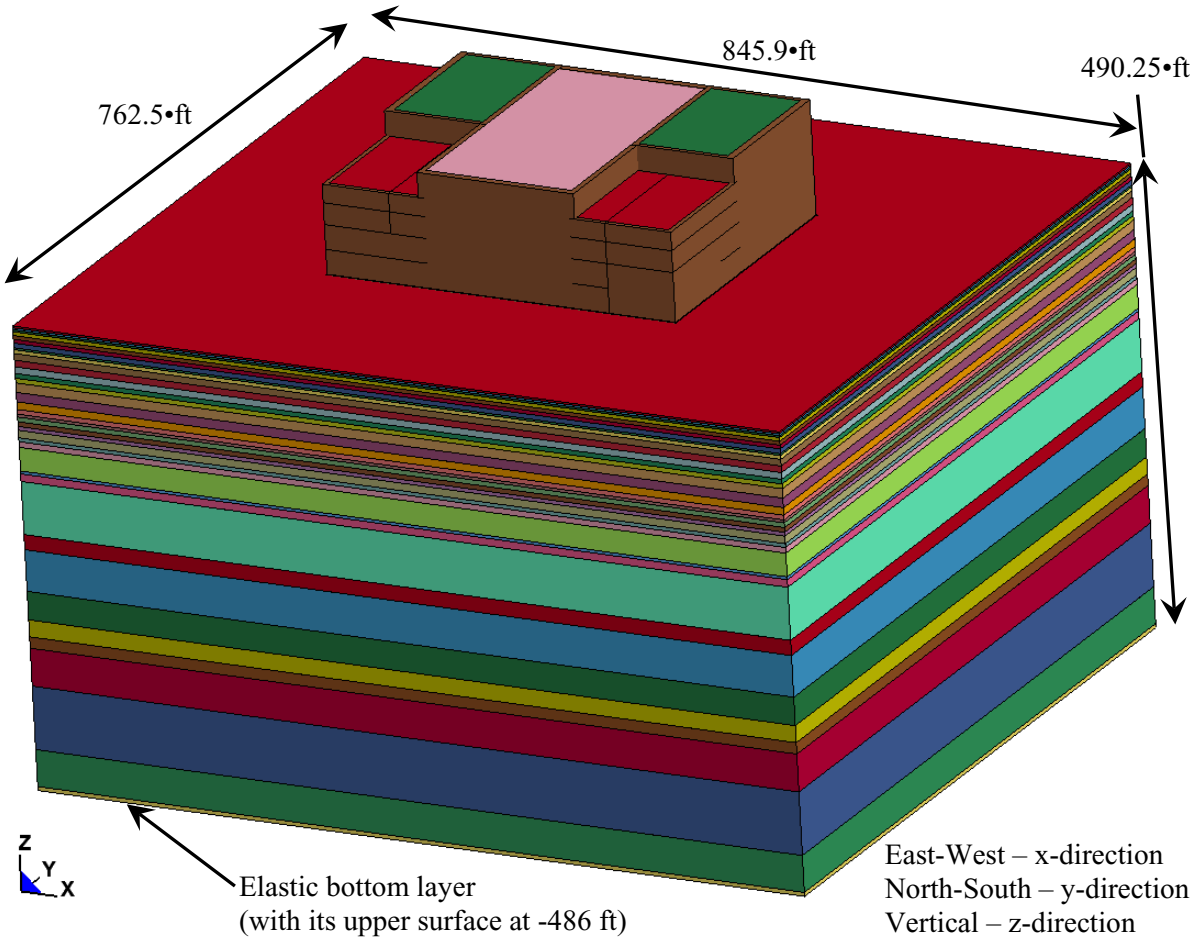

Figure 5.1-1. NLSSI finite element mesh.

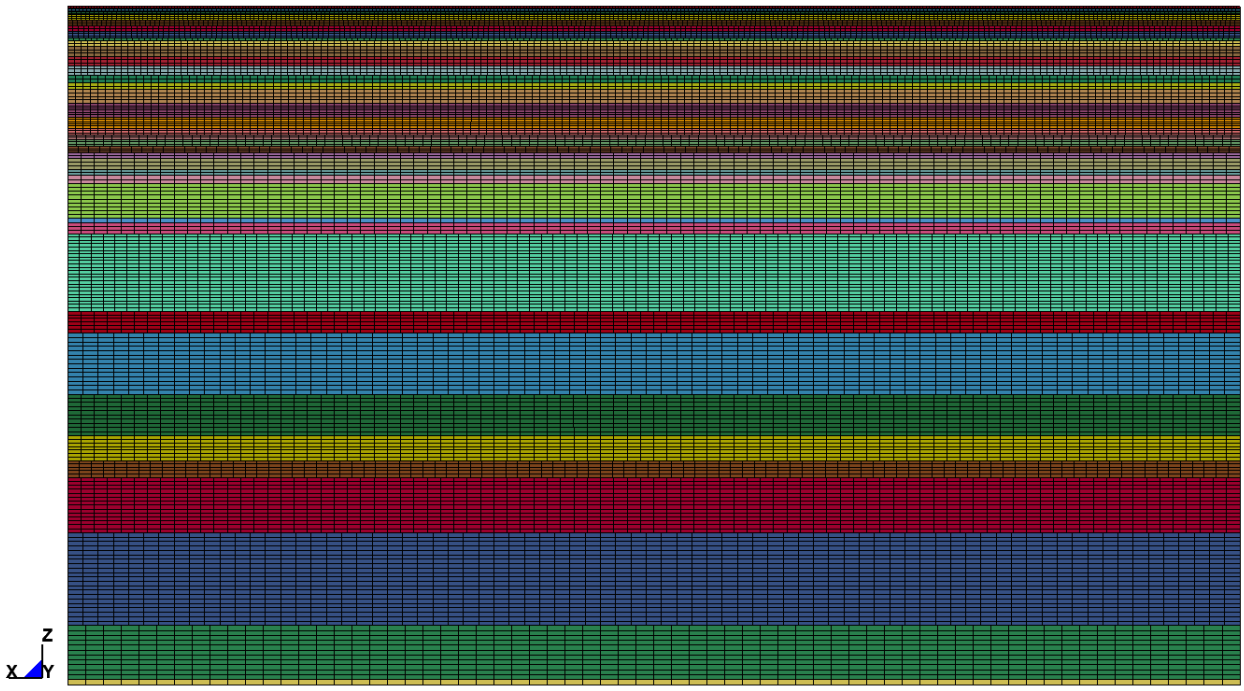

Figure 5.1-2. Soil mesh.

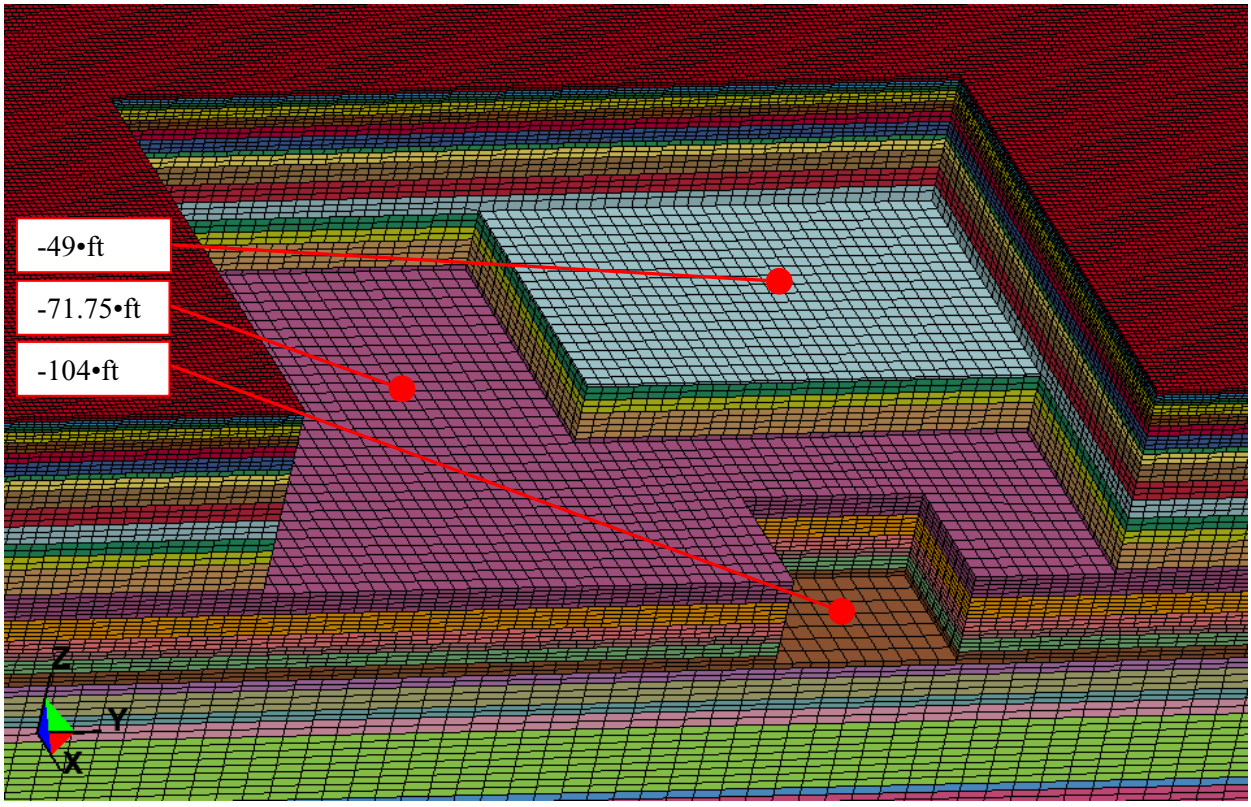

Figure 5.1-3. Soil mesh cut-away showing the area where soil has been removed for the structure.

5.2 Contact Modeling

Because of the contact chatter that occurs with penalty contact algorithms in the soil-structure interaction, contact is modeled using finite elements with a constitutive model that mimics frictional contact (with a coefficient of friction of 0.5). The mesh (shown in Figure 5.2-1) is constrained to the structure and continuous with the soil and it is a foot thick. The constitutive model for the mesh is defined for elastic/perfectly plastic behavior which varies with hydrostatic pressure (mean effective stress). Single element model tests were performed to establish the adequacy of the approach. The testing showed that having a Poisson's ratio near 0.5 produces the closest match to frictional sliding when different compression loads are used with the same initial conditions. To ensure that the elements are stable, a Poisson's ratio of less than 0.5 is necessary. Using the surface (softest) soil shear modulus and ensuring that the bulk modulus is less than or equal to the concrete, a Poisson's ratio of 0.494 can be used. Test models for the range of compressive loads likely in the model runs showed that the maximum error (using a Poisson's ratio of 0.494) was less than 0.5%.

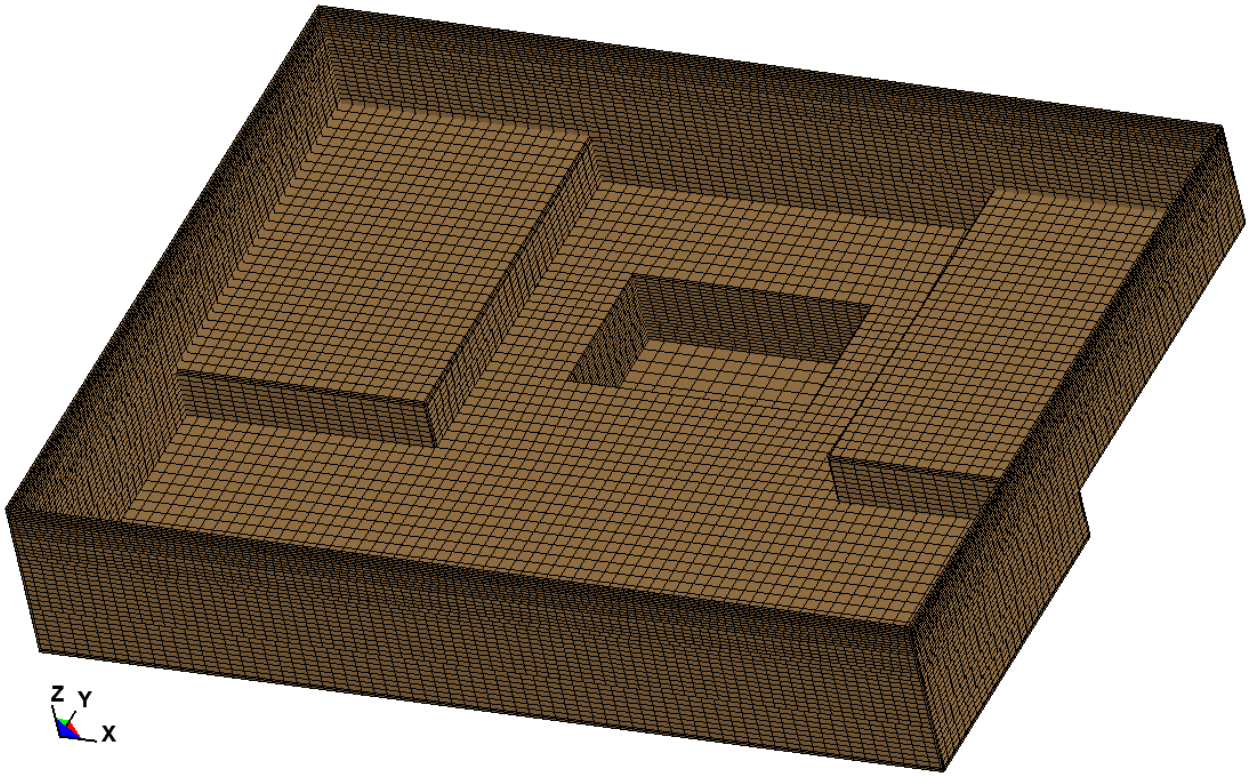

Figure 5.2-1. Contact mesh.

As an example of the contact chatter that occurs with penalty contact, the following scoping calculation results (shown in Figure 5.2-2) were produced. These are 1.0•DBE, x-direction acceleration time history results for node 6 on the structure (identified in Figure 4.1-6). The penalty contact is defined with "*CONTACT_AUTOMATIC_SURFACE_TO_SURFACE_ID" and has parameter definitions of "VDC=50", "SOFT=2", and "SBOPT=5". This definition is intended to accommodate contact between materials of dissimilar stiffness and/or dissimilar mesh densities and a very high (50%) viscous damping is used.

For comparison to the penalty contact results, results from a model run with the contact mesh (shown in Figure 5.2-1) and results from a model run with constraints between the soil and structure are shown. Only the first four seconds of the model run are shown. During this time frame, impact or sliding should not occur due to the low seismic accelerations and due to node 6 being on the deepest portion of the structure. Consequently, all three sets of results should produce the same plot.

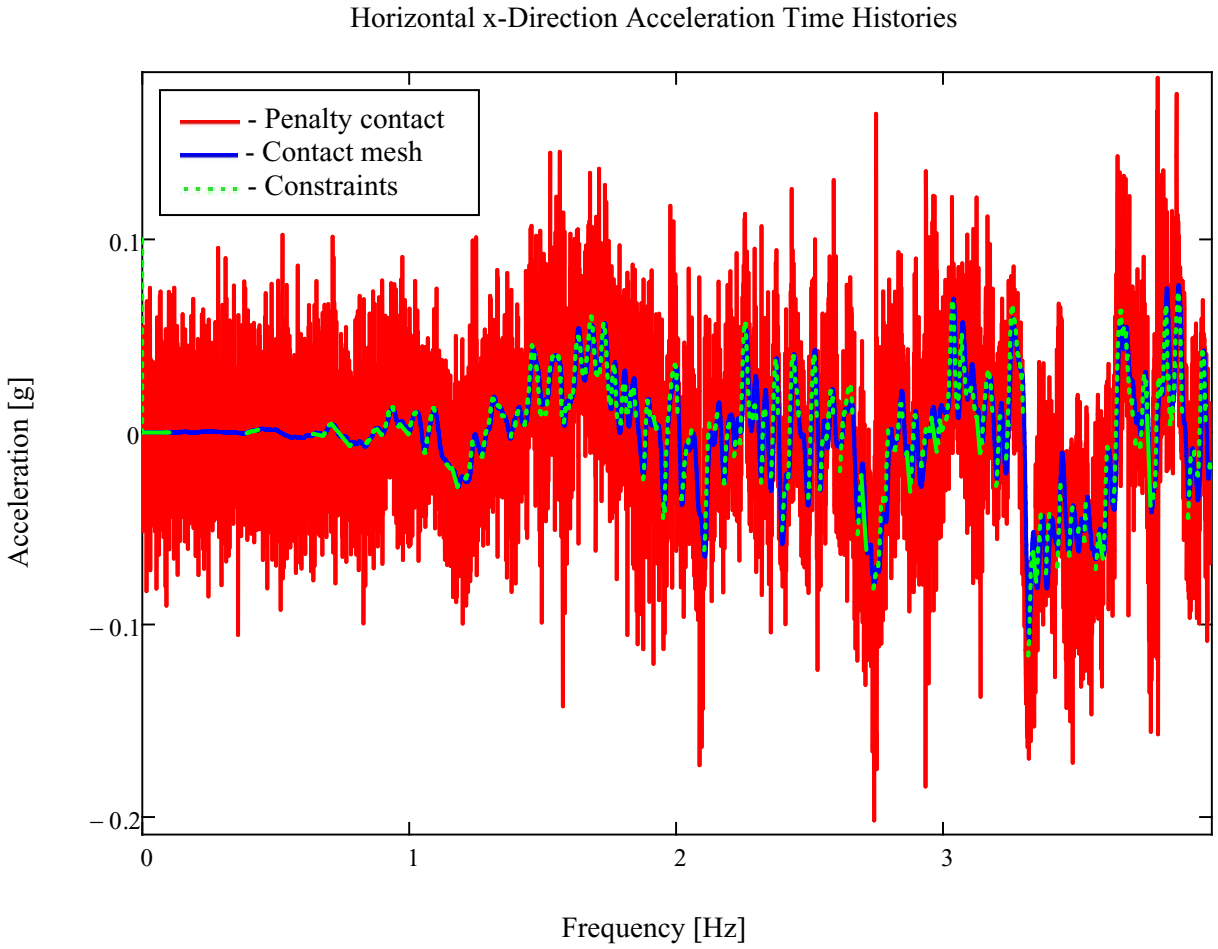

Figure 5.2-2. Node 6, x-direction acceleration time history comparison between.

As can be seen in Figure 5.2-2, the penalty contact results for this example have significant chatter even with high damping. The contact mesh results have negligible chatter and agree well with the constrained results which can be expected. This is why the contact mesh approach is used for this study.

5.3 Soil Response

To study soil response, output acceleration time histories were gathered at points in the soil from the NLSSI model (shown in Figure 5.3-1 with the points identified in Table 5.3-1) and a soil column model (shown in Figure 5.3-2 with the points identified in Table 5.3-2). Both models are run with a 1.0•DBE seismic input and the NLSSI model is performed with the structure constrained to the soil. The soil column uses the nonlinear soil mesh described in Appendix B down to 486 ft. It then uses the same

elastic element and boundary conditions as the NLSSI model. In the absence of the structure, the two models should produce equivalent output at a given depth. However, differences in high frequency seismic waves can be expected. This is because the NLSSI model is meshed to only pass up to 30 Hz vertically traveling shear waves above 71.75 ft with at least 10 elements per wavelength. Below 71.75 ft it is meshed to pass up to 50 Hz vertically traveling shear waves with at least 10 elements per wavelength. The soil column model is meshed to pass up to 67 Hz vertically traveling shear waves with at least 10 elements per wavelength in all of the mesh.

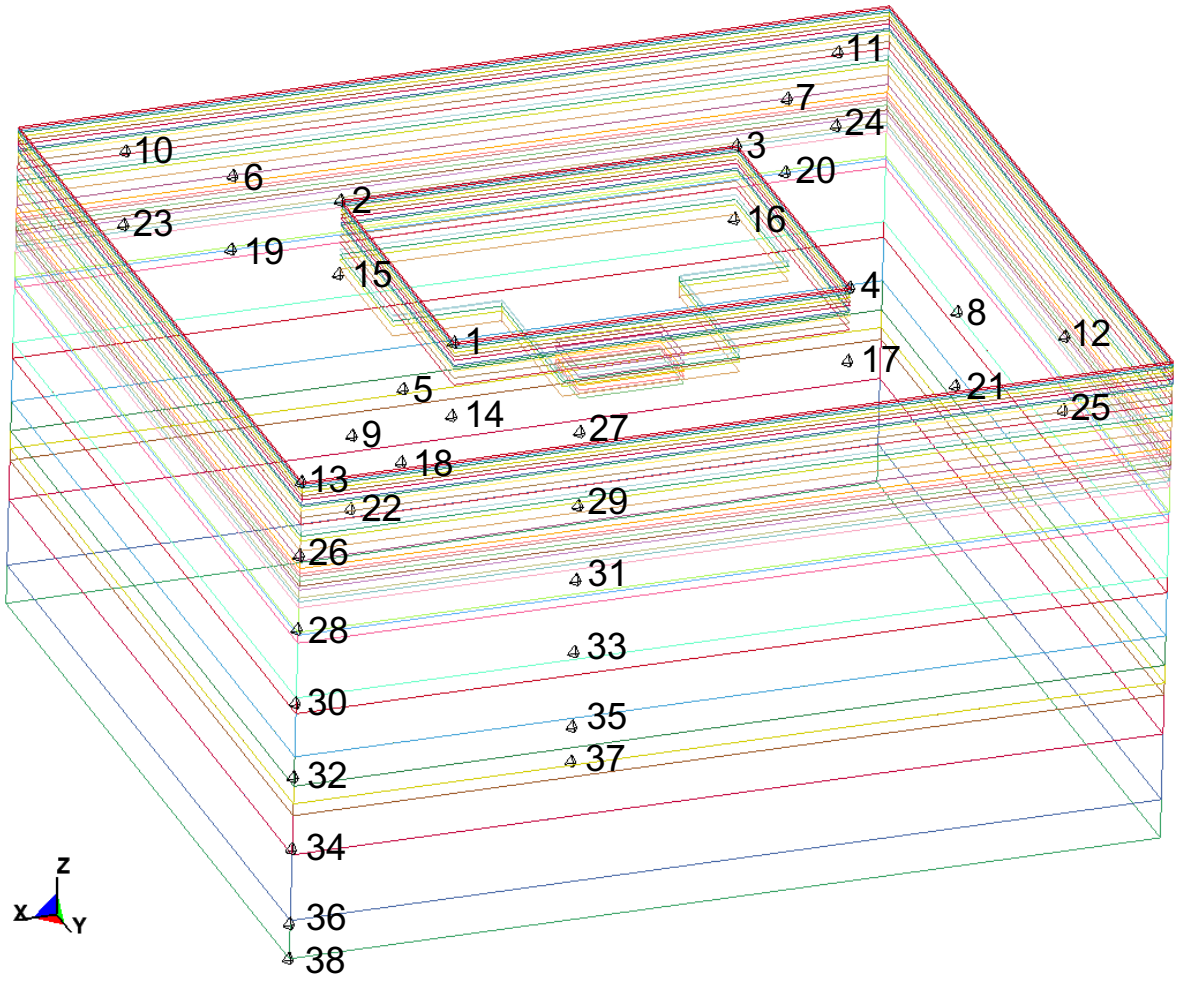

Figure 5.3-1. NLSSI soil model output points. (Points are identified with a number.)

Table 5.3-1. Figure 5.3-1 output point definitions.

Points	Nodes	Coordinates			Points	Nodes	Coordinates		
		x	y	z			x	y	z
1	35922	192.3	152.5	0.0	20	2011012	-269.2	-228.8	-75.0
2	22587	192.3	-152.5	0.0	21	2003997	-269.2	228.8	-75.0
3	64312	-192.3	-152.5	0.0	22	2055824	346.1	305.0	-75.0
4	77542	-192.3	152.5	0.0	23	2045871	346.1	-305.0	-75.0
5	37216	269.2	228.8	0.0	24	2035012	-346.1	-305.0	-75.0
6	33401	269.2	-228.8	0.0	25	2066894	-346.1	305.0	-75.0
7	73802	-269.2	-228.8	0.0	26	2105608	422.9	381.3	-75.0
8	77686	-269.2	228.8	0.0	27	2588303	38.5	76.3	-150.2
9	127964	346.1	305.0	0.0	28	2644206	422.9	381.3	-150.2
10	213818	346.1	-305.0	0.0	29	2913513	38.5	76.3	-225.3
11	183150	-346.1	-305.0	0.0	30	2947901	422.9	381.3	-225.3
12	157305	-346.1	305.0	0.0	31	3057518	38.5	76.3	-301.0
13	282710	423.0	381.3	0.0	32	3118949	422.9	381.3	-301.0
14	1976225	192.3	152.5	-75.0	33	3242933	38.5	76.3	-374.3
15	1983992	192.3	-152.5	-75.1	34	3320261	422.9	381.3	-374.3
16	2010964	-192.3	-152.5	-75.1	35	3466457	38.5	76.3	-450.5
17	2001940	-192.3	152.5	-75.0	36	3501707	422.9	381.3	-450.5
18	1976979	269.2	228.8	-75.0	37	3466467	38.5	76.3	-486.0
19	1984216	269.2	-228.8	-75.0	38	3501717	422.9	381.3	-486.0

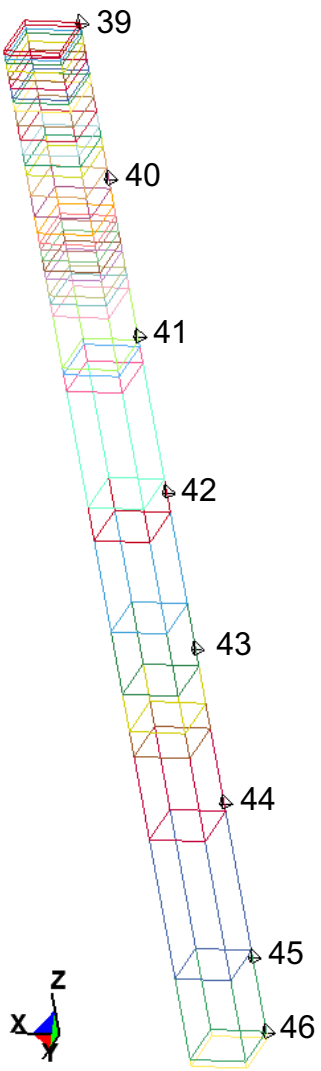

Figure 5.3-2. Soil column output points. (Points are identified with a number.)

Table 5.3-2. Figure 5.3-2 output point definitions.

Points	Nodes	Coordinates		
		x	y	z
39	1	0.0	0.0	0.0
40	309	0.0	0.0	-75.0
41	493	0.0	0.0	-150.9
42	657	0.0	0.0	-226.0
43	793	0.0	0.0	-301.4
44	937	0.0	0.0	-375.6
45	1061	0.0	0.0	-449.8
46	1113	0.0	0.0	-486.0

The output response spectra for the studied points in the soil are shown in Figures 5.3-3 to 5.3-9. In the plots, "Pt" indicates "point," "Av" indicates "the average of the listed points," "EW" indicates "East-West (or x-) direction," "NS" indicates "North-South (or y-) direction," and "V" indicates "vertical (or z-) direction."

Figures 5.3-3 and 5.3-4 show acceleration response spectra at specific points on the soil surface. Points 1 – 12 are points in the soil radiating outward from the structure. Points 13 and 39 are points on the constrained boundary condition of the NLSSI and soil column models respectively. Being on the constrained boundary condition indicates that the output for these nodes represents the output for all of the nodes at the given elevation that are constrained to move together. Figure 5.3-3 shows how much scatter occurs in points in the soil at the same distance from the structure but in a different direction. Some scatter can be expected due to local waves that have reflected from the structure. Figure 5.3-4 provides a comparison of how the response changes with distance from the structure. Soil column results are also compared (which would represent not having a structure). The plot shows that there is a significant reduction in response at the points nearest the structure as compared to the soil column response. Moving outward, the second set of points show response peaks with a significant increase relative to the soil column response. Further outward, the response becomes similar to that of the soil column. This is a good indication that the boundary conditions have been placed far enough away to produce accurate results. (There is high frequency response that is more significant in the soil column than the NLSSI model. This is related to the NLSSI shallow soil being sized to only pass up to 30 Hz waves efficiently.)

Figures 5.3-5 and 5.3-6 show acceleration response spectra at specific points at a soil depth of 75 ft. Points 14 – 25 are points in the soil radiating outward from the structure. Points 26 and 40 are points on the constrained boundary condition of the NLSSI and soil column models respectively. Figure 5.3-5 shows how much scatter occurs in points in the soil at the same distance from the structure but in a different direction. Figure 5.3-6 provides a comparison of how the response changes with distance from the structure. Soil column results are also compared (which would represent not having a structure). The plot shows a similar yet less dramatic trend as seen in the response spectra at the soil surface. One outlier is the high peak at 11 Hz for the average of points 22, 23, 24, and 25 in the vertical response. Because this shows up in all four points, it doesn't appear to be an anomaly. This could be related to being near the change from 50 Hz mesh to 30 Hz mesh. It could also be an indicator that the boundary conditions should be further away. However, points 26 and 40 have pretty good agreement which tends to indicate that the boundary conditions have been place far enough away to produce accurate results.

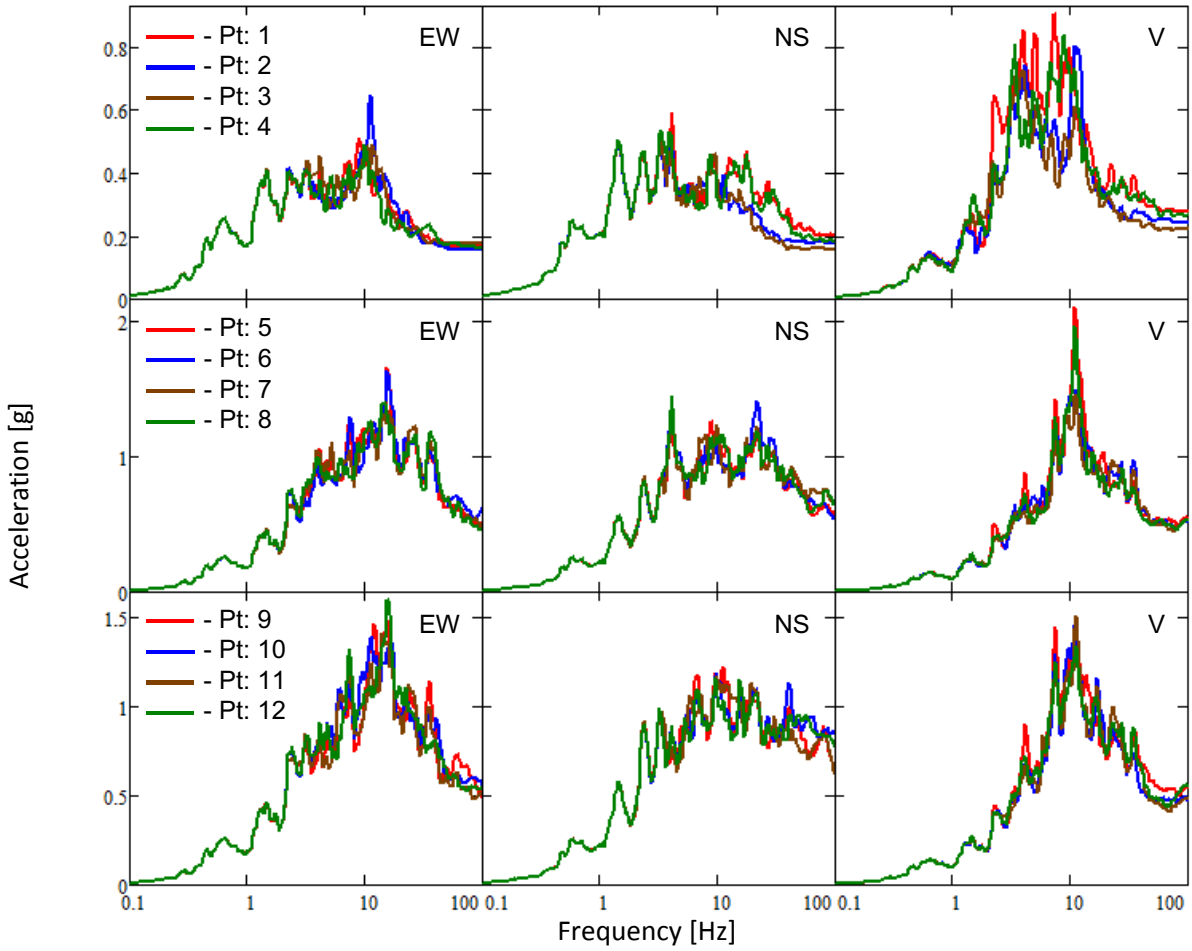

Figure 5.3-3. Soil surface acceleration response spectra (5% Damped) at specific points.

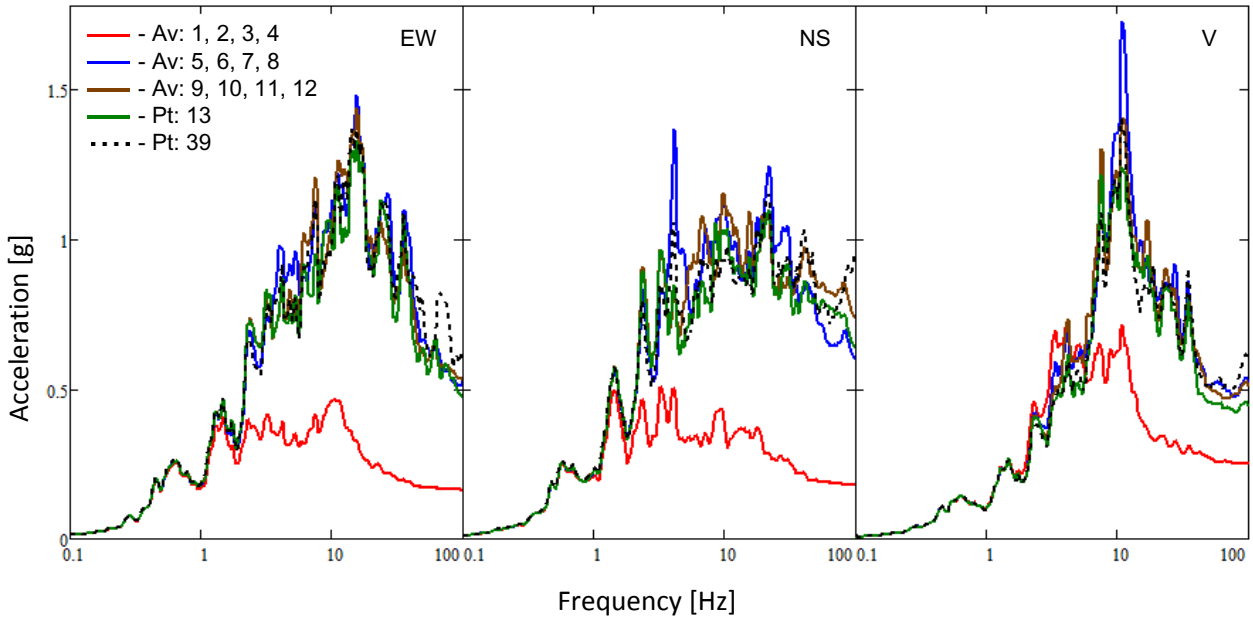

Figure 5.3-4. Soil surface acceleration response spectra (5% Damped) comparison.

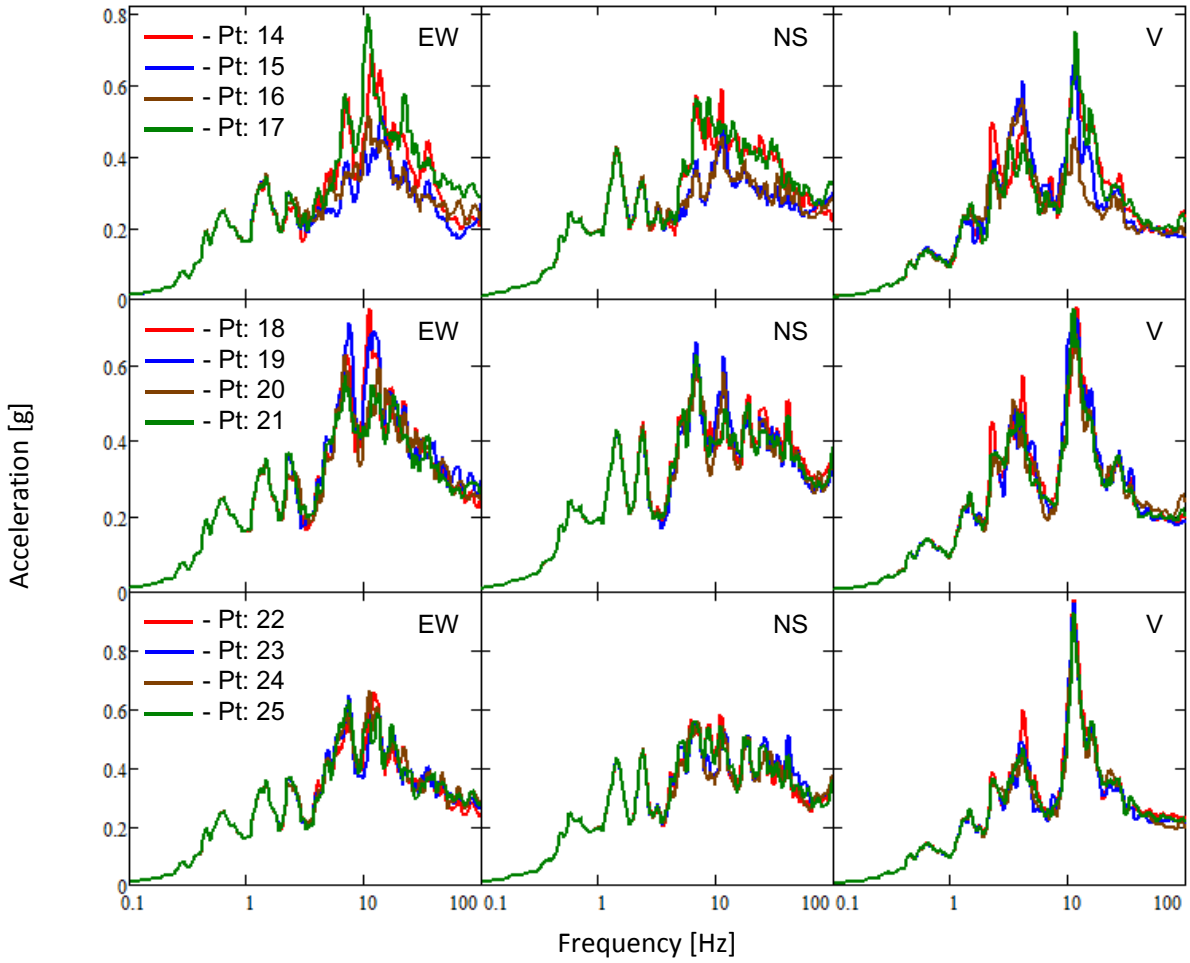

Figure 5.3-5. Acceleration response spectra at a depth of 75 ft (5% Damped) for specific points.

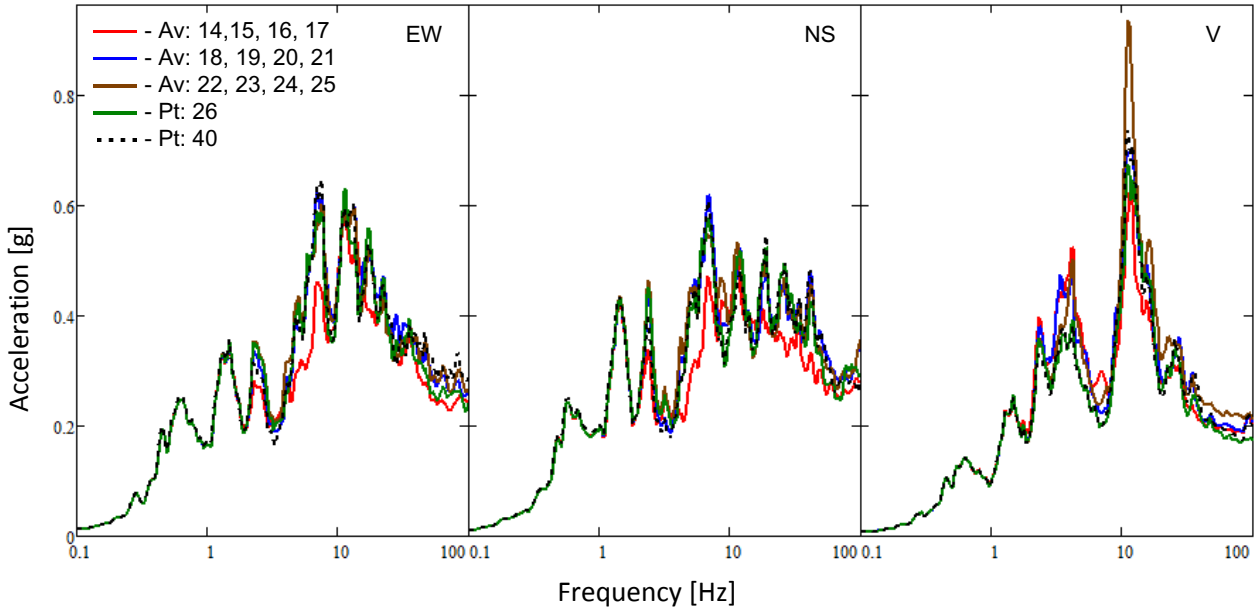

Figure 5.3-6. Acceleration response spectra at a depth of 75 ft (5% Damped) comparison.

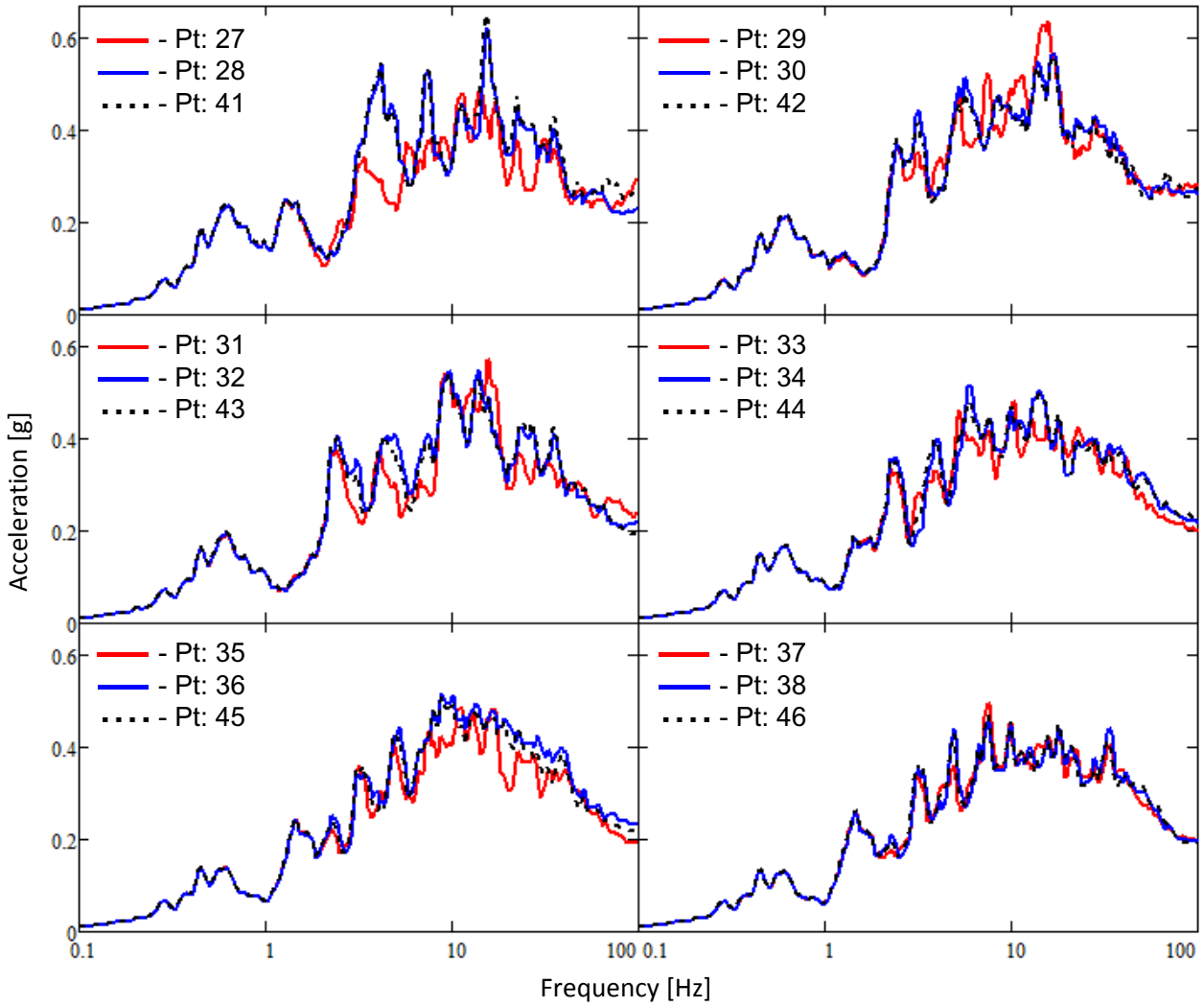

Figure 5.3-7. East-West acceleration response spectra (5% Damped) for selected points below 75 ft.

Figures 5.3-7 to 5.3-9 show the acceleration response spectra for a point under the reactor area of the structure, a point on the constrained boundary, and an equivalent point in the soil column. The output is at approximately 75 ft intervals except the last interval which occurs at the bottom of the nonlinear soil. The response spectra for the points on the constrained boundary and soil column compare very well. Also, as can be expected, the points under the reactor differ significantly from those on the constrained boundary near the structure. But, the difference reduces to an insignificant amount at the bottom of the soil column. These results tend to indicate that the model is adequately sized and it should be producing accurate results.

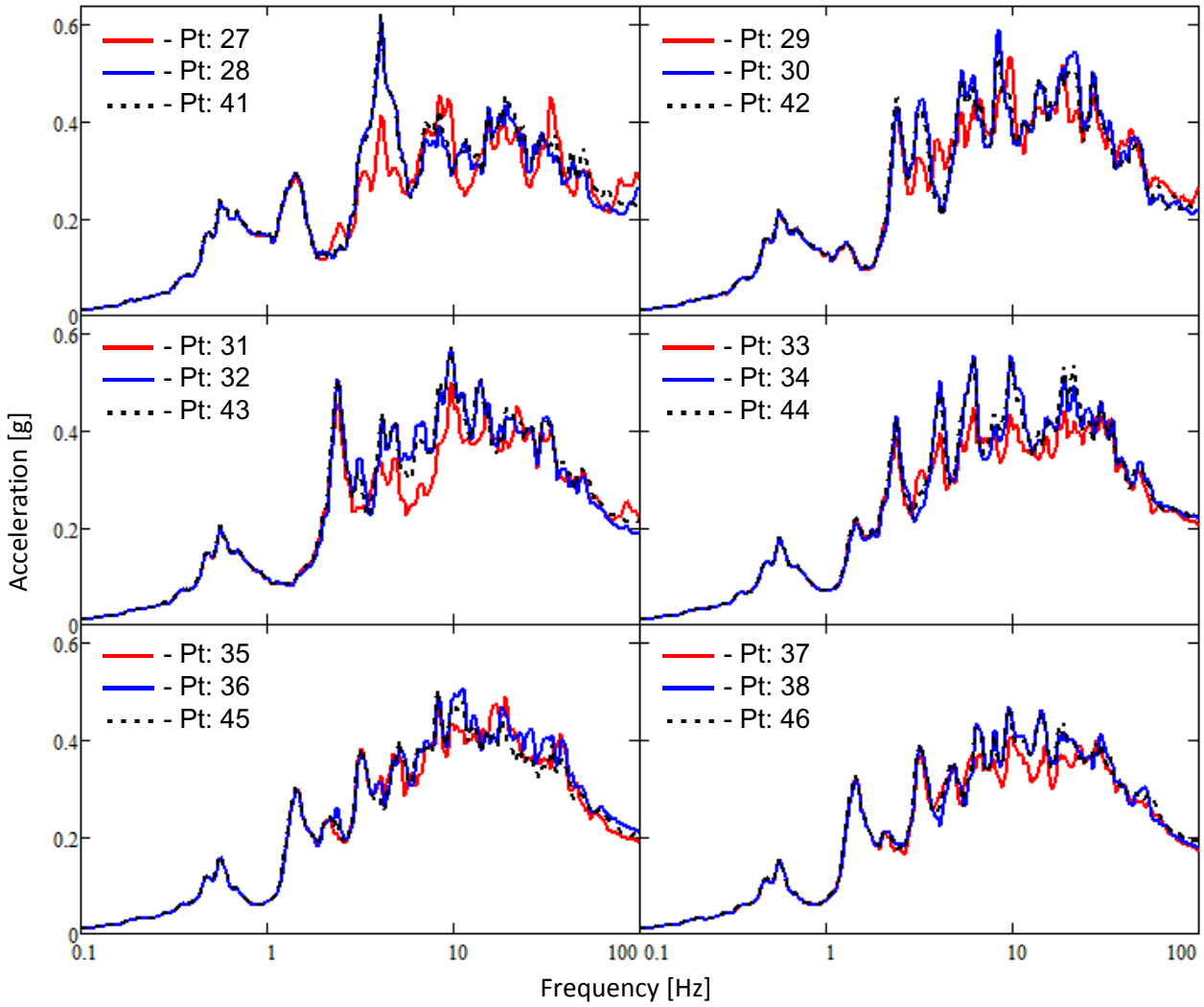

Figure 5.3-8. North-South acceleration response spectra (5% Damped) for selected points below 75 ft.

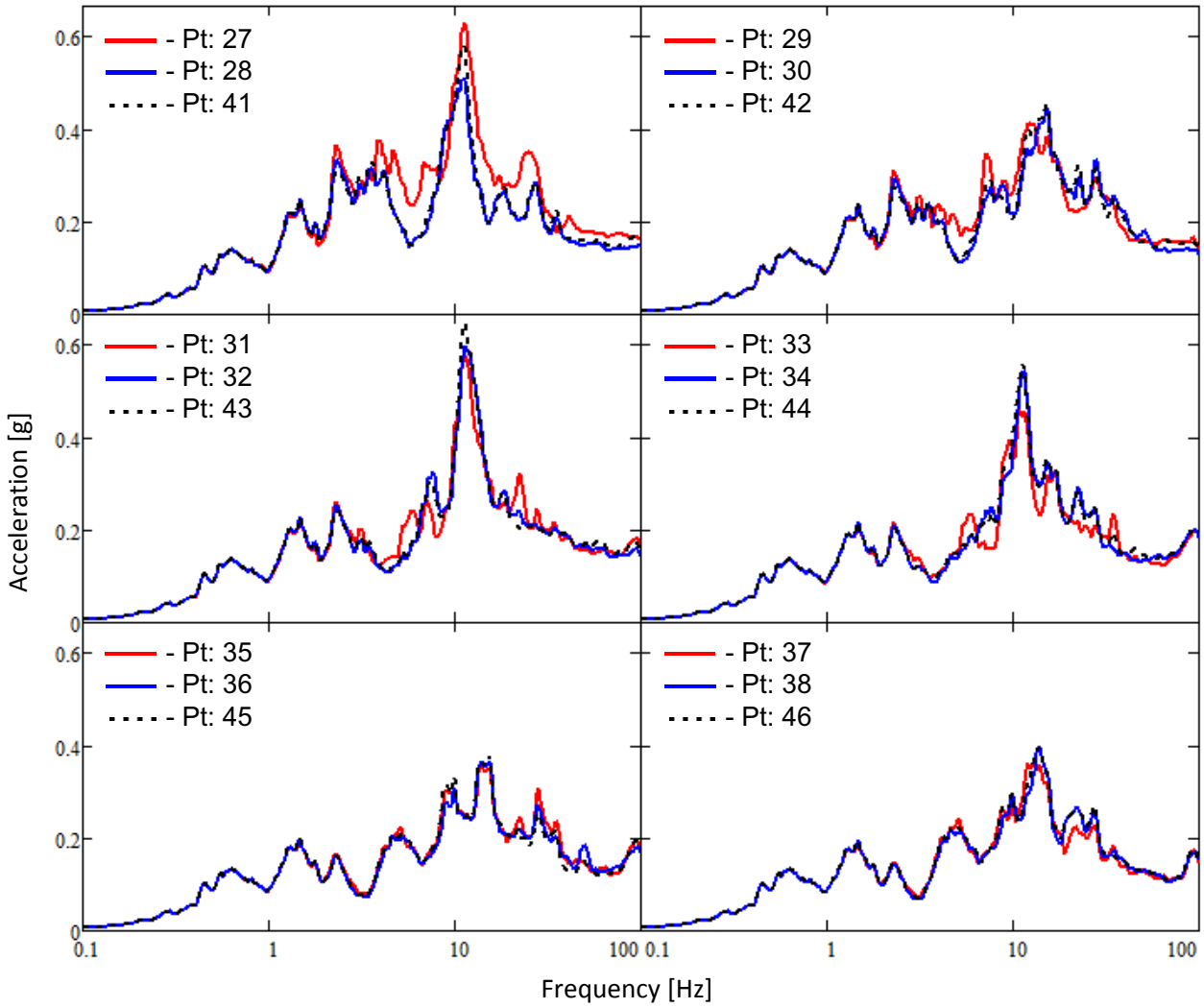

Figure 5.3-9. Vertical acceleration response spectra (5% Damped) for selected points below 75 ft.

6. NLSSI Compared with SASSI

6.1 Overview

The NLSSI model runs discussed in this section (one with the structure constrained to the soil and one with the structure in contact with the soil) are performed with LS-DYNA using the NLSSI model (shown in Figure 5.1-1). The linear SSI model runs discussed in this section are performed with SASSI. The SASSI model is generated in part by converting the Abaqus/Standard version of the structural model into a form that can be read into SASSI (shown in Section 4.1). The soil model used in SASSI is discussed in Cuesta et al. (2016). The SASSI analysis follows the standard method currently used for SSI evaluation.

When comparing results between the NLSSI and linear SSI, there are important model differences that must be considered. Further study is important to quantify these differences. Below are some of these differences and a brief discussion of each:

- The input soil material properties do not exactly match for the nonlinear and linear models (as shown in Section B.1 of Appendix B). The current nonlinear soil constitutive model accepts a nonlinear stress versus strain curve. This is not sufficient to be exactly equivalent to the Vogtle site G/Gmax and damping ratio curves. Consequently, the NLSSI stress versus strain curves were defined to minimize the error. Because the linear SSI analysis was following the standard method for SSI evaluation, the Vogtle site G/Gmax and damping ratio curves were used. While this did not produce an obvious error in the soil column results, less difference between the NLSSI and linear SSI results could be expected if equivalent material properties were used.
- The vertical (pressure wave) damping is different between the NLSSI and linear SSI. In the NLSSI, the damping occurs relative to shearing and not hydrostatic pressure. Since pressure waves have shearing and hydrostatic components, the effective damping is reduced. Because the linear SSI analysis was following the standard method for SSI evaluation, the vertical damping ratio was set the same as the horizontal damping ratio. This results in the NLSSI having an expected higher vertical response than the linear SSI.
- Linear SSI with SASSI is performed by running models for each of the three directions separately and then doing a square-root-sum-of-the-squares combination to combine results. This is not expected to be a large source of error. But, a more detailed study could be performed by running NLSSI models one direction at a time and comparing the results individually. A more detailed study could also be performed by generating acceleration time histories in SASSI and combining the time histories on a step-by-step basis.
- The material properties used in the linear SSI models are degraded for only one horizontal direction (which is a technique that follows the standard method currently used for SSI evaluation). Given the similarity of the shearing in the two horizontal directions, this is expected to give a reasonable approximation horizontally. Scoping evaluation in the vertical direction indicated that better agreement between NLSSI and linear SSI may be possible by degrading the vertical material properties separately. The current process results in the NLSSI having higher vertical response relative to the linear SSI. More study is necessary to determine if degrading the vertical material properties should be done in linear SSI or if the NLSSI constitutive model should be modified to reduce the vertical response.
- The SSI models are not set up to pass all of the high frequency waves through the soil and yet the response spectra are given at frequencies up to a 100 Hz. The NLSSI soil model is set up to pass

50 Hz waves with 10 elements per wave length below 71.75 ft depth (which provides input to most of the structure's base) and 30 Hz waves with 10 elements per wave length above 71.75 ft depth. As discussed on p. 16 in Cuesta et al. (2016), the SASSI soil mesh near the surface has a 15 Hz cutoff frequency, the soil mesh between 49 ft and 104 ft depth has a cutoff frequency of 18 Hz, and below the 104 ft depth the cutoff frequency is 45 Hz. The discussion on p. 16 in Cuesta et al. (2016) also notes that since the soil below the 49 ft depth drives the structure, the SASSI structure analysis is capable of representing frequencies up to 20 Hz. Given that the in-structure results are plotted to a frequency of 100 Hz, care is needed when considering the high frequency results. Also, it can be expected that the high frequency response from the SASSI model will drop off sooner than the high frequency response from the NLSSI model given the relative cut-off frequencies between the models. (As shown in the soil column evaluation in Appendix B, where the high frequency is more accuracy addressed, high frequency surface response is greater in general for NLSSI than linear SSI for the same soil column base input. This becomes less apparent for the shallower soil column used for the SSI models but remains an important topic for study.)

- The structure is linear-elastic for the NLSSI and linear SSI models; however, the structural response is not identical (as discussed in Section 4.3). For the NLSSI model, LS-DYNA is used to evaluate the structure. To get the structure into SASSI, Abaqus/Standard is used as a translator. While attempts were made to minimize the differences in the structural models, LS-DYNA and Abaqus/Standard produce unique formulations for the structure. This produces a somewhat arbitrary difference that can be seen in the Section 4.3 fixed base results.
- The linear and nonlinear approaches address the inherent nonlinearities in the soil differently. For the linear approach, soil degradation is performed to select the most appropriate stiffness and damping ratio at each soil depth. These values are then used for the entire analysis. For the nonlinear approach, the soil at each depth is given an elastic-plastic constitutive model. This causes the effective soil stiffness and effective soil damping to be modified through time as the soil is deformed. This difference alone is not expected to cause large differences in the results. However, the shape of the hysteresis loop is different for the linear and nonlinear approaches and this is significant to differences in results. The linear model hysteresis loop is smooth and causes the soil elements to pass a seismic wave smoothly with only damping occurring to reduce their amplitude. The nonlinear model hysteresis loop for this evaluation has discontinuous "pointed" ends (based on a Masing rule approach which is discussed in Stewart et al. (2008) and Hashash et al. (2001) in greater detail). This causes the soil elements to pass a seismic wave with some energy being effectively damped. But, some energy is also moved to higher frequency waves due to the discontinuous ends of the hysteresis loop. While the nonlinear model hysteresis loop should be more accurate relative to the physics of actual soil dynamics, more testing is desirable to establish the accuracy of the approach (and if modifications are necessary). For the results of this study, this is seen as an increase in high frequency response for the NLSSI results as compared to the linear SSI results.

6.2 NLSSI and SASSI Model Results Comparison for Vogtle

A comparison of the NLSSI and linear SSI results are given in Cuesta et al. (2016). This includes results from the two meshes described in Section 5.1 and results from the SASSI evaluation.

7. Results and Conclusions

This report documents development of a NLSSI methodology for a deep soil site. As free field validation, the nonlinear soil constitutive model is compared to actual data gathered by the Electric Power Research Institute (EPRI) in cooperation with the Taiwan Power Company (Taipower) at Lotung, Taiwan. The results of this portion of the study (discussed in Section 2) provide validation that the soil model used in the NLSSI evaluation can be used to accurately simulate actual seismic data.

As SSI validation, low amplitude seismic results are compared between NLSSI and the recently V&Ved version of SASSI at the Vogtle site (located approximately 15 miles East-Northeast of Waynesboro, Georgia and adjacent to Savanna River).

The first step of this process is to develop the NLSSI soil column (as discussed in Section 3) and compare it to the equivalent soil column evaluated with linear techniques (SHAKE). The soil surface response spectra results for this comparison showed good agreement between the linear and nonlinear techniques at low frequencies (< 6•Hz). Additionally, the soil surface, response spectra results showed good agreement between the linear and nonlinear techniques relative to natural frequency response of the soil column. The higher frequency response (> 6•Hz) amplitude diverged between the linear and nonlinear techniques. This difference is predictable given the differences in the linear and nonlinear hysteresis loops. Elements with the linear hysteresis loop transmit only the wave frequencies that are input to them. Elements with the nonlinear hysteresis loop transmit the wave frequencies that are input to them and convert some of the energy to higher wave frequencies. Consequently, even though the linear and nonlinear techniques in this study can have equivalent stiffness and damping, they do not transmit the seismic waves in the exact same way. The nonlinear hysteresis loop shape should be closer to the shape of actual tested soil and unreasonably high frequency content was not produced when comparing to the actual data at Lotung. Considering that the actual data at Lotung was not provided at depths equal to that at the Vogtle site, more study relative to the high frequency content is warranted. With more data, adjustments could be made to the nonlinear model as needed.

The second step of the process is to develop the structural model (as discussed in Section 4). The structural model is elastic with Rayleigh damping and is generated in LS-DYNA and in Abaqus. The LS-DYNA model is developed for the NLSSI model runs. (This is motivated by, under the current settings, LS-DYNA runs with greater speed than Abaqus.) The structural model in Abaqus is generated because Abaqus can be used as a translator to get the structural model into SASSI. Because LS-DYNA and Abaqus do not share the same element formulations, there are differences in the results. Attempts have been made to manage the differences, however. Consequently, the structural models produce similar results.

The third step of the process is to develop and run NLSSI models with the structural model and a reasonable amount of soil volume (as discussed in Section 5). Two versions of the NLSSI model are run. One with the soil constrained to the structure and one with the soil in contact with the structure. Additionally, 1•DBE and 3•DBE model runs are performed using seismic time histories developed in Cuesta et al. (2016). The soil volume used for the NLSSI models represents less than half the total Vogtle site soil column. However, it should be a reasonable volume of soil given the discussion in Section 5.3. With the shorter soil column, less difference in high frequency content can be expected when comparing linear and nonlinear techniques.

The fourth step of the process (as discussed in Section 7) is to compare the NLSSI results to the linear SSI models that are developed in Cuesta et al. (2016). The comparison plots are given in Cuesta et al. (2016), with 1•DBE results in Figures 42 – 62 and 3•DBE results in Figures 63 – 87. The process followed in Cuesta et al. (2016) is the standard SSI evaluation approach using the recently V&Ved version of SASSI. Section 6.1 (of this document) provides an overview of what should be considered when comparing these results. Considering the discussion in Section 6.1, the 1•DBE results showed good correlation between the NLSSI and linear SSI. The horizontal results for frequencies below about 10 Hz

compared the best having similar peak frequencies and amplitudes. This represents the portion of the results with the least issues that warrant additional study. Vertical results for nodes near the soil-structure interface also compared well for frequencies below about 10 Hz. Vertical results near the top of the structure show the largest discrepancies. Nodes 17 and 18 and Nodes 23 and 24 are centered on the two roofs at different elevations on the East and West sides of the structure respectively. For these nodes, there is a significant frequency shift where the peak response occurs when comparing NLSSI results to linear SSI results. Cuesta et al. (2016), Figures B44 – B47 show fixed base results for these nodes where the fixed base input is the free soil surface motion. In these results, LS-DYNA, Abaqus, and SASSI all compare well on where the peak responses occur. While the peak response results for the NLSSI and linear SSI are much lower in amplitude than the fixed base results (as expected), the frequencies where the peak responses occur match very well when comparing the NLSSI and fixed base results. The peak response frequencies for the linear SSI are significantly shifted from the fixed base results (which warrants further study). Comparing the NLSSI model with constrained soil-structure interaction to NLSSI model with the soil-structure interaction in contact, both showed similar results for most of the nodes evaluated. One node at the bottom corner of the structure (Nodes 13) showed results where the contact model increased in high frequency amplitude relative to the constrained model. This indicates that some impact occurred. The nodes at the centers of the shallowest floors in the structure (Nodes 16 and 22) showed results where the contact model decreased slightly in high frequency amplitude relative to the constrained model. This indicates that some sliding occurred (primarily in the North-South direction).

Considering the discussion in Section 6.1, similar conclusions can be made for the 3•DBE results as were made for the 1•DBE results when comparing the NLSSI and linear SSI models. Comparing the 3•DBE NLSSI model with constrained soil-structure interaction to the NLSSI model with the soil-structure interaction in contact, similar yet more significant results differences occurred than in the 1•DBE results. For the 3•DBE results, all of the nodes at the bottom corners of the structure (Nodes 13, 14, 19, and 20) showed results where the contact model increased in high frequency amplitude relative to the constrained model. This indicates that some impact occurred. Likewise, the nodes at the centers of the shallowest floors in the structure (Nodes 16 and 22) showed results where the contact model decreased significantly in high frequency amplitude relative to the constrained model. This indicates that some sliding occurred (primarily in the North-South direction).

8. Recommendations for Future Work

The recommendations for future work include performing additional deep soil site analysis where the differences between the NLSSI models and the linear SSI models, discussed in the Section 6.1, are addressed and/or minimized.

9. References

1 Cuesta, I., Mertz, G., Costantino, M. (2016). *Frequency Domain SSI Response of a Conceptual Reactor Building on the Vogtle Site*, CJC-IDA-M-002, Carl J. Costantino and Associates, Spring Valley, NY.

2 Dassault Systèmes (2012). Abaqus Software, Version 6.12-2, Dassault Systèmes Simulia Corporation, Providence, RI.

3 Deng, N. and Ostadan, F (2000). SHAKE2000, Theoretical and User Manual, A Computer Program for Conducting Equivalent Linear Seismic Response Analyses of Horizontally Layered Soil Deposits. Geotechnical and Hydraulic Engineering Services, Bechtel National Inc., San Francisco, CA.

4 Hashash, Y. M.A. and Park, D. (2001). *Non-linear one-dimensional seismic ground motion propagation in the Mississippi embayment*, Engineering Geology 62, pp. 185 – 206, www.elsevier.com/locate/enggeo.

5 LSTC (2013). LS-DYNA Software, Version smp s R7.00, Livermore Software Technology Corporation, Livermore, CA.

6 Lysmer, J., Ostadan, F., and Chin, C, C. (1999). SASSI2000, User Manual, Revision 1, A System for Analysis of Soil-Structure Interaction, University of California, Berkeley, CA.

7 Payne, S. J. (2006). *Data and Calculations for Development of Soil Design Basis Earthquake Parameters at RTC*, Research Report, INEEL/EXT-03-00943, Revision 2, INL, Idaho Falls, ID.

8 PTC (2011). Mathcad Software, Version 15.0, Parametric Technology Corporation, Needham, MA.

9 Stewart, P. S., Kwok, A. O., Hashash, Y. M.A., Matasovic, N., Pyke, R., Wang, Z., Yang, Z. (2008). *Benchmarking of Nonlinear Geotechnical Ground Response Analysis Procedures*, PEER Report 2008/04 Pacific Earthquake Engineering Research Center, College of Engineering, University of California, Berkeley, CA.

10 Stokoe, K. H., Menq, F. Y., Valle, C., Choi, W. K. (2002). *Dynamic Properties of Intact Soil Specimens from the Test Reactor Area Site for Idaho National Engineering and Environmental Laboratory (INEEL)*, Geotechnical Engineering Report GR02-2, Geotechnical Engineering Center, Civil Engineering Department, The University of Texas at Austin, Austin, TX.

Appendix A

Nonlinear Modelling of Ground Motions at Lotung LSST Site with Nested Surface Soil Constitutive Model

The Electric Power Research Institute (EPRI) in cooperation with the Taiwan Power Company (Taipower) has conducted field experiments at Lotung, Taiwan. The field experiments include gathering material property data on the soil and measuring soil motion caused by seismic events. The soil motion is measured at many locations at and below the soil surface. The resulting soil motion and material property data are useful for validation of linear or nonlinear time domain SSI analysis techniques.

The purpose of this study is to demonstrate that a nested surface nonlinear, hysteretic soil constitutive model used in a time domain, finite element analysis can reasonably reproduce the actual measured soil motions at Lotung.

A.1 Introduction

Lotung is in a seismically active region. Many earthquakes have been recorded in the field experiments at Lotung using the large-scale seismic test (LSST) array shown in Figure A.1-1. An earthquake of particular interest occurred on May 20, 1986 that had a magnitude of 6.5 (the LSST07 event). This earthquake is of particular interest because the shear and pressure waves were traveling in a near vertical direction at approximately 6° (Chang et al. 1990) from vertical. This is desirable because a single vertical array of accelerometers provides much of the data needed to numerically simulation the actual data.

Soil testing was also performed at Lotung to provide material properties for numerical simulation. The soil testing is provided in a form that is appropriate for linear software packages such as SHAKE (Deng et al. 2000) and SHAKE has been used to simulate the LSST07 event (Tang et al. 1990; EPRI 1991).

The study in this appendix is performed as validation that a nested surface nonlinear, hysteretic soil constitutive model, as used in LS-DYNA (LSTC 2013), can reasonably simulate the actual measured soil motions at Lotung. To fully realize the capabilities and limitations of this nonlinear simulation, much more data would be necessary. This would include sufficient data to fully address the nonlinear soil constitutive model for each soil type, geometry data to develop a finite element mesh of the soil volume, and much more accelerometer data to show how the seismic waves pass through the soil volume. Because this amount of data is not available and the LSST07 event provides data that is appropriate for a simplified nonlinear finite element model, a nonlinear simulation for validation is run similar to the SHAKE simulation (except it will be performed with motions in all three directions simultaneously). The expectation is that the nonlinear simulation where seismic motions are applied at the base of the model and propagate upward should produce similar results to the actual data. However, considering the potential for phenomena such as Rayleigh waves and local wave reflections, some error in the simulation can be expected.

This study is similar to that performed by Borja et al. (1999). Important differences include this study using a little different nonlinear soil constitutive model and there is no viscous damping included. The motivation for not having viscous damping added is because of the frequency dependence that most time domain models have when viscous damping is included.

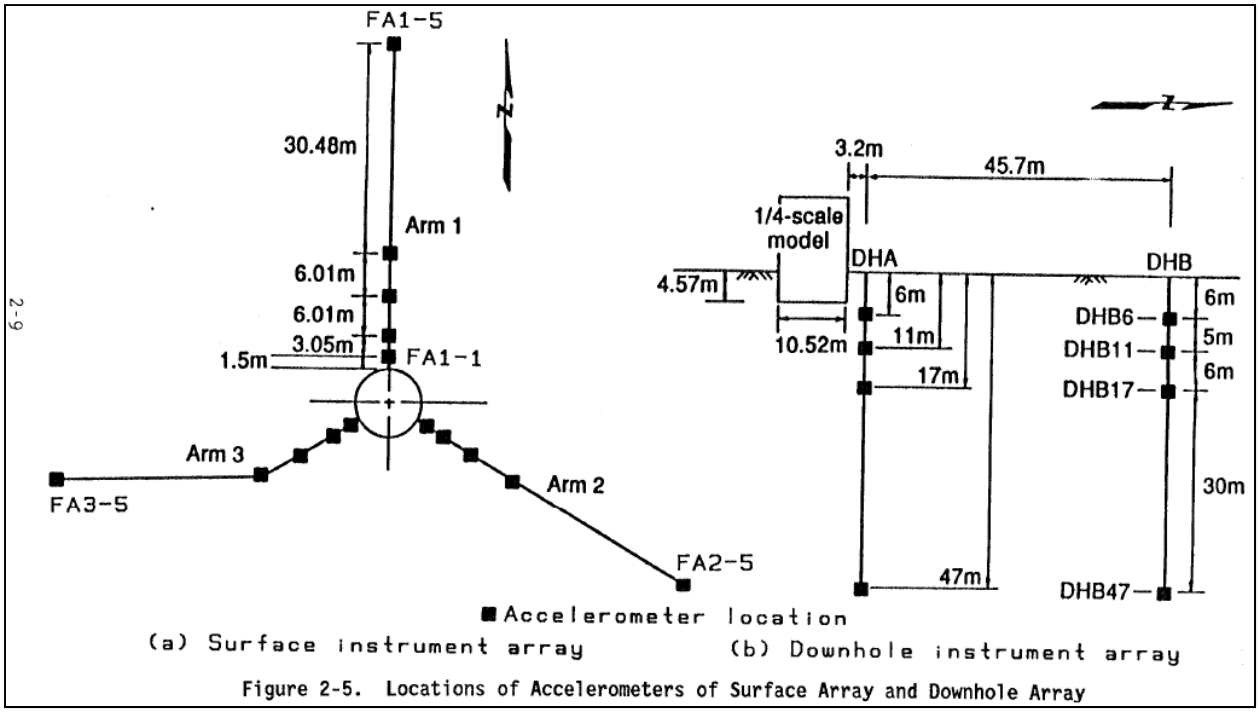

Figure 2-5. Locations of Accelerometers of Surface Array and Downhole Array

Figure A.1-1. Accelerometer array at Lotung (EPRI 1991).

A.2 Nonlinear Soil Constitutive Model

Many finite element modelling software packages may be used to evaluate a nonlinear, hysteretic soil model. One of these is LS-DYNA using a nested surface hysteretic soil constitutive model (*MAT_HYSTERETIC_SOIL). This constitutive model is of a form that includes the Drucker-Prager model and is reasonable for nonlinear soil behavior. The hysteretic soil behavior results from post yielding shear stress versus shear strain. The basic idea is based on each element having up to 10 sublayers that are each elastic/perfectly plastic with different elastic stiffness and yield stress values. The elastic/plastic behavior of each sublayer follows a kinematic hardening rule. The response of the sublayers is summed together to produce the post yielding shear stress versus shear strain curve and it is valid for a single mean effective stress (or hydrostatic stress) in the element. When running a model, the default is to have the post yielding shear stress versus shear strain curve vary as the mean effective stress varies in a given element. It can also be defined to stay constant relative to the initial conditions. Other soil parameters that are available with this constitutive model include yield function constants, dilation parameters, reference pressure, cut-off pressure, and an exponent for bulk modulus pressure sensitivity. (Note: In LS-DYNA, the modelled z-direction must be vertical for all of these parameters to work correctly.)

With sufficient soil testing, all of the soil parameters can be addressed. Given the available material properties, only the post yielding shear stress versus shear strain and exponent for bulk modulus pressure sensitivity parameters are calibrated. Additionally, model stability issues made it most convenient to define initial mean effective stresses that caused the post yielding shear stress versus shear strain curve to vary over the mesh. But, these curves were then not allowed to change with mean effective stress variations during the model runs. (The stability issues developed toward the end of the seismic time histories at relatively low accelerations and this change did not appear to cause a significant change in the results before the stability issues developed.)

A.3 Finite Element Model and Material Properties

The finite element model for this study is shown in Figure A.3-1. It consists of seven different soil layers. The seven soil layers are based on the top five layers from the best estimate layered soil properties for 7-layer profile (EPRI 1989) except the third layer (from the top) is broken into 3 layers in this study. This is done to assist in making a smooth low strain shear velocity curve (as shown in Figure A.3-2).

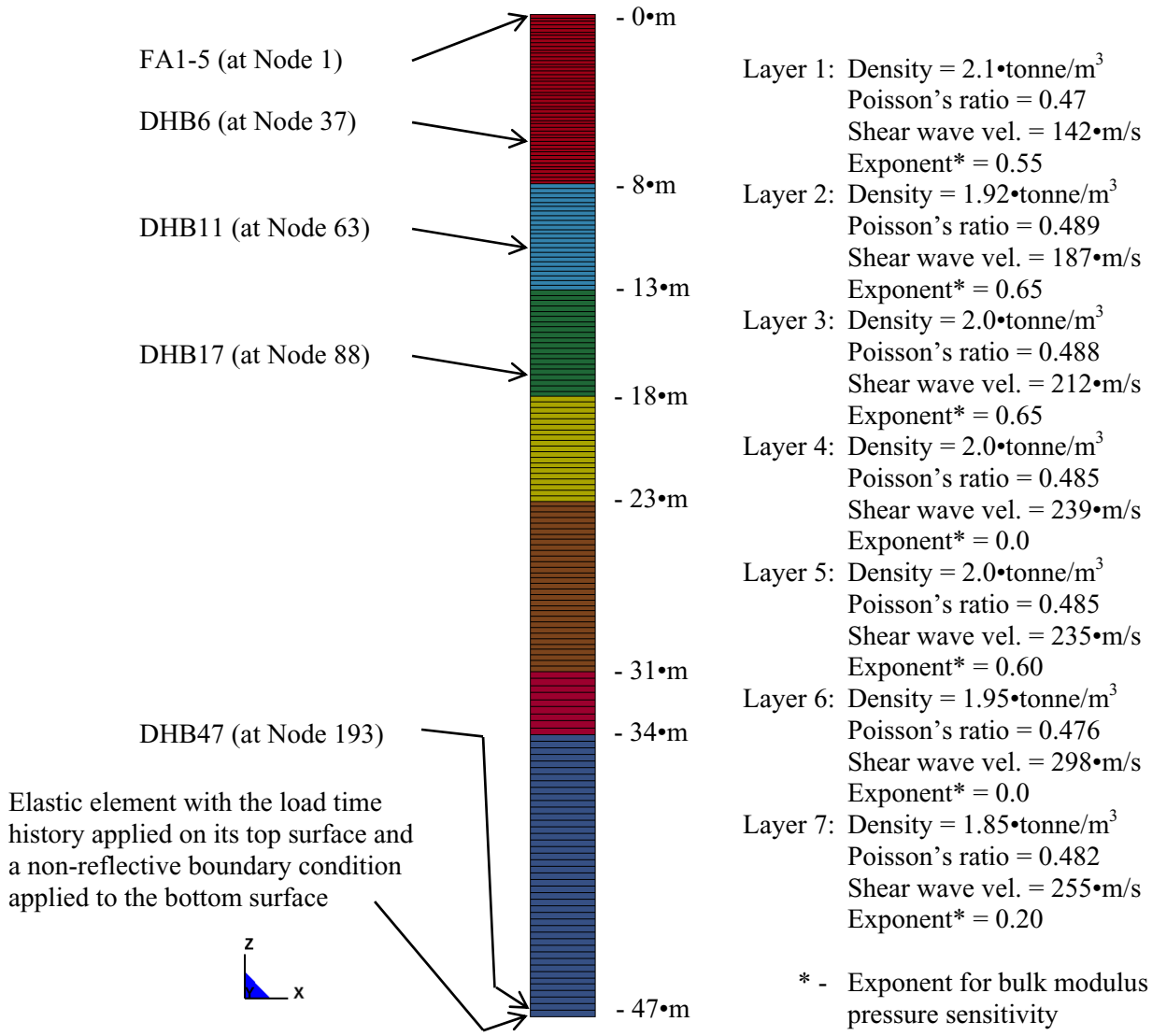

Figure A.3-1. Finite element model.

The soil material properties (as shown in Figure A.3-1) include density, Poisson's ratio, low strain shear wave velocity, and exponent for bulk modulus pressure sensitivity. The nonlinear soil model also required definitions for yield function constants, dilation parameters, reference pressure, and cut-off pressure. For all the elements, the yield functions constants were defined as $a_0 = 0.0$, $a_1 = 0.0$, and $a_2 = 1.0$. This caused the behavior to be in a classical Drucker-Prager form. The value of 1.0 given to a_2 is reasonable and has little effect on the constitutive model behavior for the problem being studied. The dilation parameters and cut-off pressure are set to zero. The reference pressure for each soil layer is

calculated as the average static pressure in the given layer (using the know density, geometry, and gravitational acceleration).

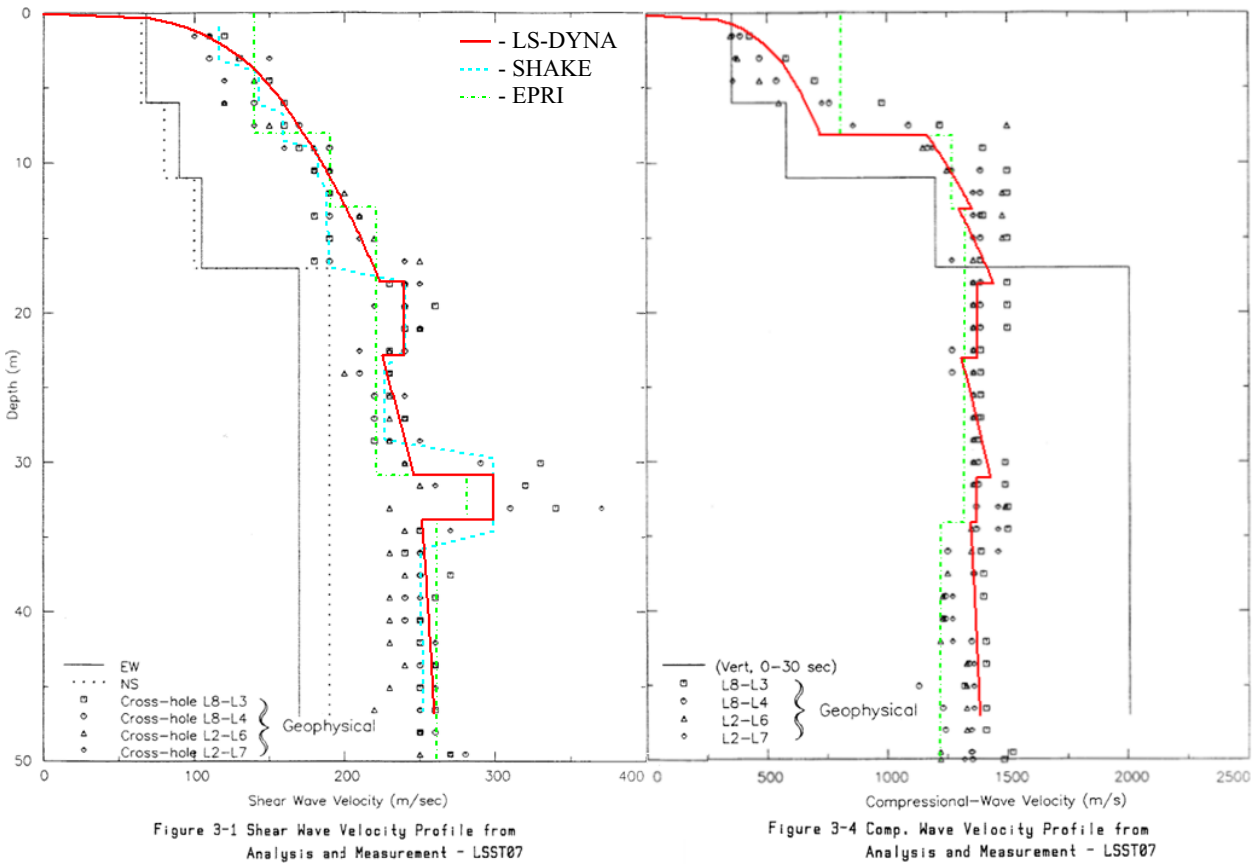

Figure A.3-2. Shear (left plot) and compressive (right plot) wave velocity profiles. The LS-DYNA, SHAKE (ref xxx), and EPRI (EPRI 1989) low strain shear velocities are superimpose onto figures from EPRI (1991).

To account for the nonlinearity of soil, the nonlinear soil constitutive model in this study uses post yielding shear stress versus shear strain to produce hysteretic behavior. This constitutive model accepts shear stress versus shear strain data (as shown in the Figure A.3-3 backbone curve). Applying a cyclic shear stress to an element with this constitutive model then produces hysteresis loops (as shown in the Figure A.3-3). The LS-DYNA soil constitutive model is limited to 10 sublayers which means that it only accepts 10 shear stress versus shear strain data points for the backbone curve. Having few data points representing significant plasticity can lead to erroneous noise being produced (Bolisetti et al. 2014) because of the significant discontinuities produced at the data points. The soil column in this study is relatively deep soil that is experiencing significant plasticity. Consequently, the backbone curves (as shown in the Figure A.3-3) have fifty points placed along a smooth curve. To accommodate this many data points, there are five superimposed elements for each element shown in Figure A.3-1. Summing the response of the five superimposed elements produces hysteresis loops similar to those in Figure A.3-3.

Because the material properties for this study are given in G/Gmax and damping versus cyclic shear stress amplitude, conversion to and from shear stress versus shear strain and energy absorbed per cycle is performed per Spears et al. (2015). Using the LS-DYNA soil constitutive model, only a shear stress versus shear strain curve may be defined. This means that the combination of G/Gmax and damping

versus cyclic shear stress amplitude is more limited for the nonlinear constitutive model used in this study (where the shape of the given G/Gmax curve determines the shape of the damping curve rather than the two curves being independent). Figure A.3-4 shows the effective G/Gmax and damping versus cyclic shear stress amplitude curves being used by LS-DYNA in this study superimposed on plots from Borja et al. (2002). Because the shape of the damping curve is dependent on the shape of the G/Gmax curve, neither curve exactly matches the test data.

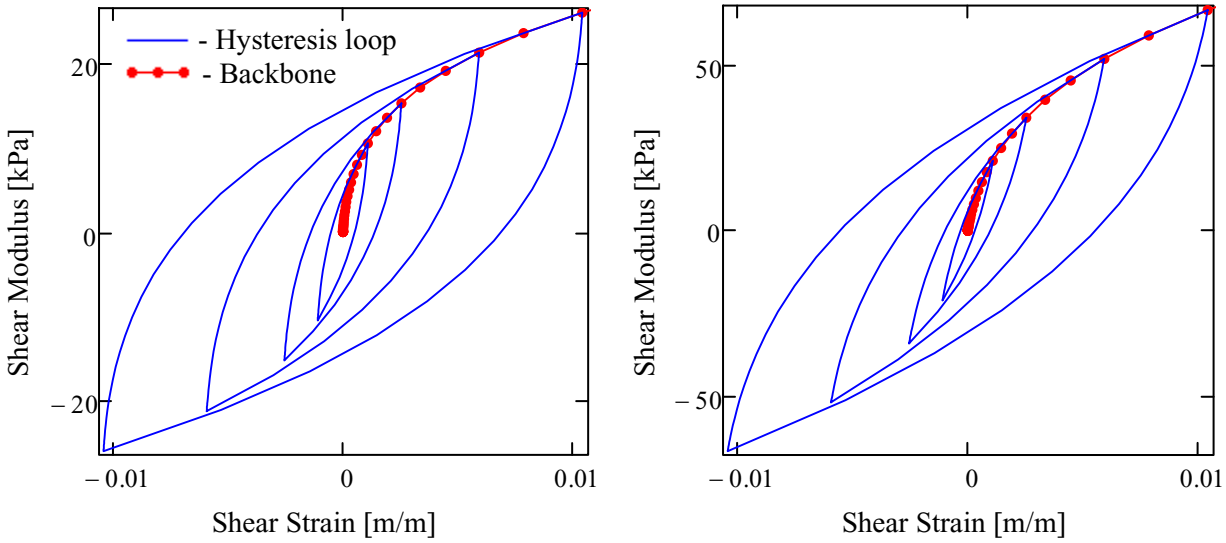

Figure A.3-3. Example hysteresis loops and backbone curves for soil near the top of the soil column (left plot) and soil near the bottom of the soil column (right plot).

The back figured data from Zeghal et al. (1995) (including the data not shown in Figure A.3-4 that goes down to seventeen meters) indicate that there is a transition of the curve shapes that progressively change with soil column depth. The test data from Stokoe (EPRI 1993) shows a relatively constant curve shape. Considering the Figure A.3-2 low strain shear velocity data, there is a fairly linear change in the low strain shear between zero and about twenty meters. Below this level, the shear velocities are more constant with sudden changes occurring with different soil layers. Consequently, for this study, the LS-DYNA curve shown in the upper plot in Figure A.3-4 is linearly transitioned to the LS-DYNA curve shown in the lower plot in Figure A.3-4 for the soil depths from zero meters to the twenty meters. The lower plot in Figure A.3-4 is then used for all soil layers below twenty meters. This strategy produces the hysteresis loops shown in Figure A.3-3.

(It should be noted that other transition strategies were tried but an exhaustive study was not performed. One strategy was to transition from zero meters to thirty-four meters similar to where the curve shape change occurred for the SHAKE data (EPRI 1991). Other strategies included changing the curves shapes to better match G/Gmax or to better match damping. The results were not drastically different; however, the study presented in this appendix produced arguably the best results of the strategies that were tried.)

The finite element boundary conditions include a free top surface and an elastic bottom element with a stiffness close to its neighboring elements which acts as a boundary condition (as shown in Figure A.3-1). The bottom element has a non-reflecting boundary condition on its bottom and a load time history on its top. This allows downward moving waves to pass out of the model while driving upward traveling waves into the model. This modelling strategy is employed because enforcing the in-layer acceleration time history at the base of the model can cause significant error. The error occurs because it is unlikely

that the model stiffness is so exact that the acceleration time history causes the downward traveling waves to pass correctly out of the model. Instead, all or part of the downward traveling waves can be erroneously reflected back into the model. However, using the modelling strategy in this study means that the load time history must represent a rock outcrop motion, which is not known. To address this problem, the load time histories are applied, the resulting accelerations are compared to the desired in layer accelerations, and the load time histories are modified iteratively to provide a better match.

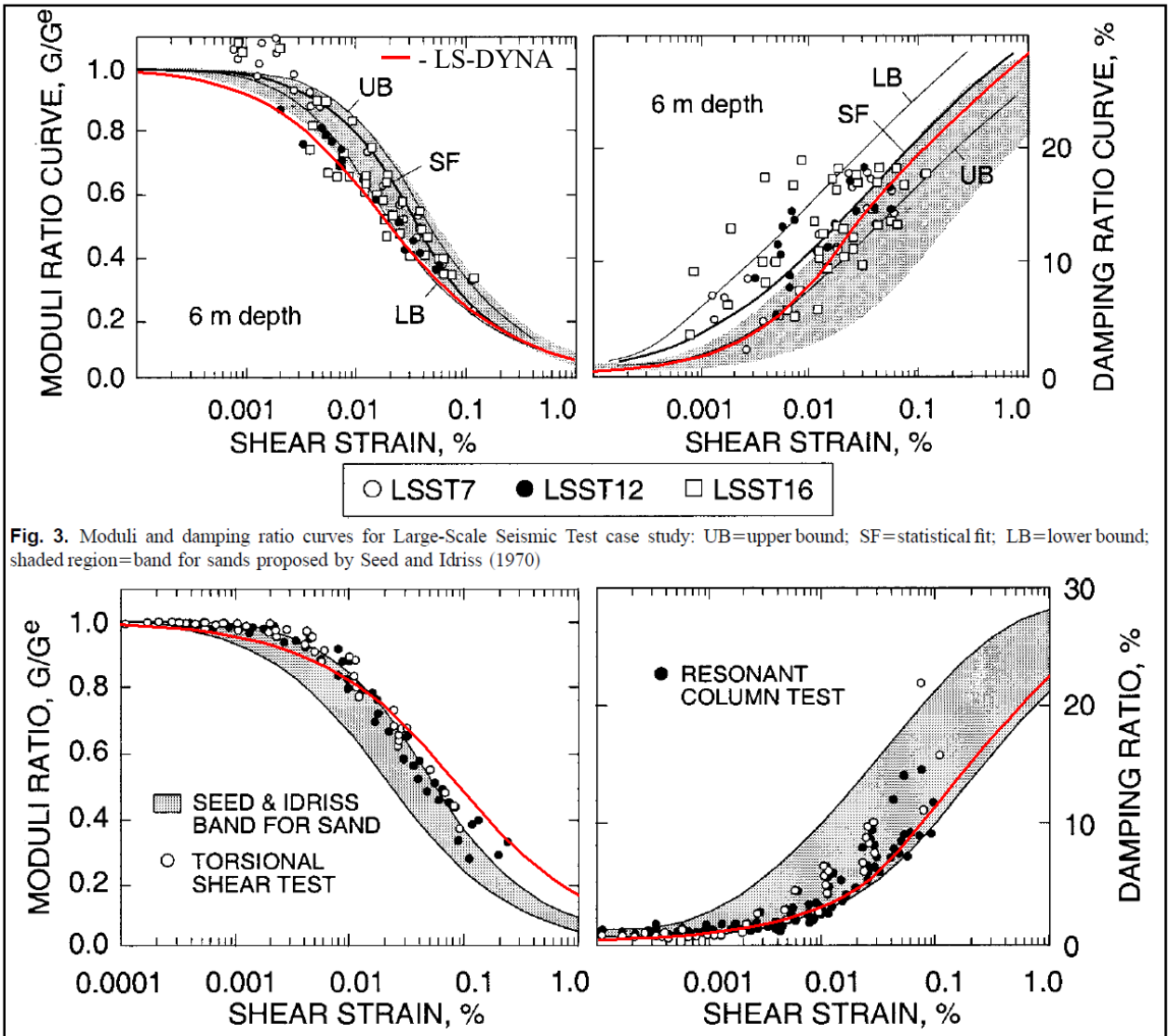

Fig. 3. Moduli and damping ratio curves for Large-Scale Seismic Test case study: UB=upper bound; SF=statistical fit; LB=lower bound; shaded region=band for sands proposed by Seed and Idriss (1970)

Fig. 2. Moduli and damping ratio curves for Large-Scale Seismic Test case study: Torsional shear and resonant column tests (Electric 1993) and band for sands proposed by Seed and Idriss (1970)

Figure A.3-4. LS-DYNA effective G/Gmax and damping versus strain curves for the shallow soils (top plots) and the deep soils (bottom plots). These curves are superimposed onto plots shown in Borja et al. (2002). The top plots also show one set of the three sets of back figured data from Zeghal et al. (1995) and the bottom plots also show test data from Stokoe (EPRI 1993).

A.4 Results and Discussion

The results for this study are shown in Figures A.4-1 to A.4-4. Figures A.4-1 to A.4-3 show the actual recorded test data and the LS-DYNA results for the acceleration at the bottom and top of the modelled soil column in each direction. The acceleration time history match is much better at the bottom than the top because load time history is input into the bottom. It is not an exact match at the bottom because the load time history is iterated to produce a good soil column motion match given the soil material properties. Though the soil constitutive model and material properties cannot be expected to be exact, even if they were, an exact motion match cannot be expected due to the lack of actual data to properly model the 3d nature of the seismic waves. However, given that the seismic waves are traveling in a near vertical direction for the studied seismic event, a good match to the actual data should be possible. Figures A.4-1 to A.4-3 show that the nonlinear soil constitutive model produces a good acceleration time history match with the actual data for this study.

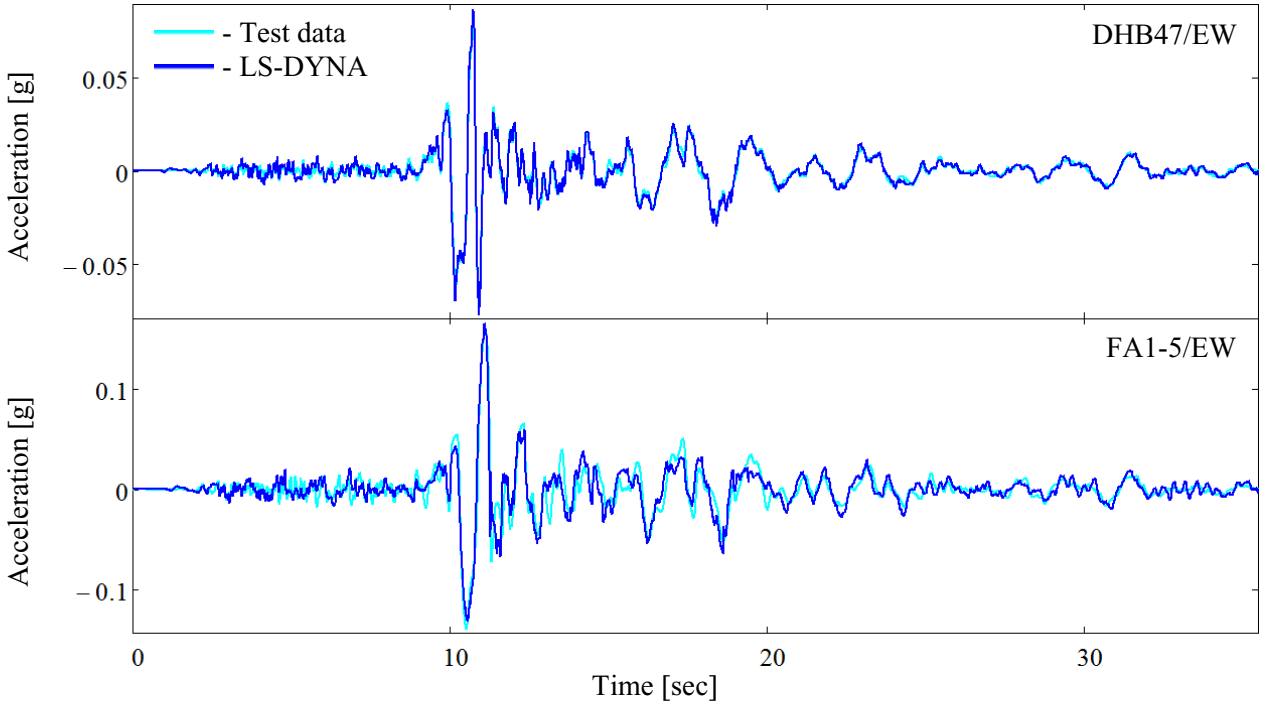

Figure A.4-1. Test data and LS-DYNA acceleration time histories in the East-West direction at a depth of 47•m and at the soil surface.

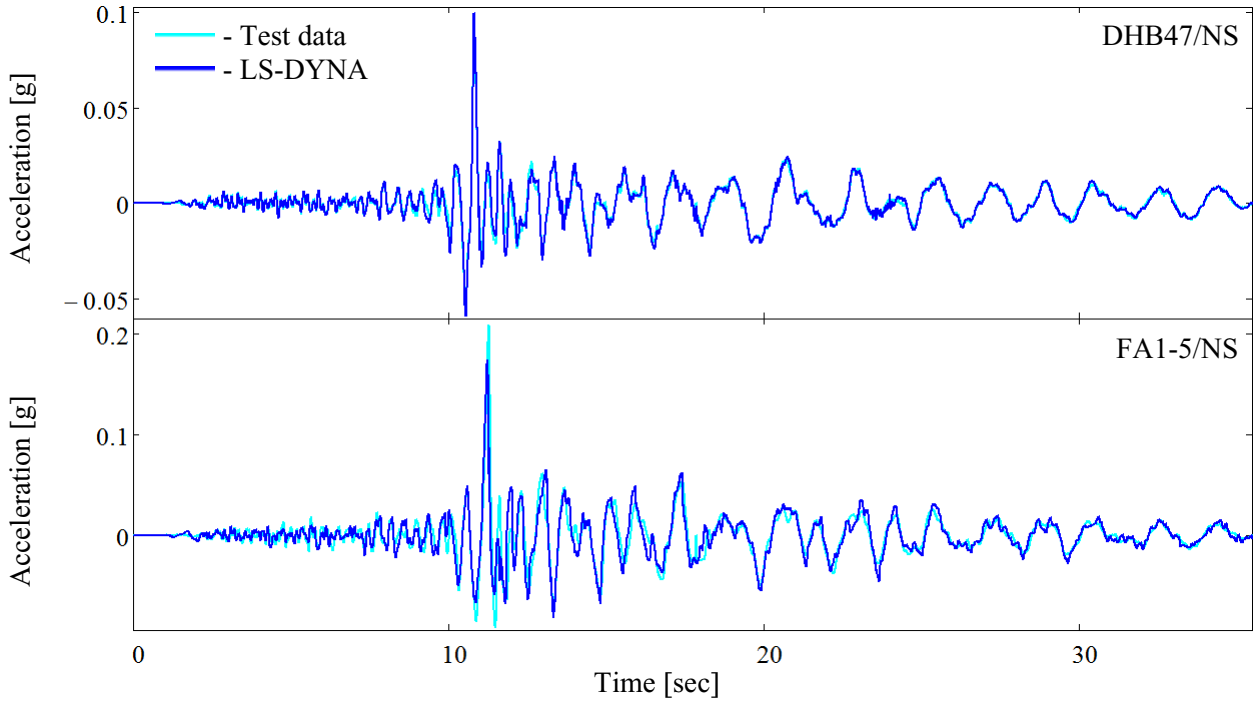

Figure A.4-2. Test data and LS-DYNA acceleration time histories in the North-South direction at a depth of 47•m and at the soil surface.

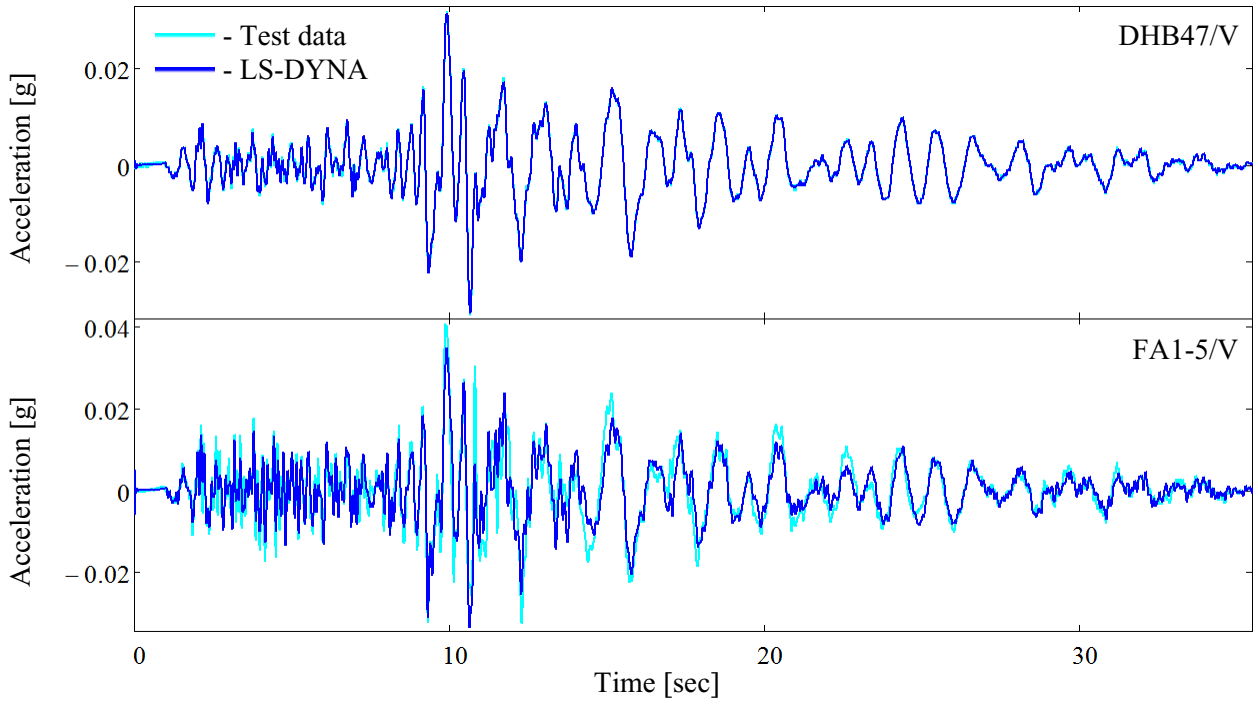

Figure A.4-3. Test data and LS-DYNA acceleration time histories in the vertical direction at a depth of 47•m and at the soil surface.

Figure A.4-4 shows a 5% damped response spectra comparison between the actual test data and the LS-DYNA results. The plots show response spectra for all of the locations and directions where actual data is provided that is applicable to this study. In general, the response spectra peaks occur at similar frequencies with similar acceleration amplitudes between the LS-DYNA results and the actual data. This indicates that the LS-DYNA model is producing good results. The peak amplitudes do not closely match at all frequency locations, however. Notable frequency locations where a better match could likely be achieved with a more exhaustive material property study include the East-West amplitude peaks at 2.5 Hz and the North-South amplitude peaks at 1.2 Hz, 1.8 Hz, 2.2 Hz and 2.7 Hz. Notable frequency locations where a better match seems unlikely with a more exhaustive material property study include the 2.9 Hz peak in DHB11/NS and the vertical amplitude peak at 0.6 Hz. These can most likely be explained with the 3d nature of the actual seismic waves that is not being fully captured by the recorded data and/or inaccuracies with the nonlinear soil constitutive model selected for the study. A better match for the vertical amplitude peaks at 3.2 Hz and 4.2 Hz may be possible with the inclusion of dilation in the soil constitutive model.

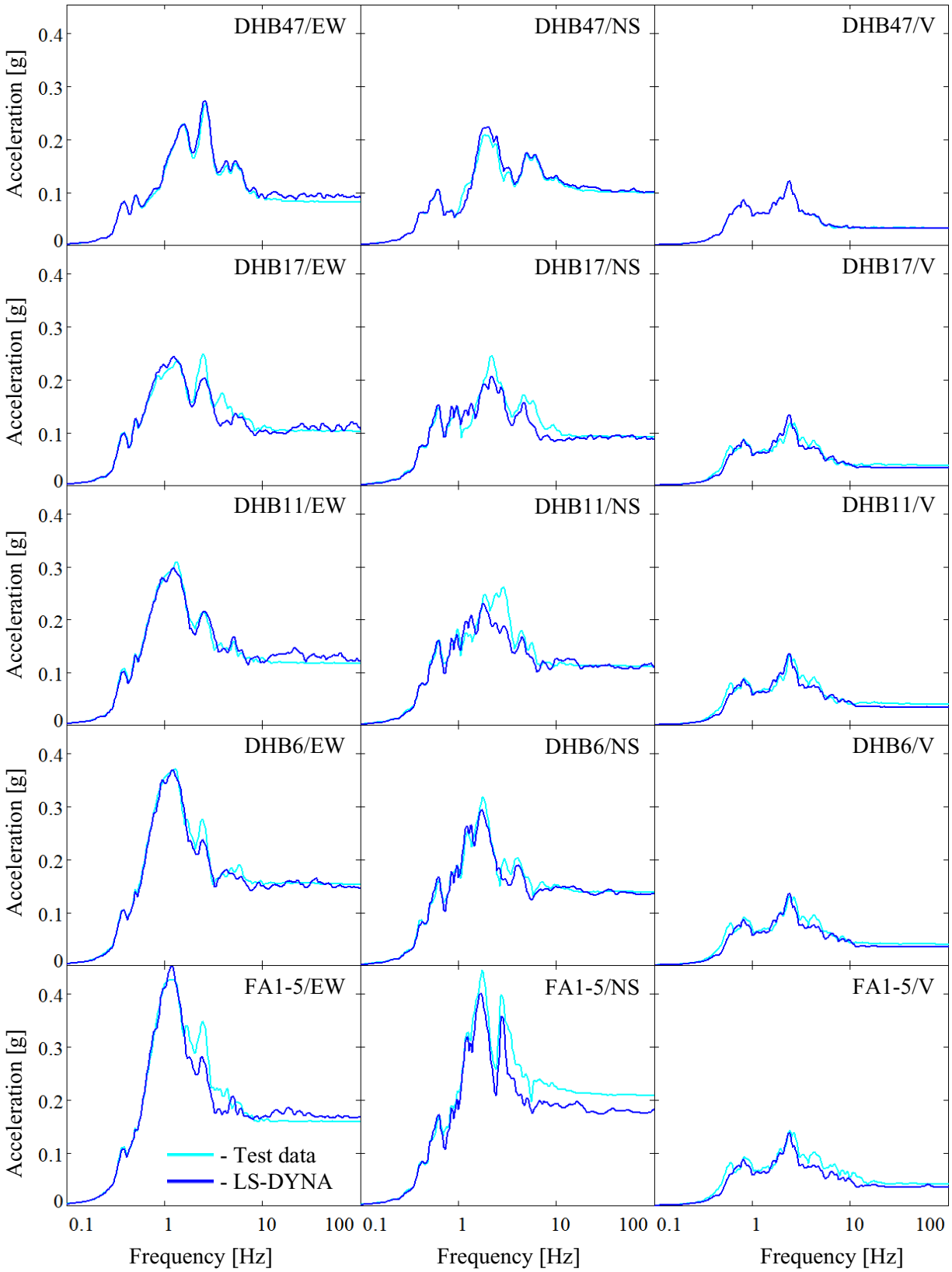

Figure A.4-4. Response spectra comparison (5% damped) between the actual test data and the LS-DYNA results.

A.5 Conclusions

As data for validation, EPRI in cooperation with Taipower has conducted field experiments at Lotung using the LSST array. The field experiments include gathering material property data on the soil and measuring soil motion caused by seismic events. The study in this appendix provides validation that a nested surface nonlinear hysteretic soil constitutive model can reasonably simulate the LSST07 event at Lotung in a time domain, finite element analysis.

A.6 References

American Society of Civil Engineers (ASCE) (1998). *Seismic Analysis of Safety-Related Nuclear Structures and Commentary*, ASCE/SEI4- 98, Reston, VA, USA.

Bolisetti, C., Whittaker, A. S., Mason, H. B., Almufti, I., Willford, M., (2014). "Equivalent linear and nonlinear site response analysis for design and risk assessment of safety-related nuclear structures," *Nuclear Engineering and Design 275*, 107-121, Elsevier, www.elsevier.com/locate/necengdes.

Borja, R. I., Chao, H. Y., Monta´ns, F. J., and Lin, C. H. (1999). ''Nonlinear ground response at Lotung LSST site.'' *J. Geotech. Eng.*, 125(3), 187–197.

Borja, R. I., Duvernay, B. G., and Lin, C. H. (2002). ''Ground Response in Lotung: Total Stress Analyses and Parametric Studies.'' *J. Geotech. Geoenviron. Eng.* 128(1), 54-63.

Chang, C. Y., Mok, C. M., Power, M. S., Tang, Y. K., Tang, H. T., and Stepp, J. C. (1990). ''Equivalent linear and nonlinear ground response analyses at Lotung seismic experiment site.'' *Proc., 4th U.S. Nat. Conf. on Earthquake Engrg.*, 1, Earthquake Engineering Research Institute, Oakland, Calif., 327–336.

Deng, N. and Ostadan, F (2000). "SHAKE2000," *Theoretical and User Manual, A Computer Program for Conducting Equivalent Linear Seismic Response Analyses of Horizontally Layered Soil Deposits*. Geotechnical and Hydraulic Engineering Services, Bechtel National Inc., San Francisco, CA, USA.

EPRI (1989). ''Proceedings: EPRI/NRC/TPC Workshop on Seismic Soil-Structure Interaction Analysis Techniques Using Data from Lotung, Taiwan." *Tech. Rep. No. NP-6154*, Electric Power Research Institute, Palo Alto, Calif., Vol. 1, Table 1-1.

EPRI (1991). ''Post-Earthquake Analysis and Data Correlation for the ¼-scale Containment Model of the Lotung Experiment.'' *Tech. Rep. No. NP-7305-SL*, Electric Power Research Institute, Palo Alto, Calif.

EPRI (1993). ''Guidelines for determining design basis ground motions - Vol. 1: Method and guidelines for estimating earthquake ground motion in Eastern North America.'' *Tech. Rep. No. TR-102293*, Electric Power Research Institute, Palo Alto, Calif.

LSTC (2013). "LS-DYNA, Version smp s R7.00," *LS-DYNA Keyword User's Manual, Volume II*, Livermore Software Technology Corporation, Livermore, CA, USA.

Seed, H. B., and Idriss, I. M. (1970). ''Soil moduli and damping factors for dynamic response analysis.'' *EERC Rep. 70-10*, Univ. of California, Berkeley, Calif.

Spears, R. E. and Coleman, J. L., (2015). "Calibrating Nonlinear Soil Material Properties for Seismic Analysis Using Soil Material Properties Intended for Linear Analysis." In: Proceedings of the 23rd SMiRT Conference, Manchester, United Kingdom.

Tang, H. T., Tang, Y. K., and Stepp, J. C. (1990). Lotung large-scale seismic experiment and soil-structure interaction method validation, *Nucl. Eng. Des.*, 123, 197–412.

Zeghal, M., Elgamal, A.W., Tang, H. T., and Stepp, J. C. (1995). ''Lotung downhole array. II: Evaluation of soil nonlinear properties.'' *J. Geotech. Eng.*, 121(4), 363–378.

Appendix B

Vogtle Site Soil Column Comparison Using Linear and Nonlinear Techniques

The Vogtle site is located approximately 15 miles East-Northeast of Waynesboro, Georgia and adjacent to Savanna River. The site consists of many soil layers spanning down to a depth of 1058 feet. Being a well-documented (Southern Company 2014) deep soil site, Vogtle makes a good location to compare deep soil column, linear and nonlinear evaluation techniques.

The purpose of this study is to show results for a deep soil column evaluated with linear techniques using SHAKE (Deng et al. 2000) and with nonlinear techniques with LS-DYNA (LSTC 2013) and with Abaqus (Dassault Système,s 2012).

B.1 Material Properties

The material properties for Vogtle site include shear velocity, density, Poisson's ratio, G/Gmax versus shear strain, and damping ratio versus shear strain for each layer. The shear velocity for the entire soil column is given in Figure B.1-1. The remaining material properties are given in Sections B.1.1 – B.1.14.

For linear analysis (SHAKE), the G/Gmax and damping ratio curves are those from the Vogtle data (Southern Company 2014). For nonlinear analysis (LS-DYNA/Abaqus), the G/Gmax and damping ratio curves approximate those from the Vogtle data using Spears et al. (2015). Since the nonlinear model curve shapes are more limiting than those for the linear model (considering the nonlinear constitutive model being used), the nonlinear model G/Gmax and damping ratio curves are defined in a manner that minimizes the differences between them and the Vogtle data. Additionally, Rayleigh damping is defined for all of the soil elements that causes a 1% damping ratio at 0.6•Hz (and 0.5% damping ratio at 100•Hz).

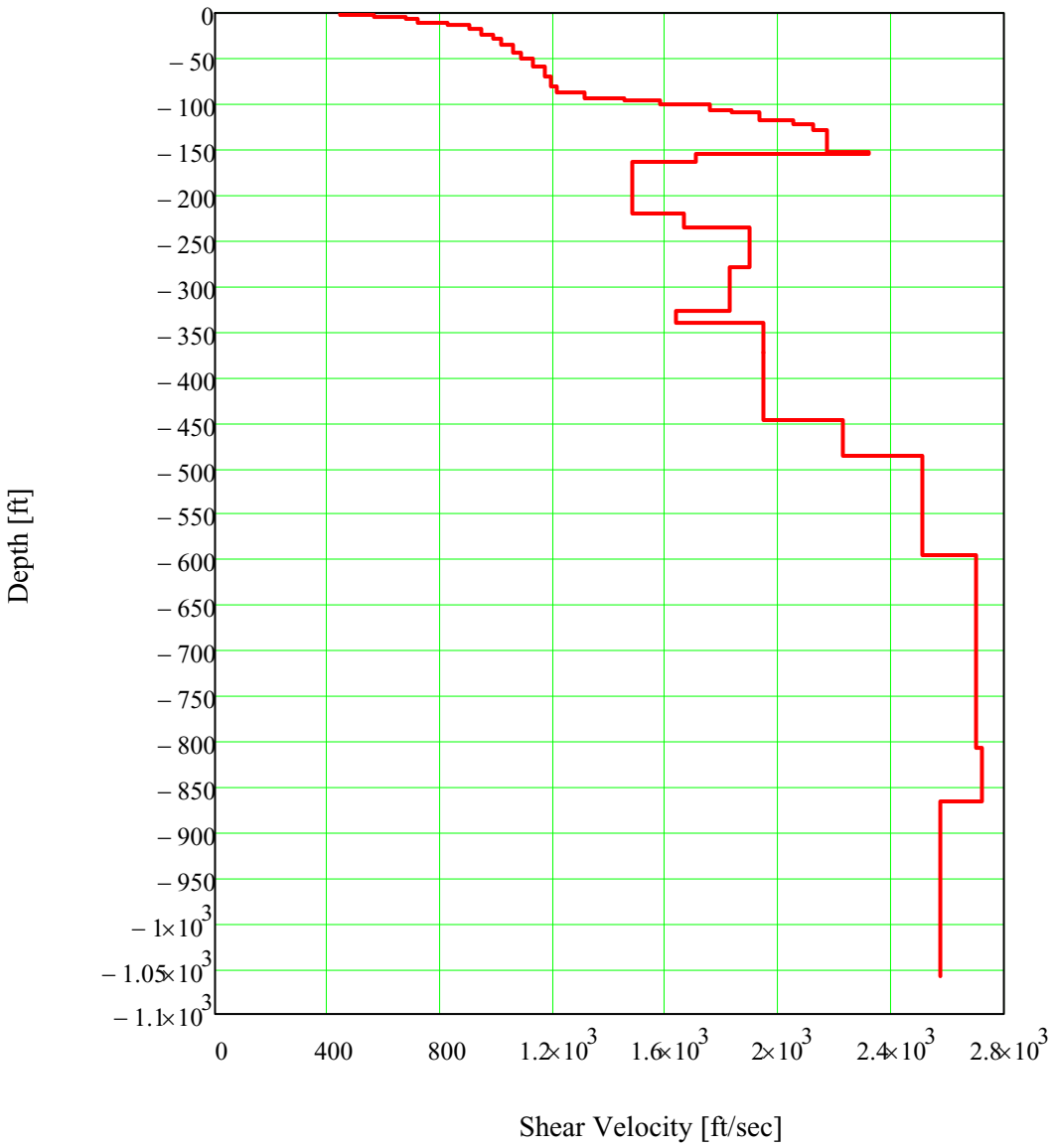

Figure B.1-1. Shear velocity plot for the Vogtle soil column used for the linear and nonlinear models.

B.1.1 Backfill (Depth 0 Feet to 25 Feet)

The material properties used for backfill at depths of 0•ft to 25•ft are given below.

$\rho_o = 123 \cdot \frac{lbm}{ft^3}$ Density

$\nu_o = 0.24$ Poisson's ratio

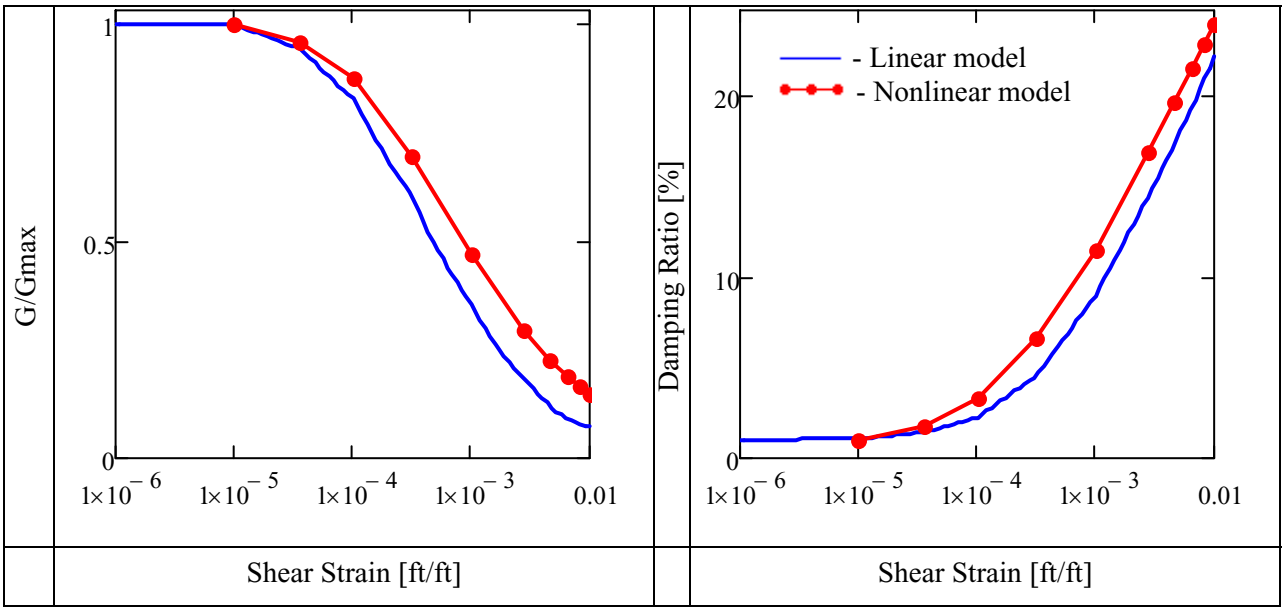

Figure B.1.1-1. Linear and nonlinear model G/Gmax and damping ratio for backfill at depths of 0•ft to 25•ft.

B.1.2 Backfill (Depth 25 Feet to 55 Feet)

The material properties used for backfill at depths of 25•ft to 55•ft are given below.

$\rho_o = 123 \cdot \frac{lbm}{ft^3}$ Density

$\nu_o = 0.24$ Poisson's ratio

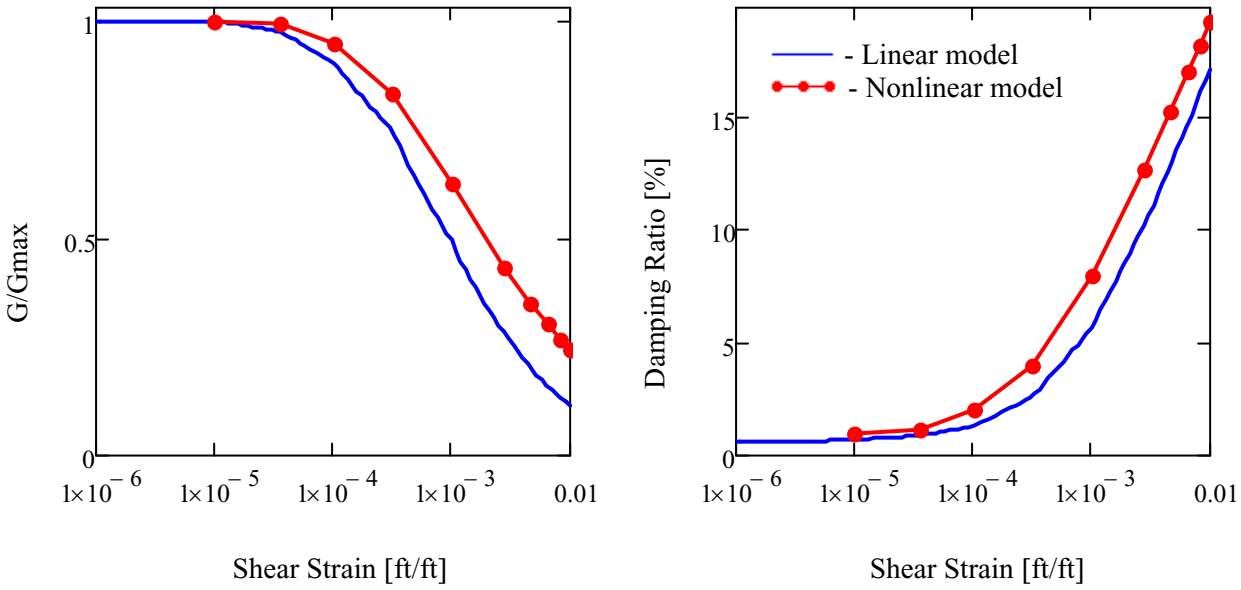

Figure B.1.2-1. Linear and nonlinear model G/Gmax and damping ratio for backfill at depths of 25•ft to 55•ft.

B.1.3 Backfill (Depth 55 Feet to 88 Feet)

The material properties used for backfill at depths of 55•ft to 88•ft are given below (below the water table).

$\rho_o = 133 \frac{lbm}{ft^3}$ Density

$\nu_o = 0.45$ Poisson's ratio

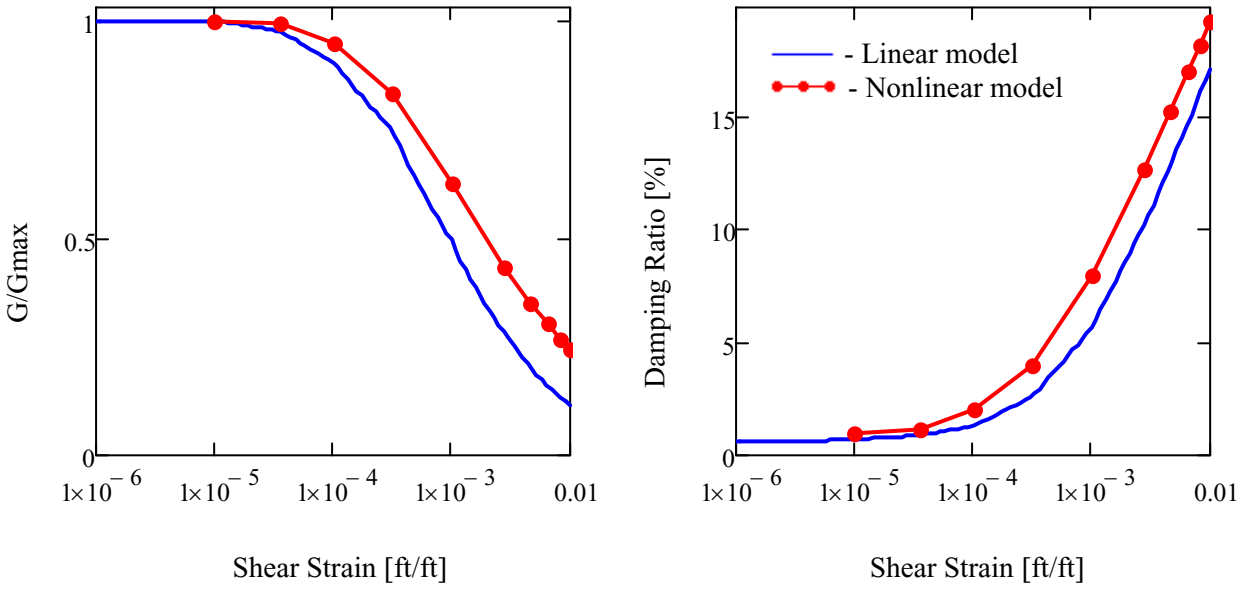

Figure B.1.3-1. Linear and nonlinear model G/Gmax and damping ratio for backfill at depths of 55•ft to 88•ft.

B.1.4 Blue Bluff Marl Low Plasticity Index (Depth 88 Feet to 156 Feet)

The material properties used for blue bluff marl with low plasticity index at depths of 88•ft to 156•ft are given below.

$\rho_o = 115 \frac{lbm}{ft^3}$ Density

$\nu_o = 0.45$ Poisson's ratio

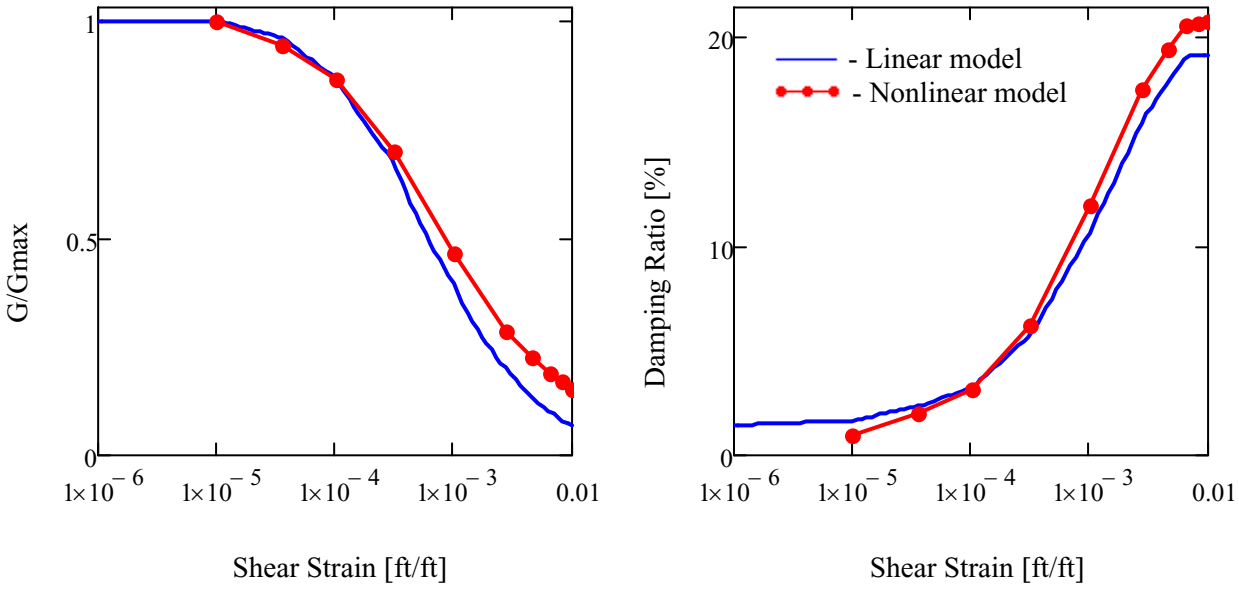

Figure B.1.4-1. Linear and nonlinear model G/Gmax and damping ratio for blue bluff marl with low plasticity index at depths of 88•ft to 156•ft.

B.1.5 Lower Sands Still Branch Sand (Depth 156 Feet to 220 Feet)

The material properties used for lower sands still branch sand at depths of 156•ft to 220•ft are given below.

$\rho_o = 123 \frac{lbm}{ft^3}$ Density

$\nu_o = 0.45$ Poisson's ratio

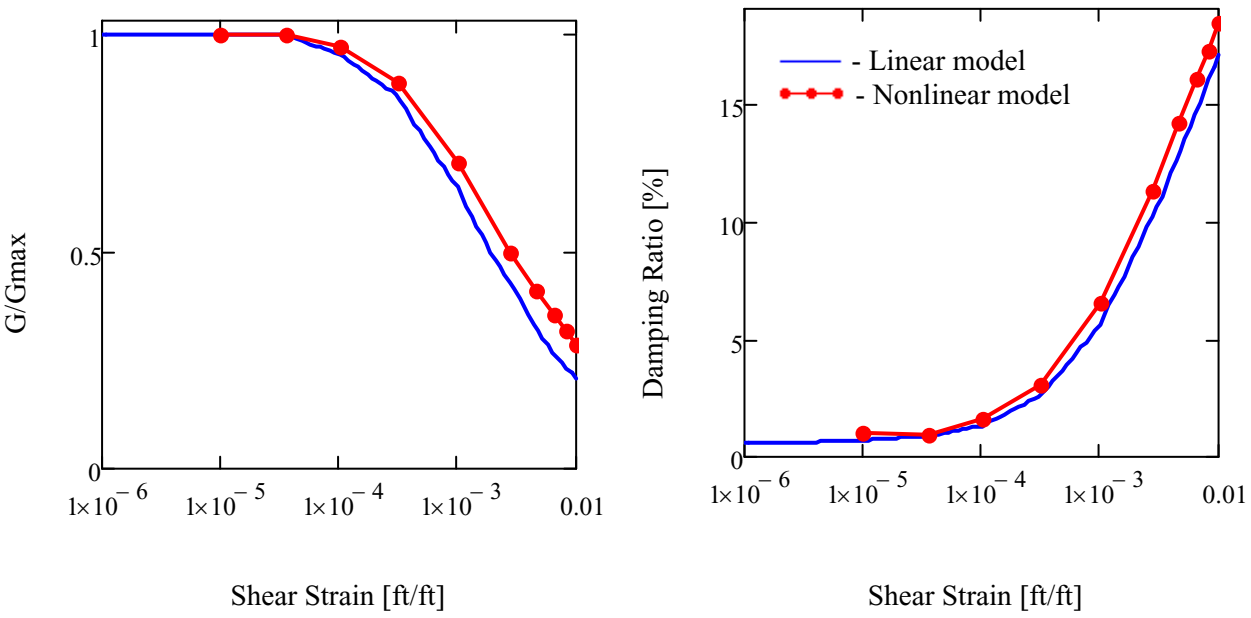

Figure B.1.5-1. Linear and nonlinear model G/Gmax and damping ratio for lower sands still branch sand at depths of 156•ft to 220•ft.

B.1.6 Lower Sands Congaree Sand (Depth 220 Feet to 310 Feet)

The material properties used for lower sands congaree sand at depths of 220•ft to 310•ft are given below.

$\rho_o = 128 \frac{lbm}{ft^3}$ Density

$\nu_o = 0.45$ Poisson's ratio

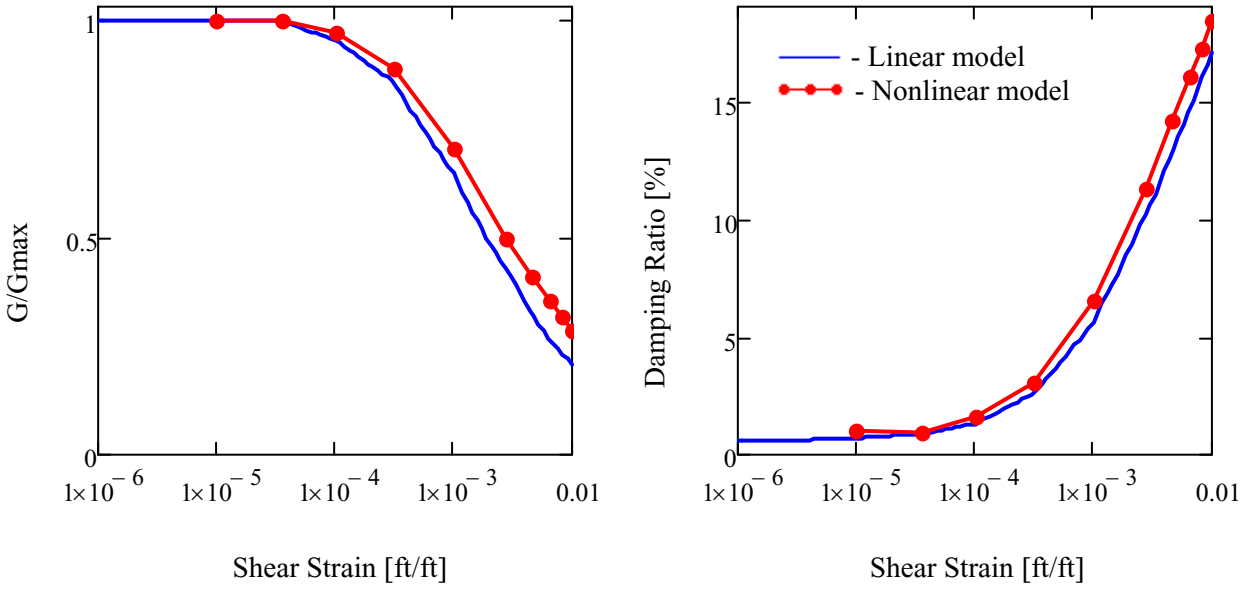

Figure B.1.6-1. Linear and nonlinear model G/Gmax and damping ratio for lower sands congaree sand at depths of 220•ft to 310•ft.

B.1.7 Lower Sands Congaree Clay (Depth 310 Feet to 340 Feet)

The material properties used for lower sands congaree clay at depths of 310•ft to 340•ft are given below.

$\rho_o = 128 \frac{lbm}{ft^3}$ Density

$\nu_o = 0.45$ Poisson's ratio

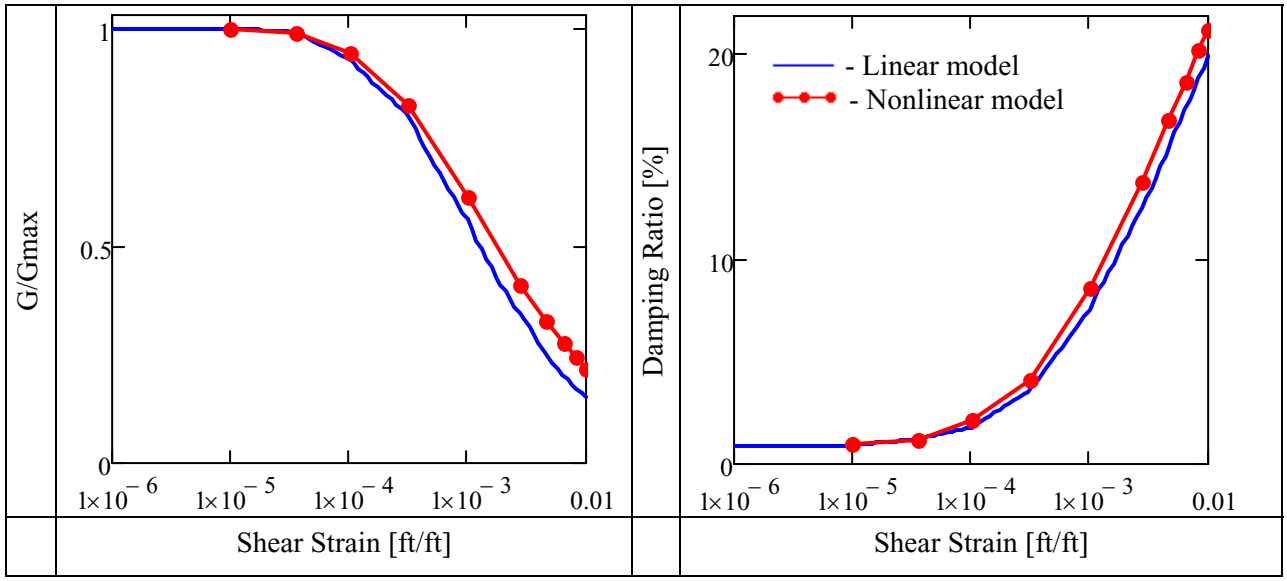

Figure B.1.7-1. Linear and nonlinear model G/Gmax and damping ratio for lower sands congaree clay at depths of 310•ft to 340•ft.

B.1.8 Lower Sands Snapp Clay (Depth 340 Feet to 380 Feet)

The material properties used for lower sands snapp clay at depths of 340•ft to 380•ft are given below.

$\rho_o = 127 \frac{lbm}{ft^3}$ Density

$\nu_o = 0.45$ Poisson's ratio

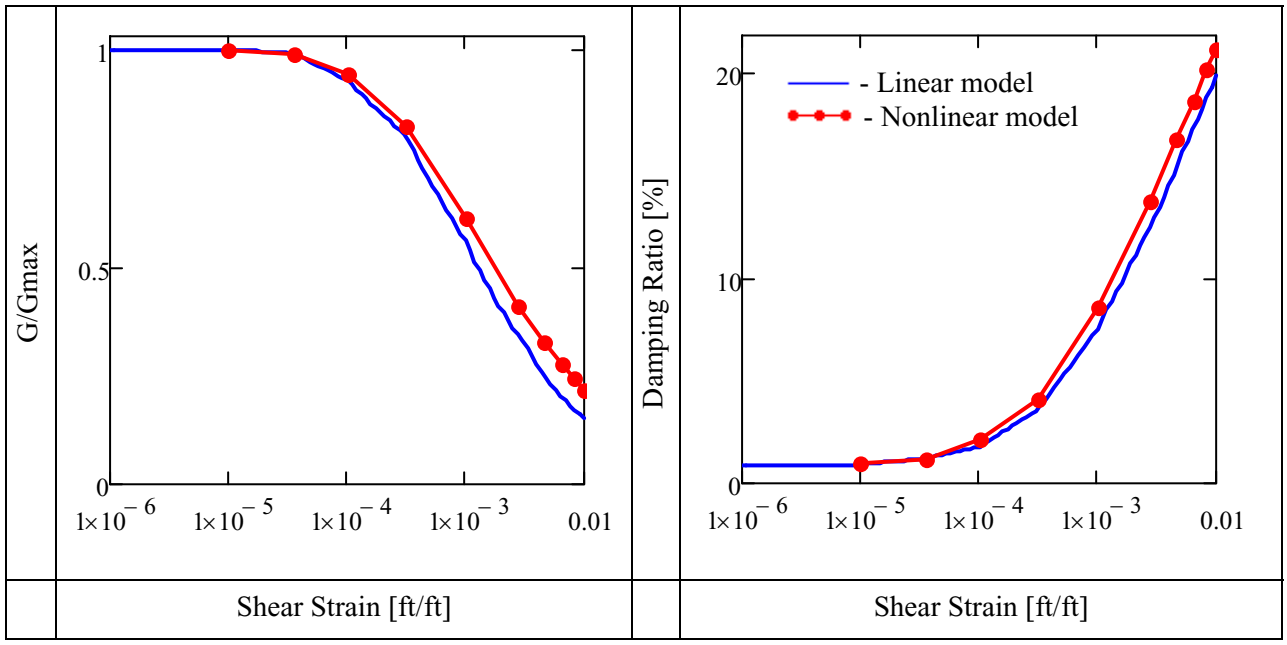

Figure B.1.8-1. Linear and nonlinear model G/Gmax and damping ratio for lower sands snapp clay at depths of 340•ft to 380•ft.

B.1.9 Lower Sands Snapp Sand (Depth 380 Feet to 447 Feet)

The material properties used for lower sands snapp sand at depths of 380•ft to 447•ft are given below.

$\rho_o = 127 \frac{lbm}{ft^3}$ Density

$\nu_o = 0.45$ Poisson's ratio

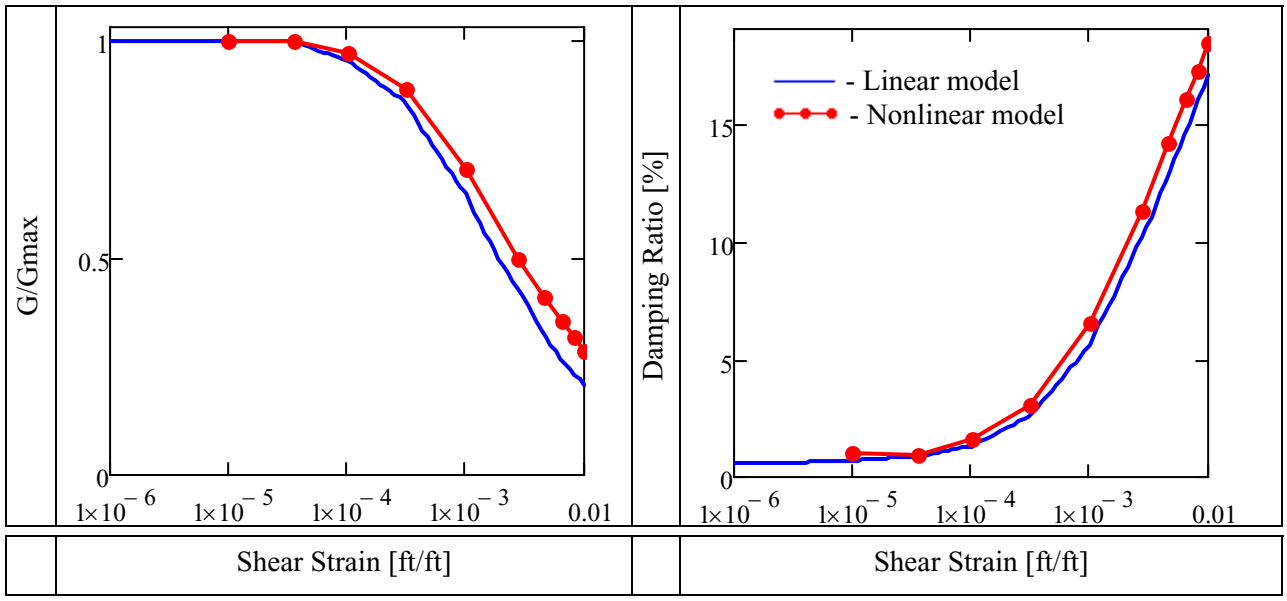

Figure B.1.9-1. Linear and nonlinear model G/Gmax and damping ratio for lower sands snapp sand at depths of 380•ft to 447•ft.

B.1.10 Lower Sands Black Mingo Sand (Depth 447 Feet to 486 Feet)

The material properties used for lower sands black mingo sand at depths of 447•ft to 486•ft are given below.

$\rho_o = 127 \frac{lbm}{ft^3}$ Density

$\nu_o = 0.45$ Poisson's ratio

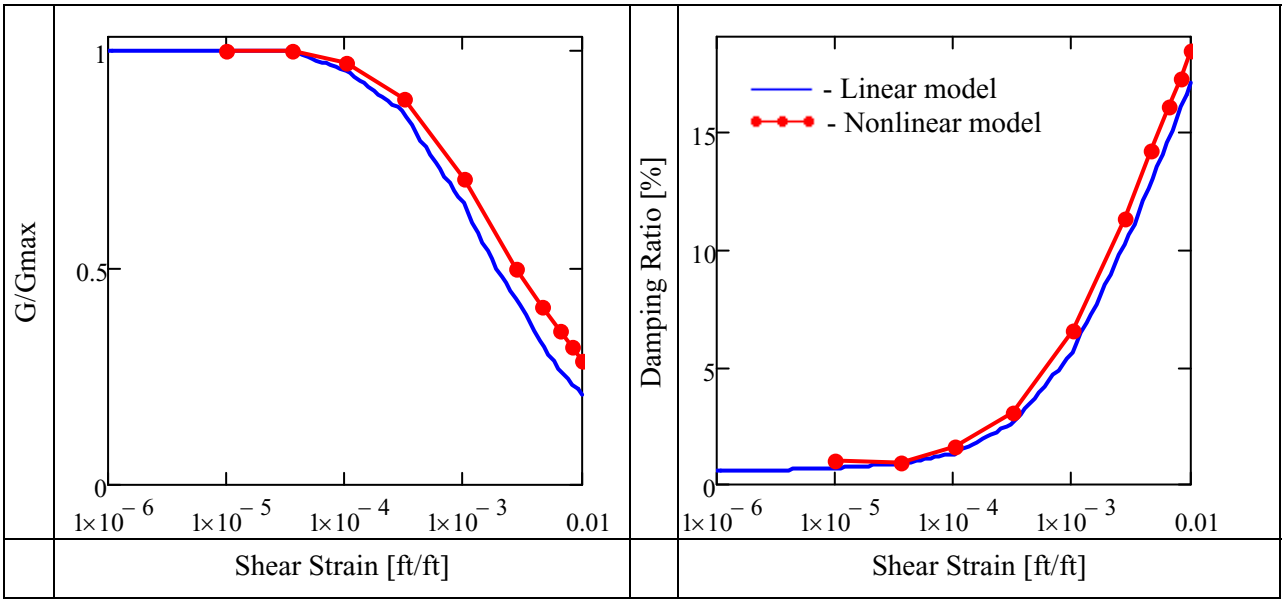

Figure B.1.10-1. Linear and nonlinear model G/Gmax and damping ratio for lower sands black mingo sand at depths of 447•ft to 486•ft.

B.1.11 Lower Sands Steel Creek Sand (Depth 486 Feet to 596 Feet)

The material properties used for lower sands steel creek sand at depths of 486•ft to 596•ft are given below.

$\rho_o = 127 \frac{lbm}{ft^3}$ Density

$\nu_o = 0.45$ Poisson's ratio

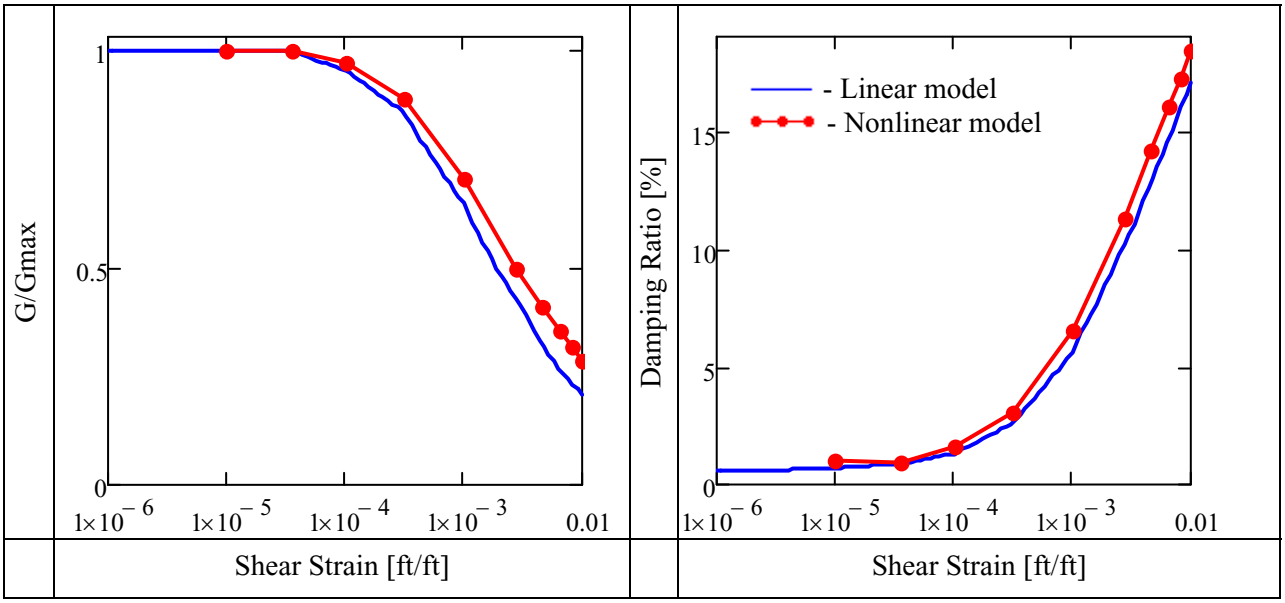

Figure B.1.11-1. Linear and nonlinear model G/Gmax and damping ratio for lower sands steel creek sand at depths of 486•ft to 596•ft.

B.1.12 Lower Sands Gaillard Sand (Depth 596 Feet to 807 Feet)

The material properties used for lower sands gailard sand at depths of 596•ft to 807•ft are given below.

$\rho_o = 127 \frac{lbm}{ft^3}$ Density

$\nu_o = 0.45$ Poisson's ratio

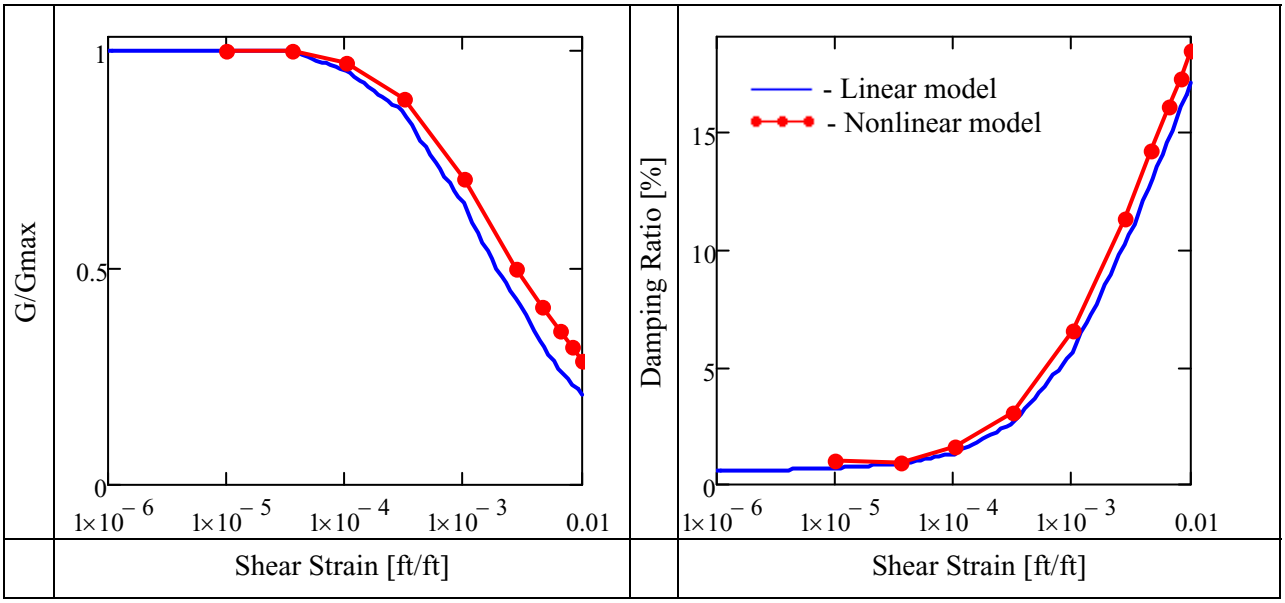

Figure B.1.12-1. Linear and nonlinear model G/Gmax and damping ratio for lower sands gailard sand at depths of 596•ft to 807•ft.

B.1.13 Lower Sands Pio Nono Sand (Depth 807 Feet to 867 Feet)

The material properties used for lower sands poi nono sand at depths of 807•ft to 867•ft are given below.

$\rho_o = 127 \frac{lbm}{ft^3}$ Density

$\nu_o = 0.45$ Poisson's ratio

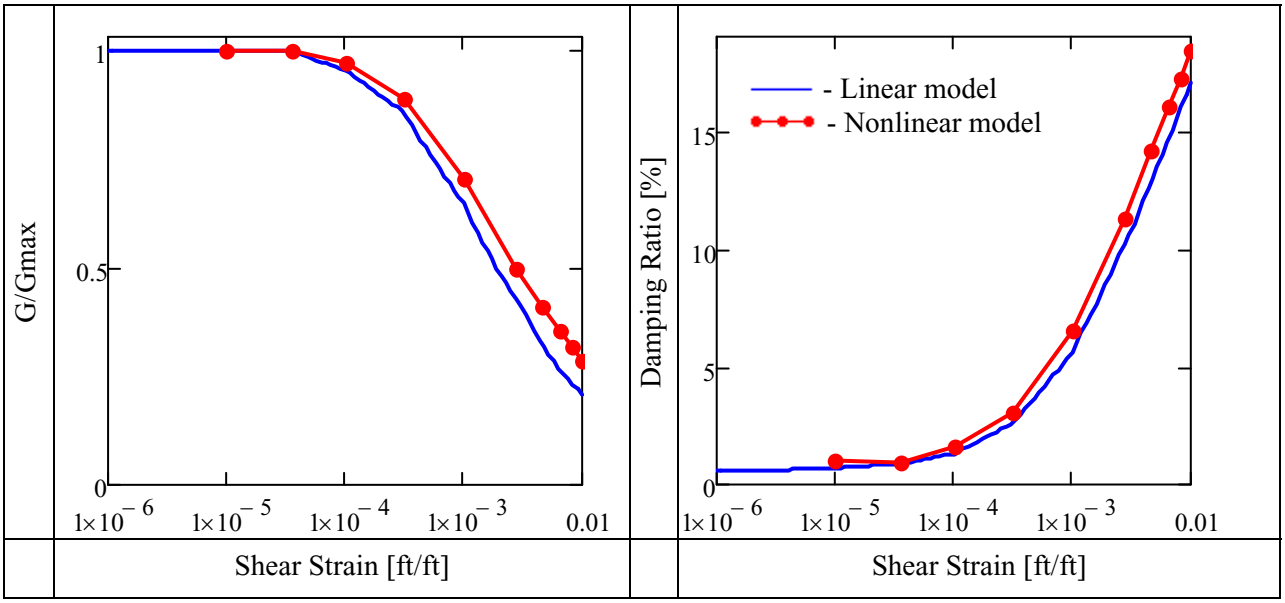

Figure B.1.13-1. Linear and nonlinear model G/Gmax and damping ratio for lower sands poi nono sand at depths of 807•ft to 867•ft.

B.1.14 Lower Sands Cape Fear Sand (Depth 867 Feet to 1058 Feet)

The material properties used for lower sands Cape Fear sand (depth 867 ft to 1058 ft) are given below.

$\rho_o = 127 \frac{lbm}{ft^3}$ Density

$\nu_o = 0.45$ Poisson's ratio

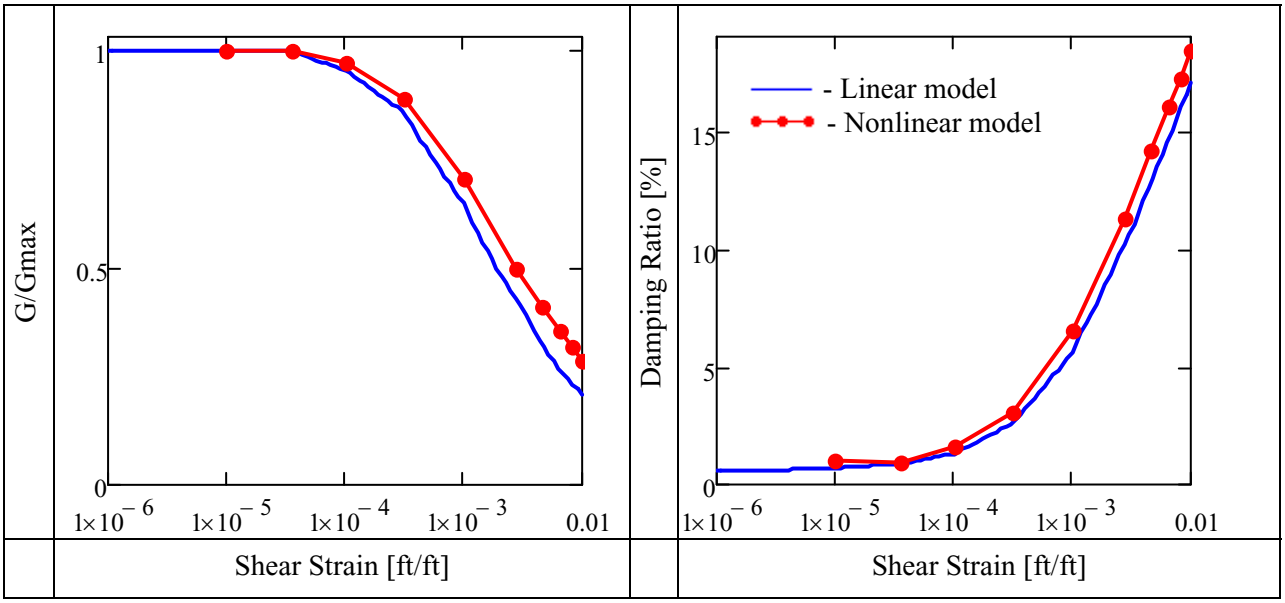

Figure B.1.14-1. Linear and nonlinear model G/Gmax and damping ratio for lower sands Cape Fear sand at depths of 867 ft to 1058 ft.

B.2 Nonlinear Soil Constitutive Model

Many finite element modelling software packages may be used to evaluate a nonlinear, hysteretic soil model. One of these is LS-DYNA using a nested surface hysteretic soil constitutive model (*MAT_HYSTERETIC_SOIL). Another one is Abaqus using the same constitutive model. This constitutive model is of a form that includes the Drucker-Prager model and is reasonable for nonlinear soil behavior. The hysteretic soil behavior results from post yielding shear stress versus shear strain. The basic idea is based on each element having up to 10 sublayers that are each elastic/perfectly plastic with different elastic stiffness and yield stress values. The elastic/plastic behavior of each sublayer follows a kinematic hardening rule. The response of the sublayers is summed together to produce the post yielding shear stress versus shear strain curve and it is valid for a single mean effective stress (or hydrostatic stress) in the element. When running a model, the default is to have the post yielding shear stress versus shear strain curve vary as the mean effective stress varies in a given element. It can also be defined to stay constant relative to the initial conditions. Other soil parameters that are available with this constitutive model include yield function constants, dilation parameters, reference pressure, cut-off

pressure, and an exponent for bulk modulus pressure sensitivity. (Note: In LS-DYNA, the modelled z-direction must be vertical for all of these parameters to work correctly.)

For all the elements, the yield functions constants were defined as a0 = 0.0, a1 = 0.0, and a2 = 1.0. This caused the behavior to be in a classical Drucker-Prager form. The value of 1.0 given to a2 is reasonable and has little effect on the constitutive model behavior for the problem being studied. The dilation parameters and cut-off pressure are set to zero. The reference pressure for each soil layer is calculated as the average static pressure in the given layer (using the know density, geometry, and gravitational acceleration).

B.3 Finite Element Model

The nonlinear finite element model for this study is shown in Figure B.3-1. It consists of fourteen different soil layers as described in Sections B.1.1 to B.1.14. To better compare with the SASSI model, each "step" in the shear velocity plot (Figure B.1-1) is defined with a separate material property (that is not allowed to change with changes in hydrostatic stress). This produces the 41 nonlinear soil layer definitions (shown as different colors in Figure B.3-1).

The mesh boundary conditions include being free at the top. There is an elastic element at the bottom of the mesh and it has seismic motion input as a load time history at its top (1058•ft depth) and it has a non-reflecting boundary condition its bottom (1072•ft depth). On the horizontal boundaries of the model, each set for four nodes at an elevation is constrained to move together. This mimics an infinite horizontal continuum.

The finite element mesh, element heights are set to pass up to 67•Hz waves with at least 10 elements per wave length. This causes the mesh to be finer in the soft soils and coarser in the stiffer soils.

Two versions of the nonlinear finite element model are performed. The first is run in LS-DYNA and it uses 10 shear stress versus shear strain data points (based on the G/Gmax, shear wave velocity, and density shown in Section B.1). This model is called the 10 sublayer model. The second is run in Abaqus/Explicit and it uses a shear stress versus shear strain curve with 100 data points. This model is called the 100 sublayer model. The 100 data points are established by first putting a cubic fit curve in log space through the 10 data points used by LS-DYNA. The 100 data points are then placed along even intervals of the smooth curve. The 100 data point model is intended to reduce erroneous noise produced by significant discontinuities along the shear stress versus shear strain curve.

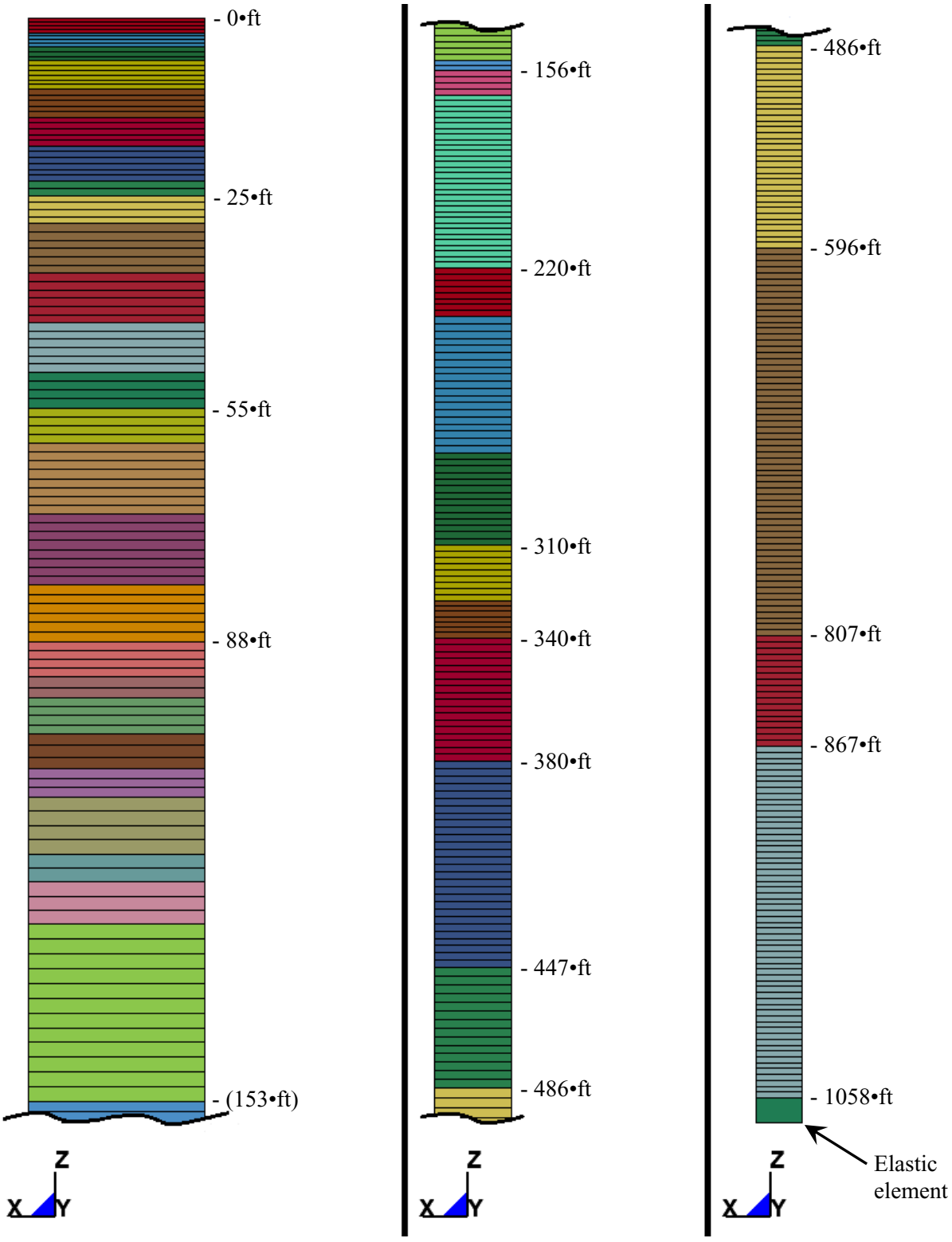

Figure B.3-1. Finite element model.

B.4 Input Seismic Time History

The seismic time history (shown in Figure B.4-1) for the soil column study is in one direction and is established from the surface down to a depth of 1058•ft using SHAKE. The time history development is performed in Cuesta et al. (2016).

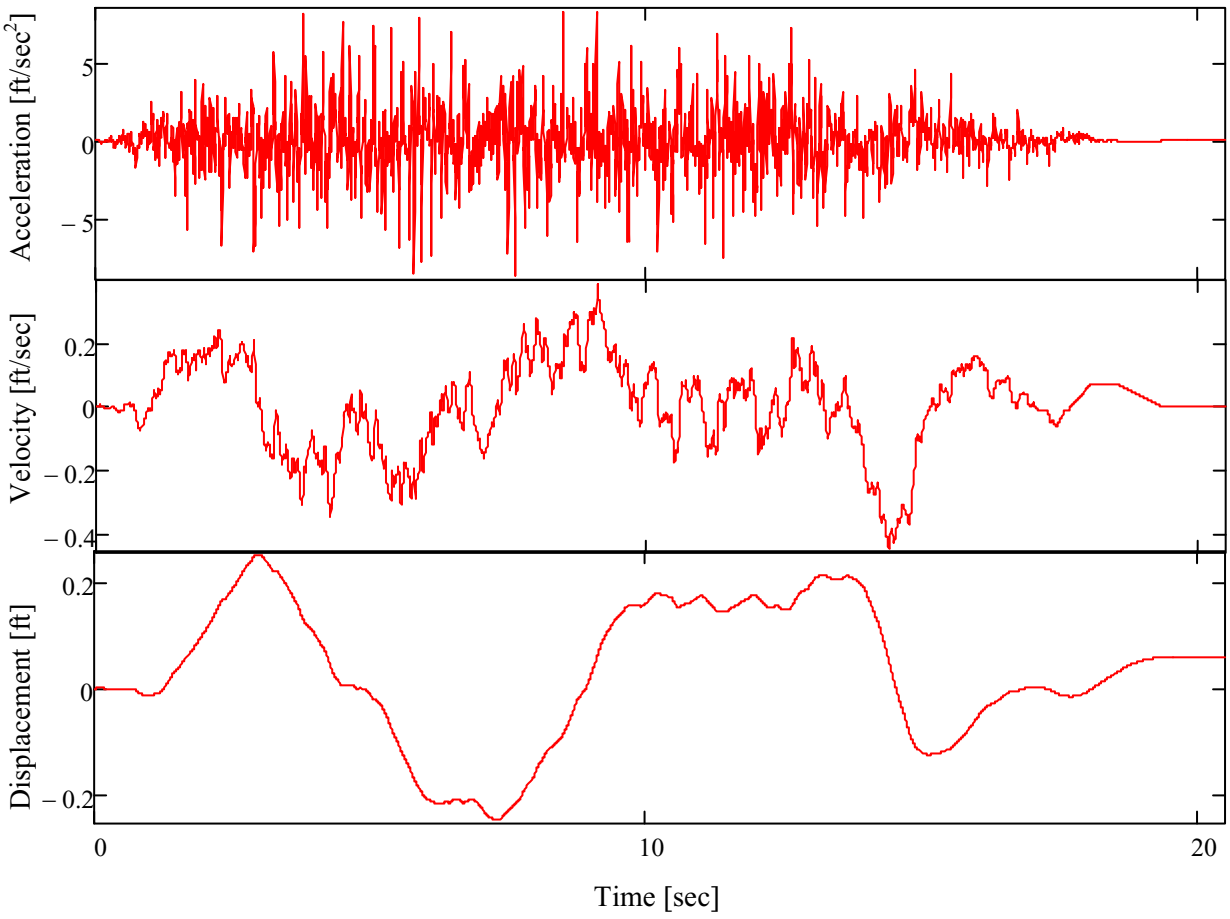

Figure B.4-1. Input, rock outcrop seismic time history at 1058•ft.

Using this process, there is substantial amount of high frequency content in the time history. Consequently, care is needed relative to the time step that is used for time history input. To ensure that the time history was being correctly input into the soil column model, preliminary models were run with just the elastic element. Running just this element with the load time history at its top and non-reflective boundary conditions at its bottom, the top of the model should produce the rock outcrop seismic acceleration (at 1058•ft). Using the typical time step of 0.005•sec, significant error is produced in this model run as there is not enough data to capture at least 10 points in time per wavelength (with the significant high frequency content). Oversampling the data to a time step of 0.001•sec yields a much better result.

Figure B.4-2 shows three 5% damped acceleration response spectra plots. The first is for the acceleration time history in Figure B.4-1 (Desired response). The second is for the acceleration output

from the elastic element only model run where the input load time history is given at a 0.005•sec time step (Response for 0.005•sec time step). The third is for the acceleration output from the elastic element only model run where the input load time history is oversampled to a 0.001•sec time step (Response for 0.001•sec time step). Based on these results, the 0.001•sec time step input load time history is used for all of the full soil column models.

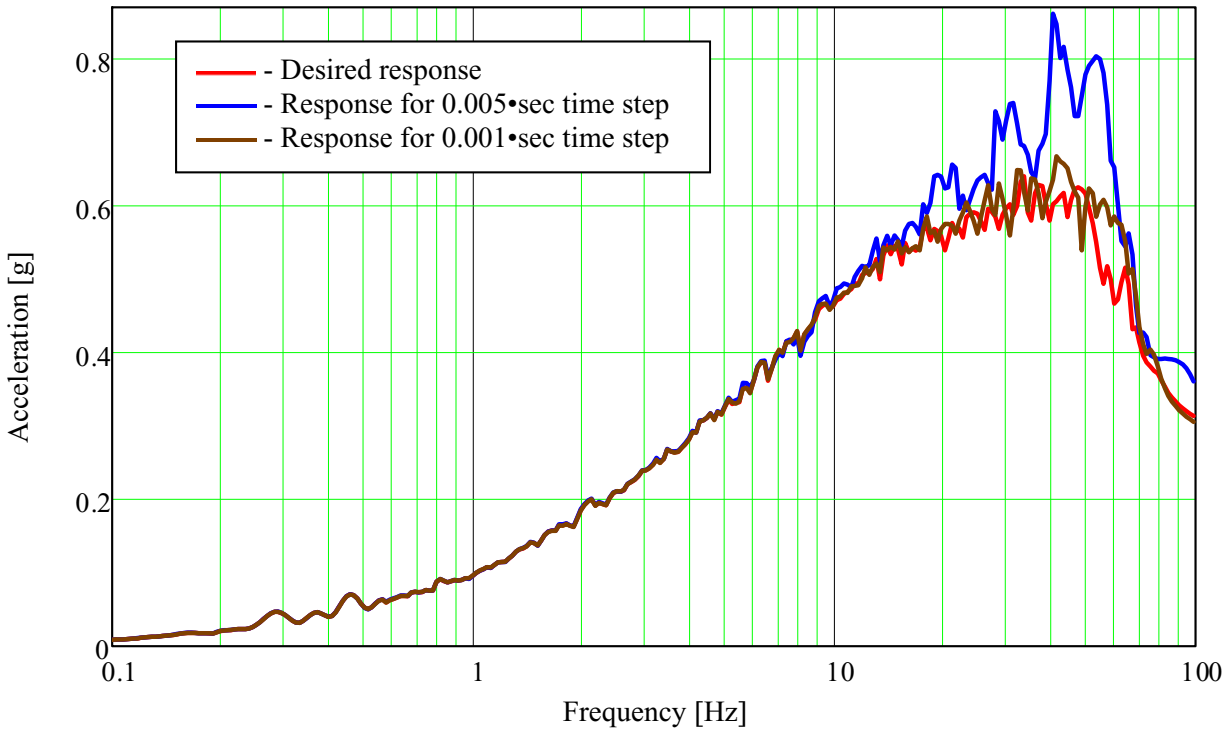

Figure B.4-1. Comparison of 5% damped response spectra for the rock outcrop seismic time history at 1058•ft.

B.5 Results and Discussion

The results for this study are shown in Figure B.5-1. As can be seen in the plot, at low frequencies (< 6•Hz), the linear and nonlinear results matched well. However, at higher frequencies (> 6•Hz), the amplitude of the linear and nonlinear results diverge. The peaks and valleys in the response occur at very similar frequencies (even for high frequencies). This indicates that the soil column natural frequencies compare well between the linear and nonlinear models. The difference in high frequency amplitude can be explained primarily with the difference in the hysteresis loops (shown in Figure B.5-2). The linear hysteresis loop is smooth and continuous. Consequently, in a linear model, an input sine wave passes through the model unaltered other than being damped. As a result, to produce a significant high frequency response at the top of a soil column, a significant high frequency input at the bottom of the soil column is necessary. In contrast, the nonlinear hysteresis loop has "pointed" discontinuous ends. This causes high frequency content to be present at the top of the soil column even when the input frequency content is only low frequency. Because the input time history for the bottom of the soil column was developed from a surface time history using linear techniques (with SHAKE), the input time has much more high frequency content than is necessary for nonlinear techniques (with LS-DYNA/Abaqus).

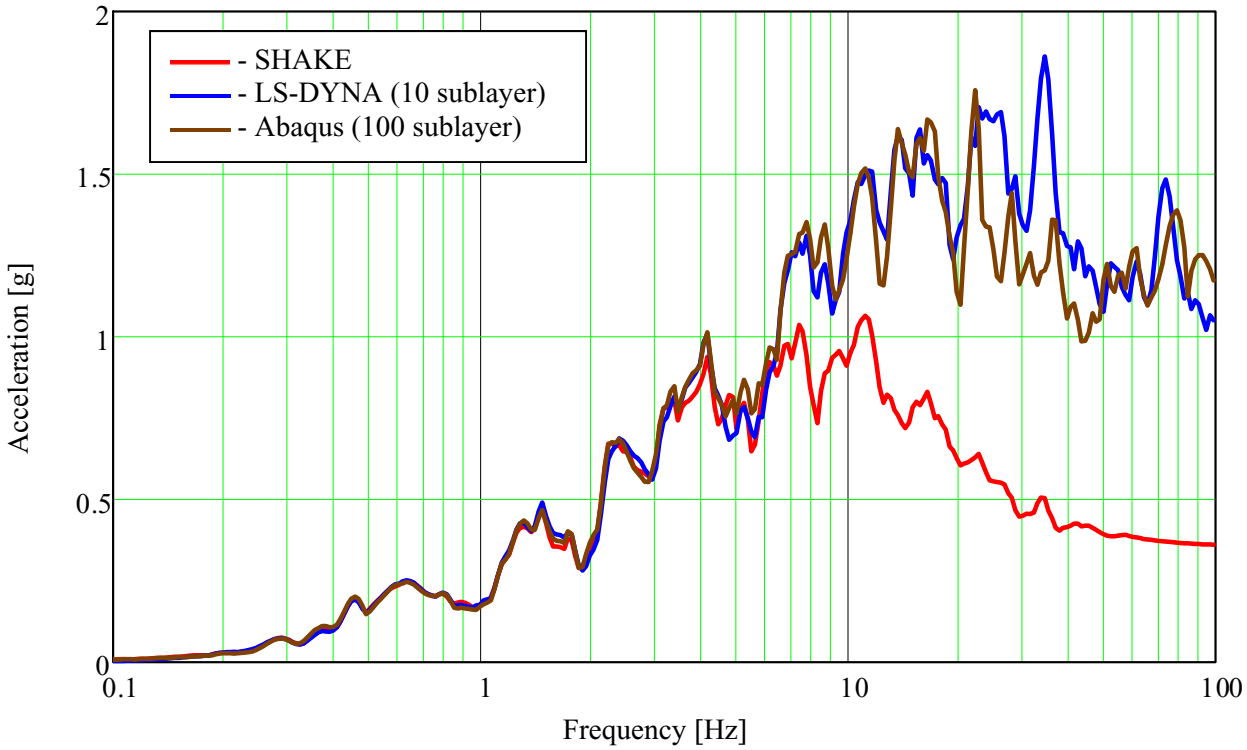

Figure B.5-1. Comparison of 5% damped response spectra for the soil column surface.

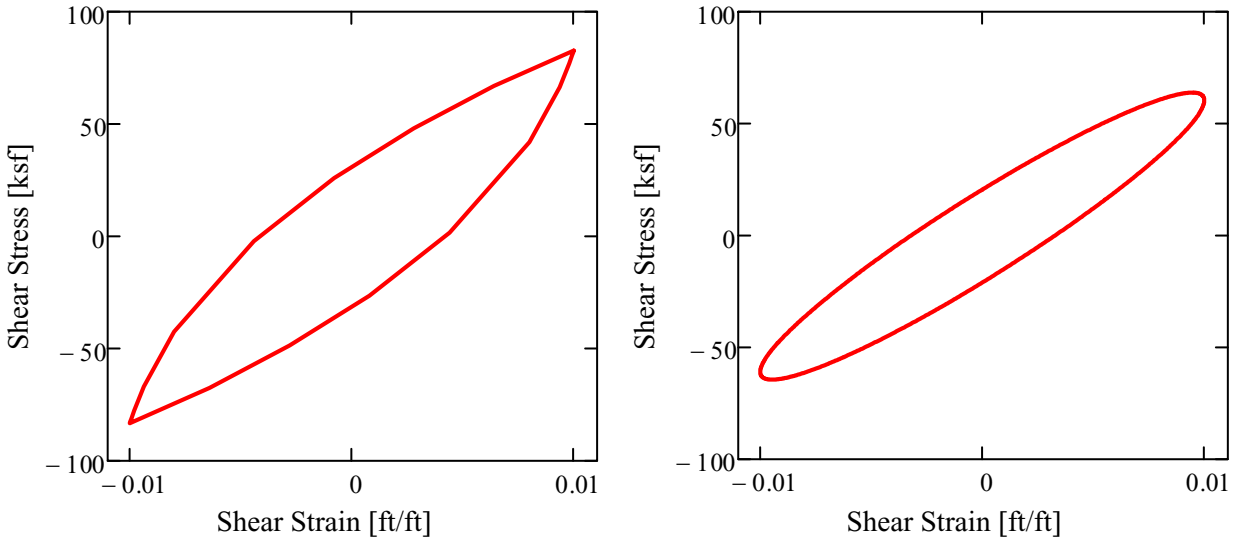

Figure B.5-2. Example nonlinear (left plot) and linear (right plot) hysteresis loops.

The comparison of the LS-DYNA (10 sublayer) results to the Abaqus (100 sublayer) results, provides an indication of erroneous noise that can be produced when the nonlinear stress versus strain curve has significant discontinuities (Bolisetti et al. 2014). It is computationally desirable to have as few sublayers

as possible. Consequently, the comparison gives an indication that there is some erroneous, high frequency noise in the 10 sublayer model but the 10 sublayer model produces accurate nonlinear response for much of the frequency range of interest.

For information, an additional nonlinear model (LS-DYNA with 10 sublayers) was run with less high frequency input at the base. To produce the modified input, a Fast Fourier transform was performed on the original time history used for input. Then the amplitudes for frequencies from 5•Hz to 25•Hz were linearly ramped down to very near zero. Amplitudes above 25•Hz were also set to very near zero. Finally an inverse transform was used to produce the modified input time history.

Figure B.5-3 shows the response spectrum of the input with less high frequency. Figure B.5-4 shows how the surface response is changed for this nonlinear model. While there is still some difference in the high frequency amplitude, this provides a much closer match to the desired surface response.

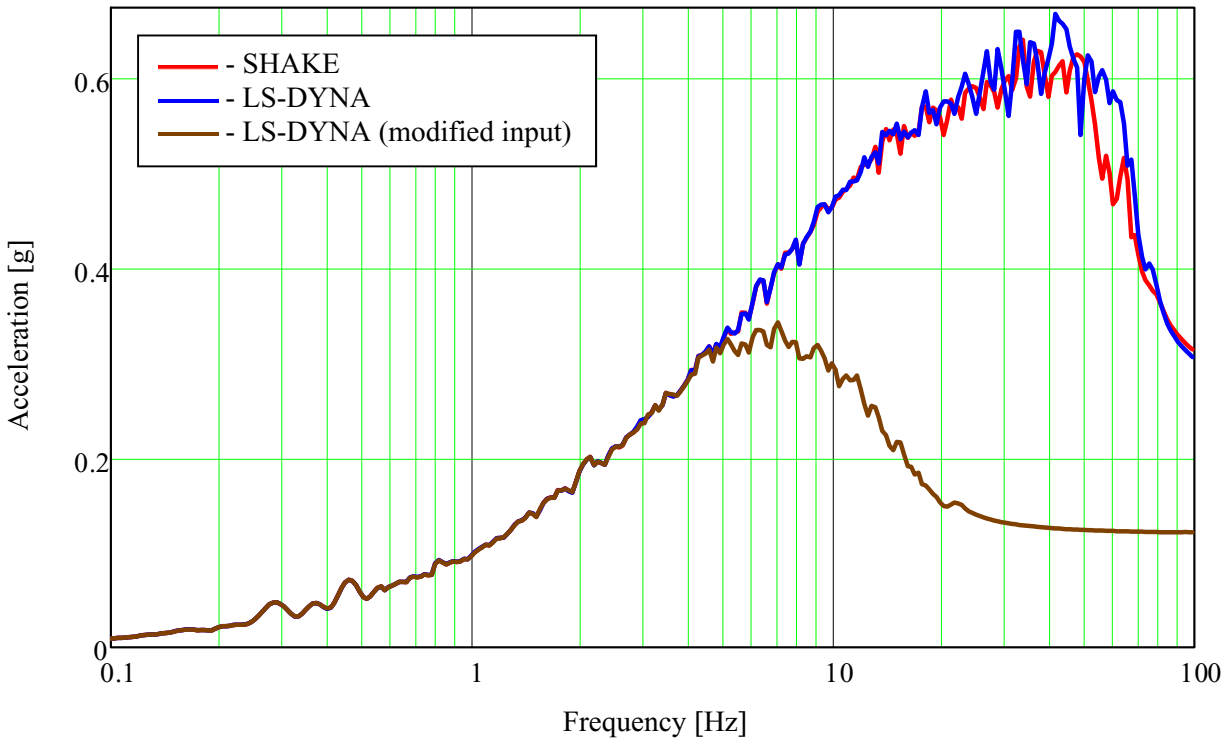

Figure B.5-3. Comparison of 5% damped response spectra for the rock outcrop seismic time history at 1058•ft including a model run with less high frequency input.

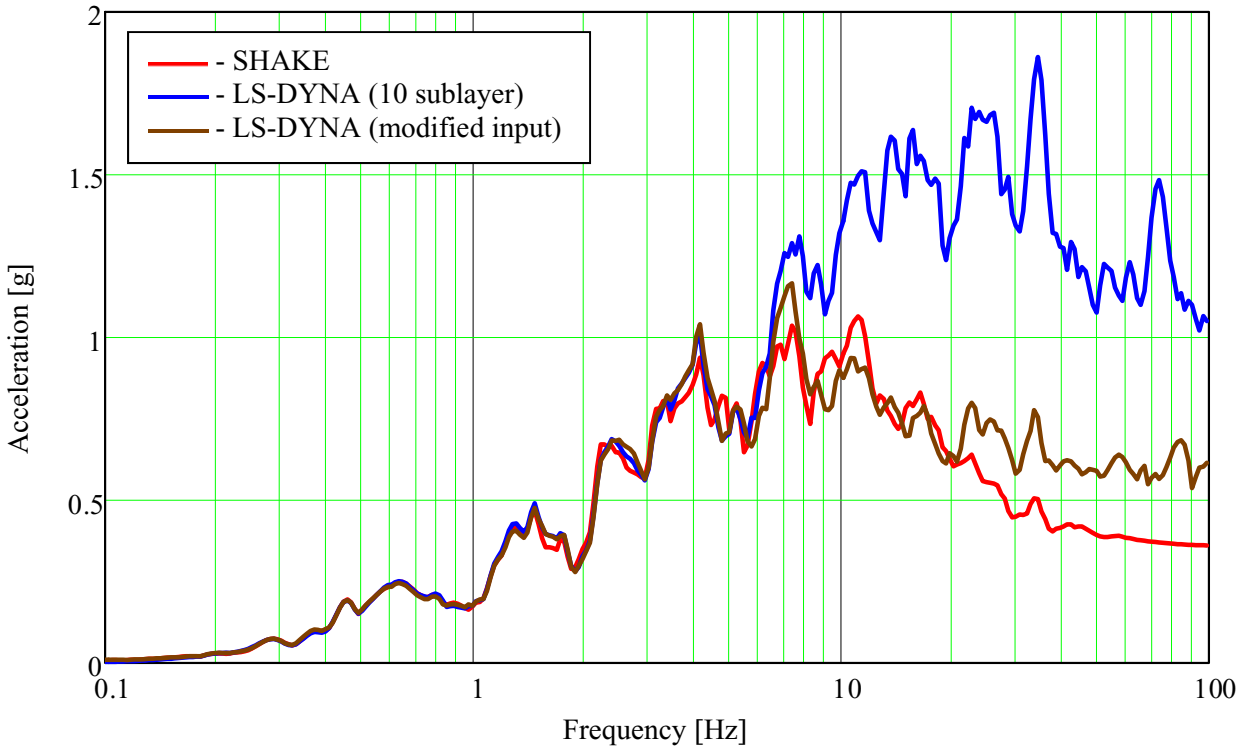

Figure B.5-4. Comparison of 5% damped response spectra for the soil column surface including a model run with less high frequency input.

B.6 Conclusions

This study shows results for a deep soil column evaluated with linear techniques (SHAKE) and with nonlinear techniques (LS-DYNA/Abaqus). The soil surface, response spectra results showed good agreement between the linear and nonlinear techniques at low frequencies (< 6•Hz). Additionally, the soil surface, response spectra results showed good agreement between the linear and nonlinear techniques relative to natural frequency response of the soil column. The higher frequency response (> 6•Hz) amplitude diverged between the linear and nonlinear techniques. This difference is predictable given the differences in the linear and nonlinear hysteresis loops.

B.7 References

1 Bolisetti, C., Whittaker, A. S., Mason, H. B., Almufti, I., Willford, M., (2014). "Equivalent linear and nonlinear site response analysis for design and risk assessment of safety-related nuclear structures," *Nuclear Engineering and Design 275*, 107-121, Elsevier, www.elsevier.com/locate/necengdes.

2 Cuesta, I., Mertz, G., Costantino, M. (2016). *Frequency Domain SSI Response of a Conceptual Reactor Building on the Vogtle Site*, CJC-IDA-M-002, Carl J. Costantino and Associates, Spring Valley, NY.

3 Dassault Système,s (2012), "Abaqus Software, Version 6.12-2," *Abaqus Analysis User's Manual*, Dassault Systèmes Simulia Corporation, Providence, RI.

4 Deng, N. and Ostadan, F (2000). "SHAKE2000," *Theoretical and User Manual, A Computer Program for Conducting Equivalent Linear Seismic Response Analyses of Horizontally Layered Soil Deposits*. Geotechnical and Hydraulic Engineering Services, Bechtel National Inc., San Francisco, CA, USA.

5 LSTC (2013). "LS-DYNA, Version smp s R7.00," *LS-DYNA Keyword User's Manual, Volume II*, Livermore Software Technology Corporation, Livermore, CA, USA.

6 Spears, R. E. and Coleman, J. L., (2015). "Calibrating Nonlinear Soil Material Properties for Seismic Analysis Using Soil Material Properties Intended for Linear Analysis." In: Proceedings of the 23rd SMiRT Conference, Manchester, United Kingdom.

7 Southern Company (2014). ''Vogtle Electric Generating Plant Units 1 and 2.'' *Enclosure 1 to SNC Letter NL-14-0344*, Southern Nuclear Operating Company, Inc., Birmingham, AL.